

Material Characterization of Weld Toe Region Using Digital Image Correlation

Master's Thesis in the Master's Programme Structural Engineering and Building Technology

ANDREA DEZŐ

MASTER'S THESIS BOMX02-17-101

Material Characterization of Weld Toe Region Using Digital Image Correlation

Master's Thesis in the Master's Programme Structural Engineering and Building Technology

ANDREA DEZÖ

Department of Civil and Environmental Engineering
Division of Structural Engineering
Steel and Timber Structures
CHALMERS UNIVERSITY OF TECHNOLOGY
Göteborg, Sweden 2017

Material Characterization of Weld Toe Region Using Digital Image Correlation

Master's Thesis in the Master's Programme Structural Engineering and Building Technology

ANDREA DEZŐ

© ANDREA DEZŐ 2017

Examensarbete BOMX02-17-101/ Institutionen för bygg- och miljöteknik,
Chalmers tekniska högskola 2017

Department of Civil and Environmental Engineering
Division of Structural Engineering
Steel and Timber Structures
Chalmers University of Technology
SE-412 96 Göteborg
Sweden
Telephone: + 46 (0)31-772 1000

Cover:

Strain field of the test specimen, obtained by means of DIC and the corresponding finite element model.

Department of Civil and Environmental Engineering. Göteborg, Sweden, 2017

Material Characterization of Weld Toe Region Using Digital Image Correlation
Master's thesis in the Master's Programme Structural Engineering and Building Technology

ANDREA DEZŐ

Department of Civil and Environmental Engineering
Division of Structural Engineering
Steel and Timber Structures
Chalmers University of Technology

ABSTRACT

Material models, properties of steel, the changes that occur during welding and different testing procedures were investigated as a starting point of the thesis work. The thesis project investigated the feasibility of using digital image correlation (DIC) in the process of material calibration. This consisted of the examination of local material properties at the weld toe of a welded joint, using digital image correlation in order to obtain the true strain field over the investigated area. The real stress-strain curves of the three material regions at the weld toe, namely, the weld material, base material and heat affected zone were obtained by means of material calibration, using an optimization function in Matlab, combined with the structural analysis capability of Abaqus. Since all weld geometries are significantly different, and the investigated area is very local, the accuracy of the Abaqus model is very important. Thus, in order to ensure a good correlation between the real test specimens and the Abaqus model, the test specimens were 3D scanned, and the obtained contour line was used in the creation of the model.

The difficulty of the task arises from the presence of three different materials in a region where stress concentration is also present. Therefore, a test-run of the material calibration was performed on a statically loaded plate having a hole in the middle, serving as source of stress concentration and consisting of two materials. The results showed that deviation between the obtained stress-strain curves and the reference stress-strain curves was under 5 %, proving that the proposed material calibration procedure worked well.

The DIC was performed on three test specimens, two of which were loaded statically and one was subjected to cyclic loading. One of the statically tested specimens was in its as welded state, while the other together with the cyclically loaded test specimen were treated with High Frequency Mechanical Impact (HFMI) treatment. The results of all three testing procedures were examined. The material calibration was performed only on the as welded statically tested test specimen. However, a detailed stress-strain curve for all three materials could not be obtained, since the plastic deformation of the investigated area was deemed to be too small.

Key words: Digital image correlation (DIC), Material calibration, Optimization function, 3D scanning, Weld toe, Base material (BM), Heat affected zone (HAZ), Weld material (WM), High Frequency Mechanical Impact (HFMI) treatment

Click here to enter text.

Click here to enter text.

Contents

1	INTRODUCTION	1
1.1	Aim and scope	1
1.2	Methodology	1
1.3	Limitations	2
2	MATERIAL PROPERTIES	3
2.1	Overview of material properties	3
2.2	Characteristic tests	4
2.2.1	Tensile test	4
2.2.2	Hardness tests	6
3	MATERIAL CHARACTERISATION OF WELDED JOINTS	12
3.1	Introduction (welding)	12
3.2	Base material (BM) - structural steel (S355-S460)	13
3.3	Weld material (WM)	16
3.4	Heat affected zone (HAZ)	19
4	HIGH FREQUENCY MECHANICAL IMPACT TREATMENT	24
4.1	Introduction	24
4.2	HFMI treatment process	26
4.2.1	Treatment defects	28
4.3	Consequences of HFMI treatment	30
5	PLASTICITY MODELS	32
5.1	Yield condition	33
5.1.1	The von Mises yield criterion	33
5.1.2	The Tresca criterion	34
5.1.3	The Hill criterion	37
5.2	Hardening rules - overview	38
5.3	Isotropic hardening	41
5.3.1	Johnson-Cook isotropic hardening	42
5.4	Kinematic hardening	43
5.4.1	Bi-linear kinematic hardening (Melan-Prager)	45
5.4.2	Multilinear kinematic hardening (Mroz)	46
5.4.3	Nonlinear kinematic hardening (AF and Chaboche)	47
5.5	Mixed hardening	48

6	EXPERIMENTAL PROCEDURES	51
6.1	Test specimens	51
6.1.1	Geometry	51
6.1.2	Material	53
6.2	Testing	55
6.3	Digital image correlation	56
6.3.1	Introduction	56
6.3.2	Specimen preparation	57
6.3.3	Convergence study – Analyzed area size	60
6.4	Results	63
6.4.1	Static test results – As welded specimen	63
6.4.2	Static test results – HFMI treated specimen	66
6.4.3	Cyclic test results	69
7	MODELLING PROCEDURES (ABAQUS + 3D SCAN)	73
7.1	3D scanning of test specimen	73
7.2	Abaqus model	76
8	MATERIAL CALIBRATION PROCEDURE	79
8.1	Simple case study	80
8.1.1	Abaqus model	80
8.1.2	Calibration procedure	82
8.1.3	Results	84
8.2	Test specimen (SAW)	87
8.2.1	Elastic region	87
8.2.2	Plastic region	90
9	DISCUSSION\CONCLUSION	93
10	FUTURE RESEARCH	94
11	REFERENCES	95
	APPENDIX I: MATLAB CODE FOR MATERIAL CALIBRATION OF SAW TEST SPECIMEN	97
	Main Matlab code for Elastic material models	97
	Main Matlab code for Plastic material models	98
	Matlab Function script code: simulationEl	101
	Matlab Function script code: simulationYield	105
	Matlab Function script code: simulationPl	108
	Matlab Function script code: simulationYieldHAZ	111
	Matlab Function script code: IntElas	114

Preface

This Master's thesis is focused on the investigation of the materials present at the weld toe region of a welded detail, using digital image correlation (DIC) in the process of material calibration in order to obtain the stress – strain curves of these materials. The study was carried out at the Division of Structural Engineering of the Department of Civil and Environmental Engineering at Chalmers University of Technology.

Many people have contributed either directly or indirectly to this study, without whom it would have been impossible to complete this research. First and foremost, I would like to show my greatest appreciation to my supervisor, Prof. Mohammad Al-Emrani, who was an endless source of wisdom and support. His invaluable assistance and comments helped me throughout my research, while his personality and sense of humour brightened my day on multiple occasions.

I am deeply grateful to Prof. Mathias Flansbjer, for conducting the tests in the laboratory of the Research Institutes of Sweden (RISE - former SP), helped me understand the testing procedures and gave me valuable insight regarding DIC.

Special thanks to Ignasi Fernandez for granting me his time and for giving me his assistance regarding the manipulation of the 3D scanner.

Finally, I would like to thank my opponents, Josef Makdesi and Fabio Lozano Mendoza for their continuous feedback.

Göteborg June 2017

Andrea Dező

Notations

Roman upper case letters

A	Constant equal to the yield stress in Johnson-Cook isotropic hardening
A_0	Initial cross-sectional area of test specimen
B	Constant representing the strain hardening in Johnson-Cook isotropic hardening
C	Constant representing the strain rate in Johnson-Cook isotropic hardening
CEV	Carbon equivalent value
D	Diameter of indenter in Brinell hardness test
D_b	Depth of HFMI treatment in base material
D_w	Depth of HFMI treatment in weld material
E	Elastic modulus
E_{HR}	Constant indentation in Rockwell hardness test
F	Force
$F(\sigma_{ij})$	Initial yield surface
G	Shear modulus
H	Plastic modulus
HB	Brinell hardness test value
HR	Rockwell hardness test value
HV	Vickers hardness test value
K	Strain hardening coefficient
K_α	Hardening parameter
K_ε	Strain concentration factor
L_0	Initial length of test specimen
R_{ij}	Stress ratio
\hat{T}	Homologous temperature in Johnson-Cook isotropic hardening

Roman lower case letters

d	Diameter of indent in Brinell hardness test
e	Depth of indentation
n	Strain hardening exponent
m	Thermal softening constant in Johnson-Cook isotropic hardening
s_{ij}	Deviatoric stress tensor

Greek upper case letters

ΔA	Cross sectional area difference due to tensile testing
ΔL	Length deformation due to tensile testing

Greek lower case letters

α_{ij}^d	Deviatoric back-stress
α_{ij}	Back-stress
ε	Engineering strain

ε^P	Plastic strain
ε_{eff}^P	Effective plastic strain
$\dot{\varepsilon}_{ij}^P$	Plastic strain rate
ε_{nom}	Nominal strain value
ε_{true}^P	True plastic strain
$\dot{\lambda}$	Plastic multiplier
ν	Poisson's ratio
σ	Engineering stress
σ_e	Equivalent von Mises stress
$\bar{\sigma}_{ij}$	Given stress in Abaqus
σ_{ij}^M	Mapping stress point
σ_{max}	Maximum principal stress
σ_{min}	Minimum principal stress
σ_{true}	True stress
σ_U	Maximum stress
σ_x	Stress in x direction
σ_y	Stress in y direction
σ_Y	Yield stress
σ_z	Stress in z direction
τ_{max}	Maximum shear stress

Abbreviation

AF	Armstrong and Frederick
AW	As-Welded
BM	Base Material
CCT	Continuous Cooling Time
DIC	Digital Image Correlation
HAZ	Heat Affected Zone
HFMI	High Frequency Mechanical Impact
HiFiT	High Frequency Impact Treatment
IIW	International Institute of Welding
PIT	Pneumatic Impact Treatment
PWT	Post-Weld Treatment
SEM	Scanning Electron Microscope
UPT	Ultrasonic Peening Treatment
WM	Weld Material

Special characters

% <i>El</i>	Percent elongation (ductility)
% <i>Ra</i>	Percent reduction of cross section area (ductility)

1 Introduction

The behaviour of a material subjected to tension can be described by the stress-strain curve of that specific material. In the case of structural steel, this can be divided into two regions, an elastic region described by Hook's law and a plastic region following the Power law. Usually, this stress-strain curve is obtained by Tensile testing, where a homogeneous test specimen, having regular geometry is subjected to uniformly increasing tensile force, until failure.

When multiple steel elements are desired to be joined, the most common method is welding. This procedure introduces not only residual stresses, but it also changes the crystalline structure of the weld zone. Thus, due to the welding of the elements, three different materials can be differentiated at the weld toe, the base material to be welded, the weld material which was added during welding and the heat affected zone, which is the area of the base material which suffered changes due to the heat input of the welding. In order to obtain the stress- strain curves of these three materials, the above mentioned tensile testing is no longer adequate, since the test specimen is not homogeneous and stress concentration appears due to the change in geometry. Thus, another method must be used.

1.1 Aim and scope

The aim of the thesis work is to investigate the feasibility of using Digital Image correlation (DIC) in the process of material calibration, in order to obtain the material parameters of a welded joint at the weld toe region.

During the thesis work, three test specimens are tested and the result of the experimental procedures are analysed. The material calibration is performed only on the simplest case, this being the statically tested welded test specimen, without any post weld treatments, due to the time limitation of the thesis work. The other two test specimens are subjected to High Frequency Mechanical Impact (HFMI) treatment in order to increase the strength of the materials at the weld toe region, and improve the weld toe geometry. One of these is tested statically, while the other is subjected to cyclic loading.

The thesis work also serves as a stepping stone for future research in using DIC for the investigation of the effect of HFMI post-weld treatment on the stress- strain curve of the materials present at the weld toe and in the description of their cyclic behaviour, when subjected to fatigue loading.

1.2 Methodology

Initially an extensive literature study is performed regarding the material models and material properties of steel, in order to understand what happens with the material during welding and how the material is described by different parameters and models.

The test specimens are prepared and tested, which is followed by the analysis of the test results.

The material calibration is performed by continuously comparing the strain data of the test specimen during static loading, obtained by means of DIC with the strain data obtained from the Abaqus analysis, which is simulating the experimental procedure.

In order to use an optimisation function from Matlab, as well as the structural analysis capabilities of Abaqus, a link is created between the two softwares by using the Abaqus2Matlab toolbox. The used optimisation function produces an educated guess of the input material properties, which is then introduced into the Abaqus model and the analysis is run again with the new material input. The input material parameters are improved until the obtained strain field from the Abaqus model is as close as possible to the strain field from the DIC experimental procedure.

1.3 Limitations

The conducted study is restricted to test specimens having a steel grade of S460, considered as regular structural steel. The investigated test specimens are slices of two full-size fillet weld details, one with and one without HFMI-treatment. Thus, the only post-weld treatment method considered is HFMI treatment.

The material calibration is limited to the statically tested as-welded test specimen, considering only three different materials located at the weld toe region, without a gradient in the case of the heat affected zone. Thus, each material is regarded as homogeneous and the exact locations of these are determined using the magnified image captured for the DIC procedure.

2 Material Properties

This chapter serves as a short overview of typical material properties and tests which are carried out in order to understand a material's behaviour under loading.

2.1 Overview of material properties

The short description of the following material properties is based on Damone, Illston (2010) and Brockenbrough, Merritt (1999).

Stress-strain curve:

The stress-strain curve is most commonly used in order to show the behaviour of a specific material under steadily increasing tensile or compressive loading. Some significant material properties can be obtained by analyzing these curves, like yield strength, tensile strength, modulus of elasticity or ductility. Two distinct regions can be differentiated on most material stress-strain curves, an initial linear region, or also called elastic region and a non-linear, plastic region. The curve can change depending on the composition and the crystalline structure of the material. Figure 2.1 shows the schematic stress – strain curve for different types of steel.

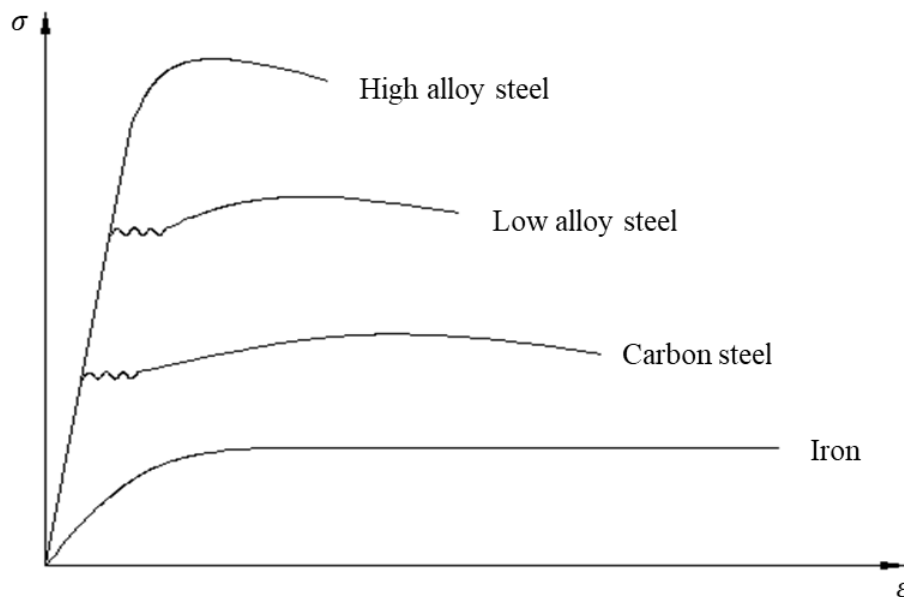


Figure 2.1 Stress strain curves for different types of steel.

Yield strength:

The yield strength is the stress value, at which a sudden increase of strain can be observed, without the increase of stress. This delimits the point up to which the material undergoes elastic deformation, having the ability to recover its initial shape in the case of unloading and above which the material experiences plastic, permanent deformation due to the applied load.

Tensile strength:

The maximum stress before failure recorded on the stress-strain curve indicates the ultimate tensile stress, or tensile strength.

Modulus of elasticity:

The modulus of elasticity is defined as the ratio between the stress and strain of the material or the slope of the stress-strain curve in the elastic region and it shows the ability of the material to withstand elastic deformation.

Ductility:

Ductility measures the ability of the material to deform plastically before failure. It is expressed as percent elongation at failure or percent reduction of cross section area in a tensile test.

Hardness:

Hardness is defined as the capability of the material to resist indentation or penetration by another material, showing the resistance of the material against plastic deformation.

2.2 Characteristic tests

2.2.1 Tensile test

This test can be performed in order to determine the tensile stress-strain curve of a material. It is regarded as a destructive test, since the specimen is destroyed in the process of obtaining the relevant material data. After placing the test specimen into the testing machine, a steadily increasing traction force is applied, acting in the longitudinal direction of the test specimen, usually until failure, while the elongation and the force acting on the specimen is recorded in time. Equation (1.1) and (1.2) can be used to calculate the engineering stress and strain values. Dividing the force (F) by the initial cross sectional area (A_0) of the specimen will result in the engineering stress (σ) value expressed in MPa in the SI system, while dividing the deformation (ΔL) in the direction of the applied force with the initial length (L_0) of the specimen gives the strain (ε) value, which is dimensionless. All these parameters are presented in Figure 2.2, showing the schematic representation of the specimen before and after testing.

$$\sigma = \frac{F}{A_0} \quad (1.1)$$

$$\varepsilon = \frac{\Delta L}{L_0} \quad (1.2)$$

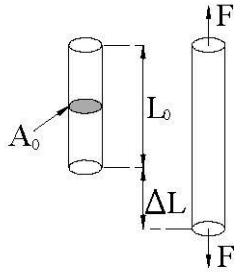


Figure 2.2 Schematic representation of the stress rupture test parameters.

As mentioned before, as a consequence of obtaining the stress-strain curve, the test will also provide values for yield strength, tensile strength, ductility and other tensile properties.

Ductility is expressed as percent elongation ($\%El$) at failure or percent reduction of cross section area ($\%Ra$) during tensile testing and it is calculated using the equation (1.3) and (1.4).

$$\%El = \frac{\Delta L}{L_0} 100\% \quad (1.3)$$

$$\%Ra = \frac{\Delta A}{A_0} 100\% \quad (1.4)$$

Figure 2.3 shows an example of a test machine used for the tensile testing.



Figure 2.3 Hualong stress rupture testing machine - RCW series.

The general behavior of a structural steel specimen during tensile testing can be seen in Figure 2.4. At stress values below the yield stress (σ_y), the material exhibits elastic behavior, characterized by elastic deformation. This is followed by the plastic region, which can be divided into two parts. Until the maximum stress is reached (σ_U), the specimen experiences uniform plastic deformation. After this point, the stress starts decreasing while a localised decrease in the cross sectional area, also called necking can be observed somewhere along the length, which leads to a ‘cup and cone’ failure type in the case of medium-strength steel.

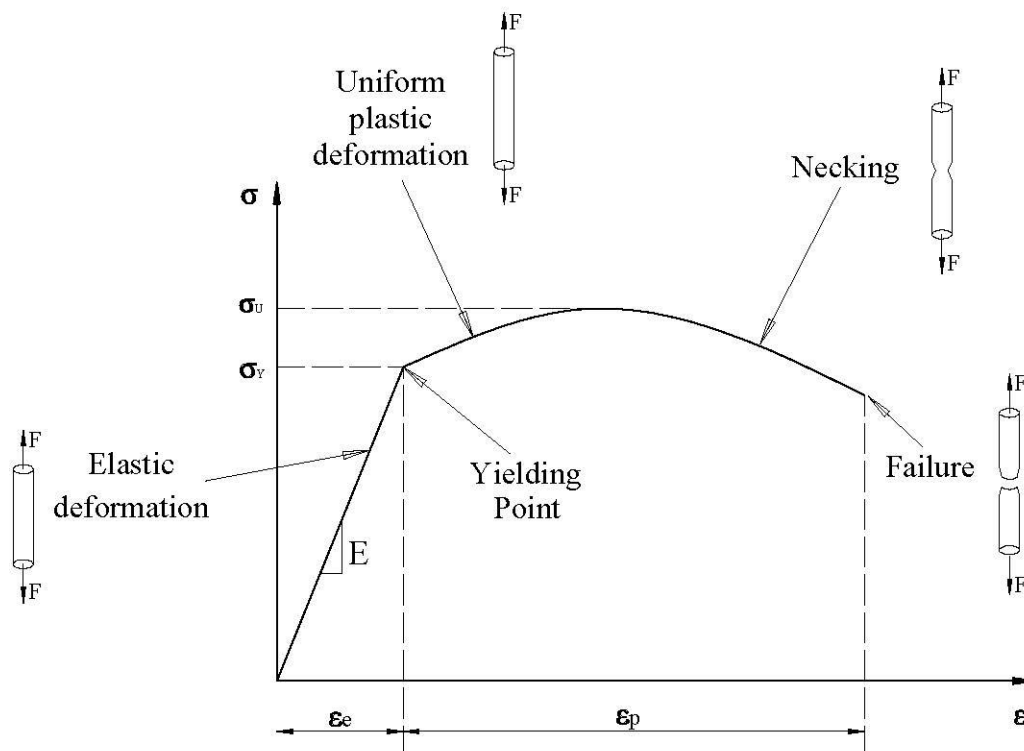


Figure 2.4 Schematic stress –strain curve of structural steel and general behaviour of the structural steel specimen during tensile testing.

2.2.2 Hardness tests

The hardness value can be obtained using multiple testing methods, usually by measuring the indentation surface left by an indenter, which is pushed into the material with a specific force and for a specific time period. Some of the most widely used hardness testing methods are the Brinell hardness test, the Vickers hardness test and the Rockwell hardness test, these being presented in this subchapter. The information regarding these tests is based on Herrmann (2011).

The hardness value is governed by the chosen measurement procedure, being regarded as a reference value scale, thus lacking a unit of measurement. The value is denoted as the hardness value obtained by the test followed for example by the letters ‘HB’ in the case of the Brinell hardness test, or ‘HV’ for the Vickers hardness test. The direct

comparison of the obtained values by different methods is not possible, however certain tables and charts are available for converting or finding the equivalent values from a different testing method. However, these are regarded as approximate equivalents.

The hardness value of a specific material is directly proportional with the bonding forces between the molecules. Since the bonding force between different molecules is stronger than between similar molecules, the hardness of steel is greater than the hardness of its individual alloying components. The hardness value is also inversely proportional to the grain size and directly proportional to the yield strength, meaning that hardness value is larger if the grain size is smaller and if the yield strength is higher.

Brinell hardness test:

This test was invented in 1900 by a Swedish engineer named Johan August Brinell and it is the oldest hardness test method, which is still in use. It is a nondestructive test. Thus the test specimen may be reused.

The indentation is produced by a carbide ball. The diameter of the ball, the applied force and the time interval of the load application may vary according to the tested material, however the relationship between the applied force and the ball size has to be the same in order to have comparable results.

The correct steps and regulations concerning the Brinell hardness test can be found in the standards: ASTM E10 and ISO 6506. For example, the minimum thickness of the test piece has to be 8-10 times higher than the depth of the produced indentation. This rule is set in place due to fact that the material zone affected by the indentation process has to be located completely inside the test specimen, otherwise the surrounding materials, like the support table would influence the outcome of the test. The distance between two indentations is also regulated, as well as the distance of the indentation from the edge of the test specimen.

Under normal circumstances the indenter is pushed against the test specimen with a given force, which is maintained for 15-30 seconds, depending on the material. The diagonal of the indentation left behind is measured, by taking the average value of two perpendicularly measured diagonals, using a portable microscope or a microscope integrated in the device. The hardness value is calculated with the formula given in equation (1.5), using the parameters presented in Figure 2.5.

$$HB = \frac{2F}{\pi D(D - \sqrt{D^2 - d^2})} \quad (1.5)$$

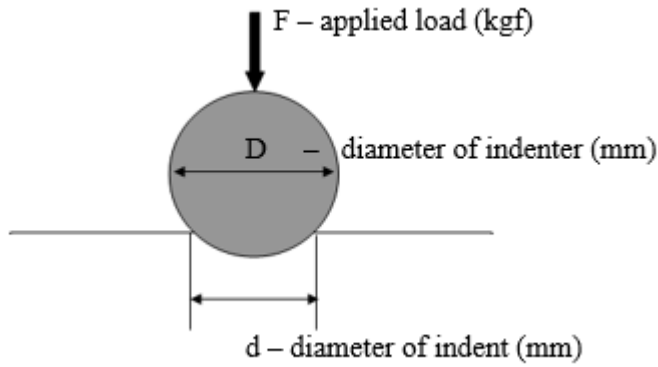


Figure 2.5 Schematic representation of the Brinell hardness testing.

In the notation of the test result, after the hardness value and the abbreviation of the test method (HB for Brinell hardness test) the diameter of the carbide ball in millimeters, the applied force in kilogram and the force application time in seconds are also presented - or denoted (ex. 270 HB 10/300/15).

An example of the test machine can be seen in Figure 2.6.



Figure 2.6 Fasne Optical Brinell Hardness Testing Machine, OPAB – 3000 model.

Vickers hardness test:

This test was created by Robert L. Smith and George E. Sandland at Vickers Ltd in 1921. In this case the indenter has a diamond pyramid shape, with a square base, having an angle of 136 degrees between the opposite faces.

The procedure of the test is similar in many ways to the Brinell hardness test, however one of the main advantages it possesses is that the indenter is kept the same for all materials tested.

The test has to be in accordance with the regulations presented in ISO 6507, for example the indentation has to be located at a distance of 2.5 times the diagonal of the indentation from the edge, and 3 times the diagonal from adjacent indentations.

When calculating the hardness value, the arithmetic mean of the two measured diagonals is used in the formula, inserted in millimeters, while the applied load is introduced as kilogram force, as presented in equation (1.6). The schematic representation of the procedure can be seen in Figure 2.7.

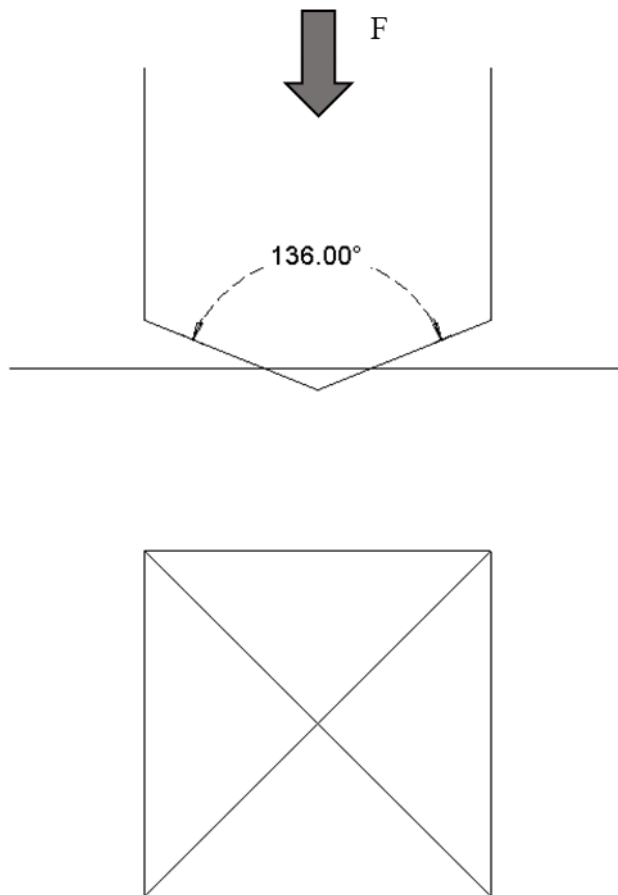


Figure 2.7 Schematic representation of Vickers hardness testing and the indentation left on the material after testing.

$$HV = \frac{2F \sin \frac{136^\circ}{2}}{d^2} \approx 1.854 \frac{F}{d^2} \quad (1.6)$$

The obtained hardness value should be followed by the letters ‘HV’, denoting the used testing method and the value of the applied force (ex. 270 HV/100).

An example of the used testing machine can be seen in Figure 2.8.



Figure 2.8 Jinan precision testing equipment Vickers hardness tester, 200HVS-5 model.

Rockwell hardness test:

This test was developed by Stanley P. Rockwell and is regulated by the ASTM E18 and ISO 6508 standards.

The indentation is produced by either a diamond cone, or a steel ball, having different dimensions and different applied loads depending on the scale on which the test is performed. There are a total of 15 scales, which depend on the material that has to be tested. An initial minor load (F_0) is applied, followed by a major load (F_1). The major load is then removed, while keeping the minor load applied on the material, this way allowing a partial recovery of the indentation. The depth of indentation (e) produced only by the major load is recorded and divided by 0.002 mm. The principle of this hardness test is shown in Figure 2.9. The Rockwell hardness value (HR) is obtained as presented in equation (1.7), by subtracting this value from a constant (E_{HR}), which is 100 units in the case of diamond indenters and 130 for steel ball indenters.

$$HR = E_{HR} - e \quad (1.7)$$

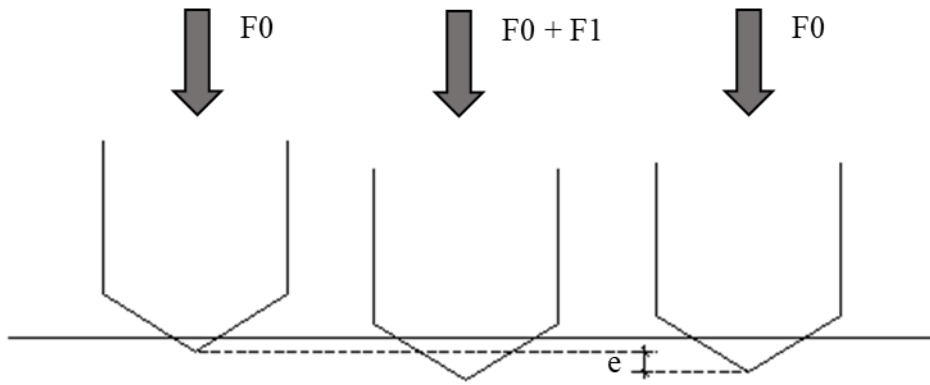


Figure 2.8 Schematic representation of Rockwell hardness testing.

The key advantage of this test compared to the other hardness tests is the test duration, since it only takes a few seconds. However, a basic knowledge of influencing factors is necessary in order to choose the correct scale, which can be considered as a disadvantage.

The hardness value is usually denoted by the obtained value, followed by the letters “HR”, showing that the testing was performed with the Rockwell method and a letter corresponding to the used scale. For example, 70 HRC, if the obtained hardness value is 70 and the chosen scale is C. In the case of regular steel, the scale C is usually chosen.

3 Material Characterisation of Welded Joints

3.1 Introduction (welding)

Welding is the process by which elements can be joined, usually metals, in the process of which due to application of heat or pressure, or both simultaneously the base material is melted locally and then left to cool down naturally. During the welding process filler material may be added, if desired. However, the filler material should have at least equivalent yield strength, ultimate tensile strength, elongation at failure and minimum Charpy V-notch energy value to the one specified for the base material, as stated in Eurocode 3-1-8 (2005).

According to the Oxford Dictionary of Construction, Surveying and Civil Engineering (2012) welding is defined as:

A technique for joining metals in which actual melting of the pieces to be joined occurs in the vicinity of the bond. A filler metal may be used to facilitate the process. In this process both similar and dissimilar metals can be used; several welding techniques exist including arc welding, gas welding, brazing, and soldering.

This joining process is widely used in the construction industry due to the advantages it presents, which include simplicity of execution, a more direct way of stress flow, and the possibility of creating complex cross sectional geometries.

Due to the applied heat, a temperature gradient can be observed in the base material, along the weld zone, which leads to metallurgical changes in the material. This is referred to as the heat affected zone (HAZ) around the weld, in the base material.

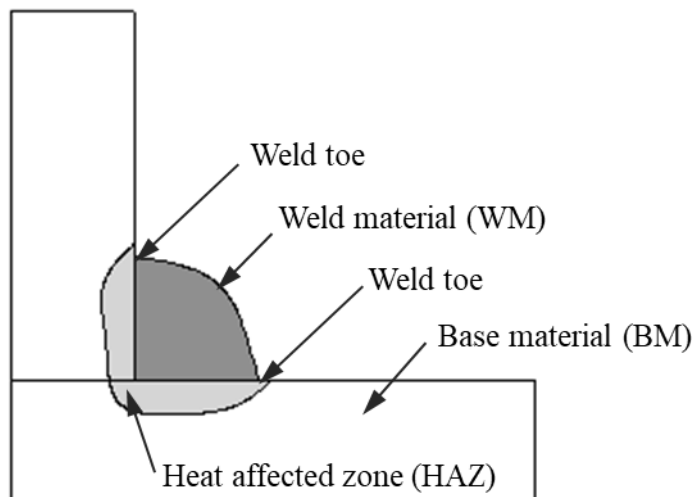


Figure 3.1 Fillet weld, showing the material regions and the location of the weld toe.

Thus in welded joints three different material regions can be differentiated at the weld toe region, as presented in Figure 3.1:

1 - Base material (BM) - Structural steel

2 - Weld material (WM) - Filler material

3 - Heat affected zone (HAZ) due to the welding process. The material properties of the base material around the weld change due to the heat input from the welding process.

In the following subchapters, the material properties of these 3 layers will be analysed.

3.2 Base material (BM) - structural steel (S355-S460)

Structural steel is a steel type used in the construction industry. In the notation of the steel grade, the letter ‘S’ stands for ‘structural’, while the upcoming number marks the minimum yield strength in MPa in the case when the specimen has a smaller thickness than 16 mm (ex. S355).

Until the yield point is reached, the material exhibits elastic behavior, characterized by linear variation between the stress and strain values and described by Hook’s law:

$$\sigma = E \cdot \varepsilon \quad (3.1)$$

The law states that the stress (σ) is equal with the product between the elastic modulus (E) and the strain value (ε).

Beyond this point, the material experiences strain hardening, up to the point of maximum stress. The variation between stress and strain is no longer linear, but can be described by a power law relationship, which states, that the change in one parameter will induce a proportional change in the second parameter. Hallomon proposed such an empirical equation, where the stress (σ) is expressed as a function of plastic strain (ε^p) (Samuel, Rodriguez, 2005):

$$\sigma = K(\varepsilon^p)^n \quad (3.2)$$

, where K is the strain hardening coefficient and n is the strain hardening exponent. These constants can be identified from a log-log plot of experimental true stress and true strain curve, as shown in Figure 3.2. If the strain hardening exponent (n) is equal to 0, the described material is considered perfectly plastic solid, whereas a value of 1 would indicate an elastic solid material.

Ludwik’s equation is a modification of equation (3.2), which includes the yield stress (σ_y) (Samuel, Rodriguez, 2005):

$$\sigma = \sigma_y + K(\varepsilon^p)^n \quad (3.3)$$

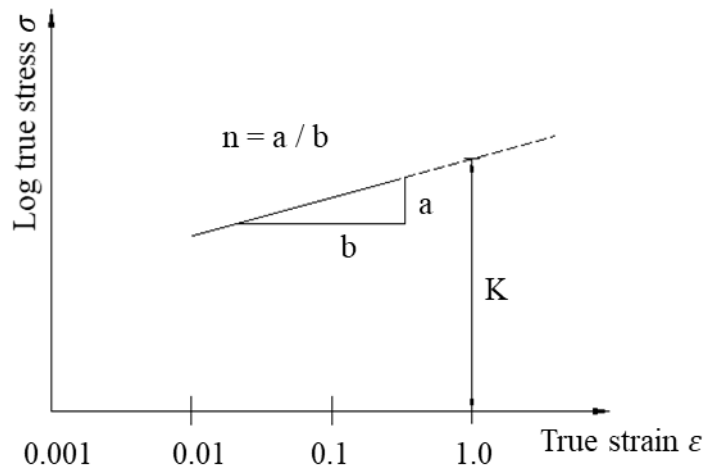


Figure 3.2 Log/log plot of true stress-strain curve.

Concerning the chemical composition of steel, it is composed of iron mixed with other alloying elements, like carbon and manganese. Some of the alloying elements are due to the steelmaking process, while other chemical elements are added deliberately to modify the material properties of the steel, as desired. For example, carbon increases the tensile strength and the hardness of steel (Brockenbrough, Merritt, 1999).

The following material properties of steel, can be considered as constant, regardless the steel type (Domone, Illston, 2010):

Modulus of elasticity, $E = 205 \text{ GPa}$

Shear modulus, $G = 80 \text{ GPa}$

Poisson's ratio, $\nu = 0.3$

Coefficient of thermal expansion $= 12 \times 10^{-6} / \text{C}^\circ$

The chemical composition, yield strength, tensile strength and minimum elongation of the most common structural steel grades are listed in the Table 3.1 (Domone, Illston, 2010). The data corresponds to flat, long, hot-rolled test specimens, having a thickness of maximum 16 mm.

CEV stand for 'Carbon Equivalent Value' and shows the sensitivity of the material to rupture due to the heating and cooling experienced by the material, when welded. It is calculated, using the percentage of alloying elements in the formula:

$$CEV = C + Mn/6 + (Cr + Mo + V)/5 + (Ni + Cu)/15 \quad (3.4)$$

Table 3.1 Material properties of common hot-rolled structural steel grades, after Domone and Illston (2010).

Grade	Min yield strength (MPa)	Tensile strength (MPa)	Min elong. at fracture (%)	Chemical composition limit (max %)							
				C	Si	Mn	P	S	N	Cu	CEV
S235	235	360-510	26	0.19		1.5	0.04	0.04	0.014	0.6	0.35
S275	275	410-560	23	0.21		1.6	0.04	0.04	0.014	0.6	0.40
S355	355	470-630	22	0.23	0.6	1.7	0.04	0.04	0.014	0.6	0.47
S450	450	550-720	17	0.23	0.6	1.8	0.04	0.04	0.027	0.6	0.49

Microscopically, steel is characterized by a crystal structure, which crystallizes cubically. Two patterns can be observed, regarding the emplacement of iron atoms: cubic system with centered volume (CC crystals) and cubic system with centered faces (FCC crystals) as presented in Figure 3.3 (Lemaitre, Chaboche, 1990).

The first one is characterized by the fact that the iron atoms are located in the corners of the cube and in its center, while in the second case the iron atoms are located in the corners and in the middle of each face.

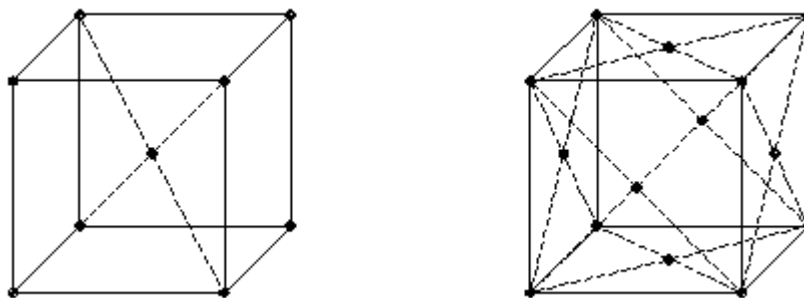


Figure 3.3 CC crystal (left) and FCC crystal (right).

Electromagnetic forces are acting between electrons of neighbouring atoms, keeping the atom structures together.

The material properties and crystalline structure of steel can change due to temperature changes, and carbon percentage. In the case of structural steel, with carbon content less than 0.8 % and at normal temperature, the crystals appear in a cubic network with centered volume. It is composed of alpha iron, also called ferrite and small regions of pearlite, located at grain boundaries. By uniting several monocrystals with random orientation a polycrystal is formed, also referred to as a crystal lattice. Since steel is a ductile material, certain defects are present in the crystal lattice, which induce the plastic deformation of the material beyond the yield limit (Lemaitre, Chaboche, 1990).

3.3 Weld material (WM)

The welding material is typically chosen according to the base material that needs to be welded. This is because the weld material has to have similar or better properties than the base material, as mentioned before and stated in Eurocode 3.

Easterling (1992) gives a good overview of the changes that occur in the weld material, induced by the welding process as well as the transformations due to the cooling period. In order to understand and be able to characterize the material properties, all the various contributions that affect the final composition of the weld deposit has to be taken into account and analyzed. A simplified portrayal of the different contributions can be seen in Figure 3.4 in the case of fusion welding.

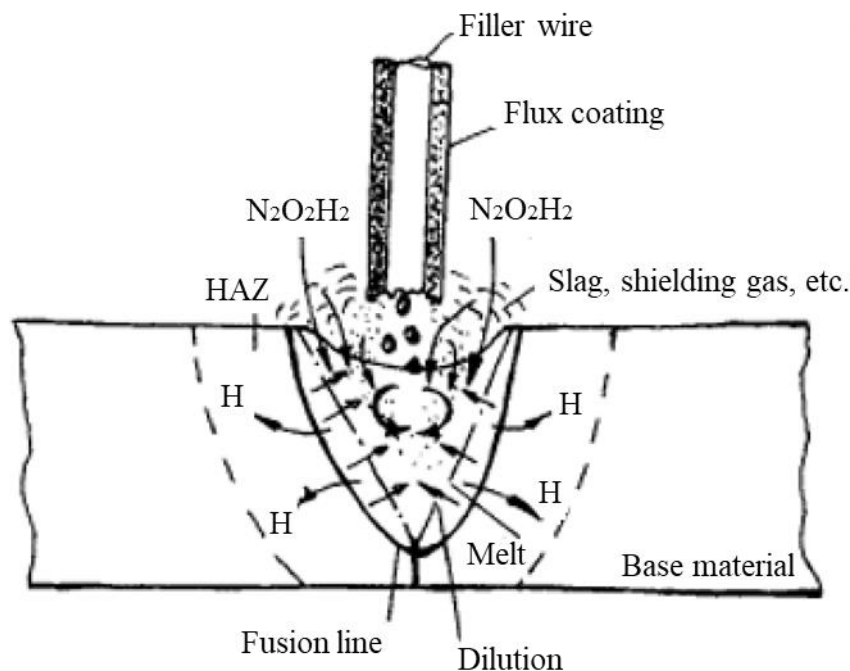


Figure 3.4 Fusion weld composition contributions, after Easterling (1992).

The chosen welding process has an influence on the weld metal composition, for example in the case of fusion welding, the basicity of the flux is of great importance. This can be expressed by the ratio between sum of basic oxides and sum of acid oxides, and it ranges usually between 0.5 and 3. According to Easterling (1992), the effect of the inclusion content is important, since the increase of the inclusion content will decrease the toughness of the weld material. More so, certain welding processes use inert shielding gases in order to protect the welding. During these welding processes, elements from the gases have the tendency to enter the weld material. Other contributions may arise from the ambient air and from the base material to be welded.

The toughness of the weld is also effected by the speed of welding. If the welding speed is increased, the orientation of crystal growth must change in order to maintain continuity, which increases the risk of segregation at the weld center line and decreases the toughness of the weld.

Due to the high heat input of the welding process, the weld becomes liquid, thus a solidification process occurs, which can be divided in three stages, epitaxial, cellular and dendritic. During epitaxial solidification, the preliminary crystal size is governed by the grain growth zone of the base metal. Thus welding processes that cause large grain growth in the heat affected zone, like submerged arc welding will also lead to large initial crystal size of the weld metal. As a result, to the solidification process, the weld material develops a cellular-dendritic structure. This is characterised by coarse columnar austenitic grains and a fine cellular network inside the grains.

Additional changes in the microstructure appear during the cooling period, from solidification temperature to ambient temperature. However, these changes are dependent on the cooling rate. With a slow cooling rate, the obtained microstructure is a mixture of ferrite and pearlite. Medium-slow cooling rate yields either Widmanstätten side plates or acicular ferrite microstructures, whereas medium-high cooling rate creates periodic pearlite microstructure. All of the above mentioned microstructures are presented in Figure 3.5.

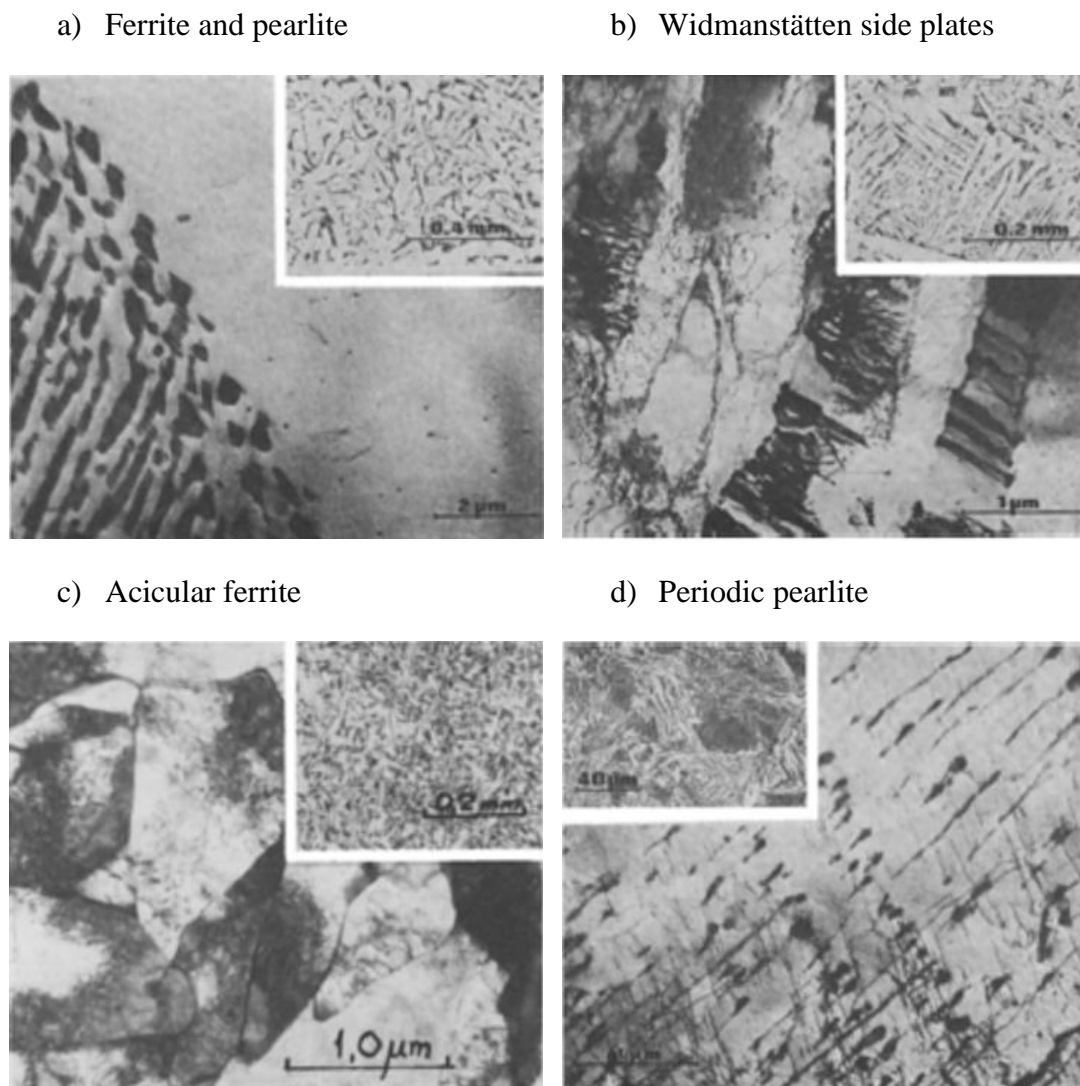
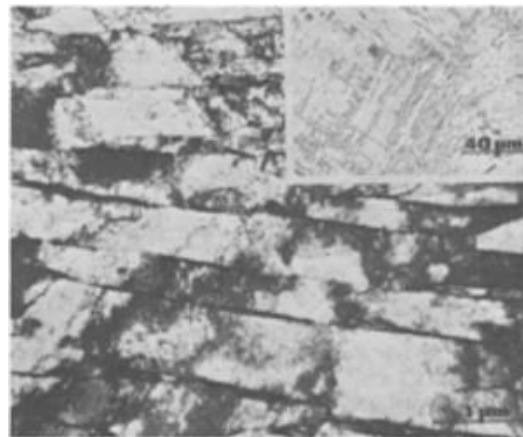
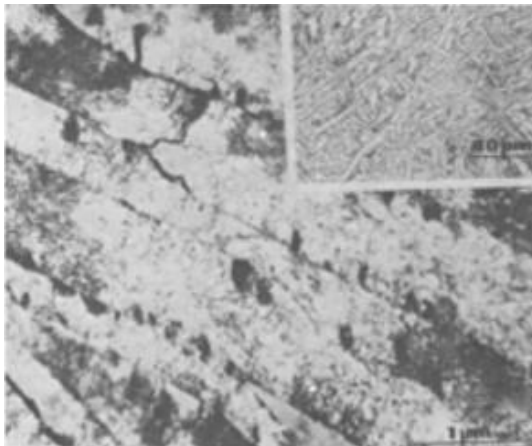


Figure 3.5 Transmission electron micrographs showing microstructures observed after cooling in weld metals, after Easterling (1992).

Upper bainite plus cementite as well as upper bainite and retained austenite microstructures occur in the case of fast cooling, see Figure 3.6 a) and b). In the case of very fast cooling lower bainite can form. However, if the time is not sufficient for carbon diffusion, lath martensite will form instead.

a) Upper bainite plus cementite

b) Upper bainite and retained austenite



c) Lower bainite

d) Lath martensite

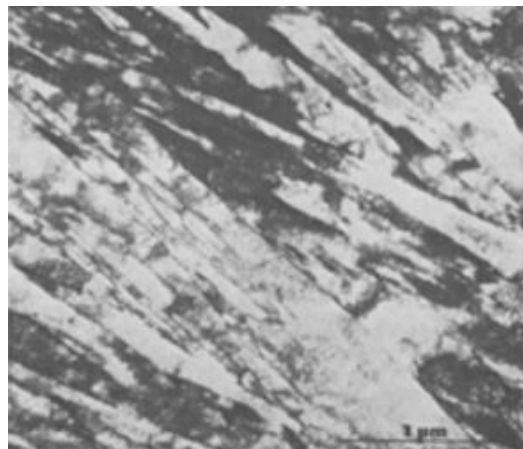
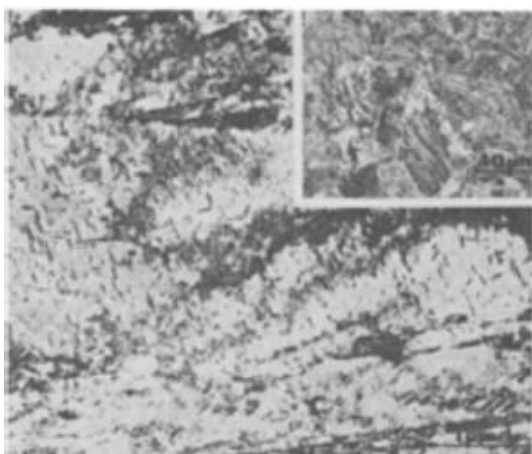


Figure 3.6 Transmission electron micrographs showing microstructures observed after cooling in weld metals, after Easterling (1992).

The influence of carbon percentage in the welding material is a good example concerning the role of alloying elements in the microstructure transformation of the weld material. Thus by increasing the carbon percentage, the bainitic and the martensitic fields get wider concerning the CCT (continuous cooling time) curve of the material.

In Figure 3.7 below, the influencing factors and their effect are marked with arrows, showing the tendency of modifying the transformation fields of the CCT curve to longer or shorter transformation time periods.

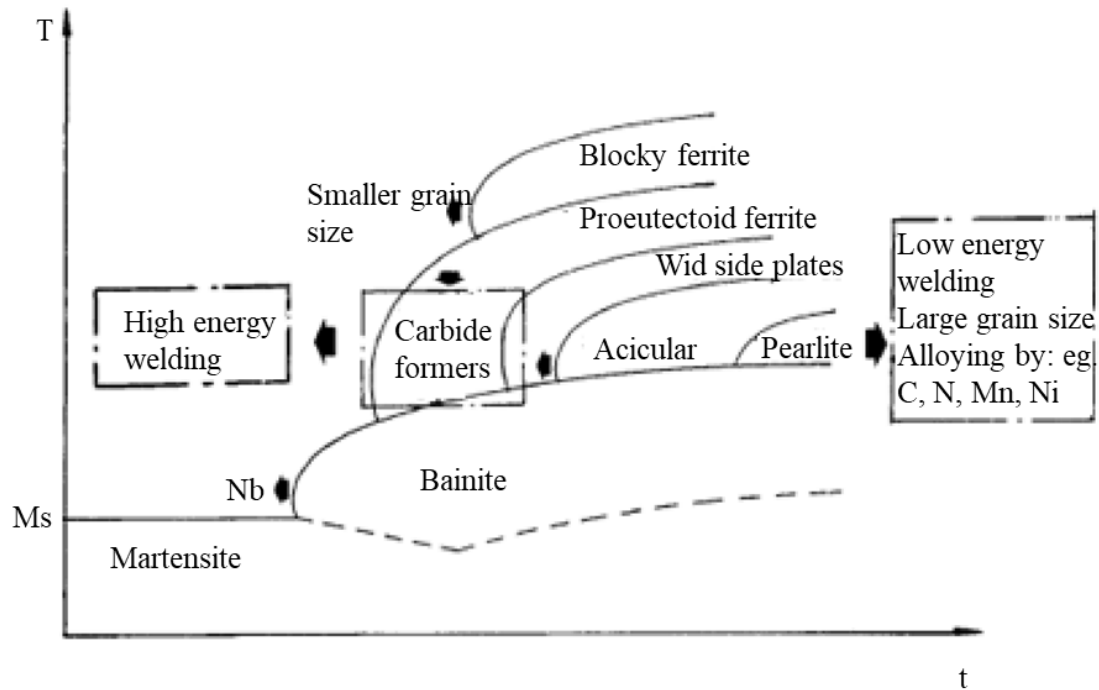


Figure 3.7 CCT diagram for steel weld material, after Easterling (1992).

3.4 Heat affected zone (HAZ)

The applied heat on the base material due to welding process introduces metallurgical changes in the material close to the weld, which have an influence on its mechanical properties, while also introducing tensile residual stresses (Phillips D. H., 2016). Some of the observed changes include grain growth, recrystallization, phase transformation, annealing and tempering. There are two phase transformations taking place during cooling, one from $\delta - FE$ to $\gamma - FE$, followed by a transformation from $\gamma - FE$ to $\alpha - FE$ (Boumerzoug et al., 2010).

The iron-carbon equilibrium diagram can be seen in Fig 3.8, which shows the phase transformations of steel, depending on the applied heat and carbon percentage of the material. It should be noted, that this diagram applies only in the case of slow cooling, since the equilibrium is not kept in the case of fast cooling (Brockenbrough, Merritt, 1999).

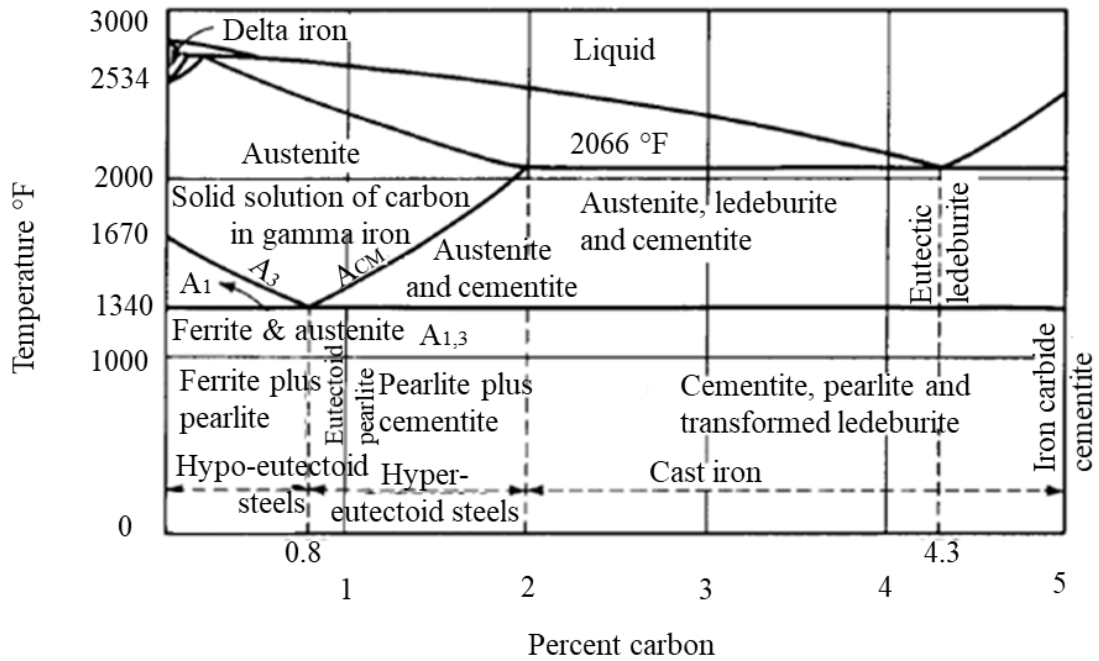


Figure 3.8 Iron-carbon equilibrium diagram, after Brockenbrough and Merritt (1999).

Since a temperature gradient is observed in the HAZ, it is understandable that it can be divided in subzones, depending on the temperature and metallurgical changes that take place under the temperature of that specific subzone. The temperature is the highest right at the fusion line, next to the weld and it decreases gradually as the distance from the weld increases, until it reaches the temperature of the BM. Figure 3.9 presents the partitioning of the HAZ.

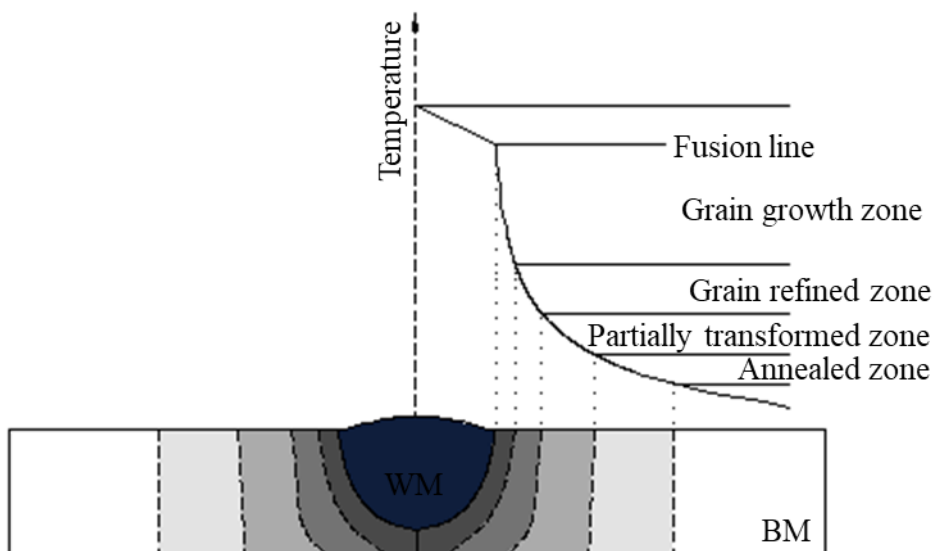


Figure 3.9 Different subzones of the heat affected zone (HAZ), after Barzin (2015) and Easterling (1992).

In the zone with the highest temperature, significant increase in grain size, compared to the base material grain size, can be observed. This zone is called the grain growth zone and it has a temperature range of approximately 1200 – 1500 °C. If the steel material has a higher CEV value (approximately 0.4), then the formation of martensite is more likely, which would also indicate a higher hardness value in this region (Easterling, 1992).

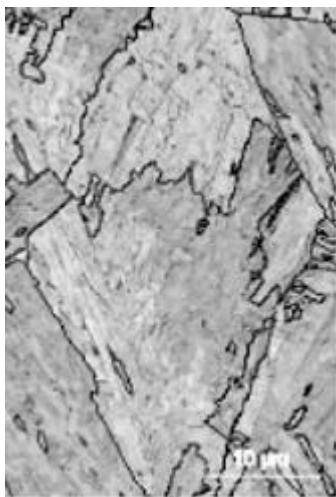
The grain refined zone is delimited in the temperature range of 900 – 1200 °C. This zone is characterised by fine grained ferrite – pearlite structure, which is produced during cooling.

In the temperature range of 650 – 900 °C the produced structure depends highly on the cooling rate and it is called the partially transformed zone. Possible developed structures are: pearlite, upper bainite, autotempered martensite or high carbon martensite.

Below 650 °C, in the annealed zone, there is no change in the microstructure of the material. However, dynamic strain ageing can take place, due to the heating cycle and residual stresses produced by the welding process. This will lead to locking the position of dislocations, increasing the brittleness of the material.

Figure 3.10 presents image quality maps of the heat affected zone and the base material, provided by Mikkola (2016). It shows significant grain size difference between the two regions.

a) HAZ



b) BM

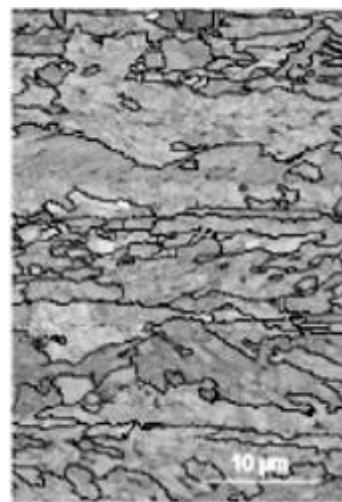
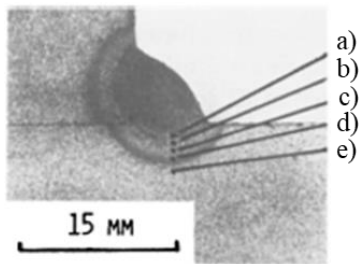
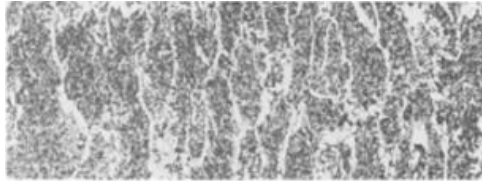


Figure 3.10 Image quality maps of the heat affected zone (HAZ) and the base material (BM), from Mikkola (2016).

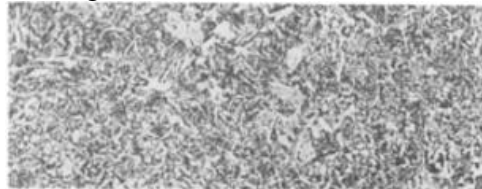
A more detailed analysis of the zones located in the HAZ was performed by Easterling (1992), by presenting optical micrographs on all of the zones and the BM as reference. These can be seen in Figure 3.11, showing clear differences in the microstructure of the zones.



a) Fusion zone



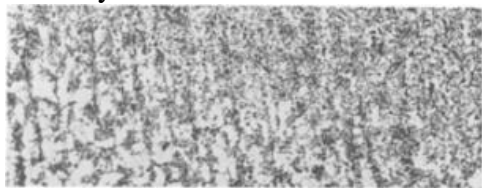
b) Grain growth zone



c) Grain refined zone



d) Partially transformed zone



e) Unchanged base material (BM)

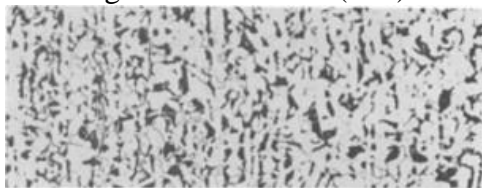


Figure 3.11 Optical micrographs of various zones in HAZ, from Easterling (1992).

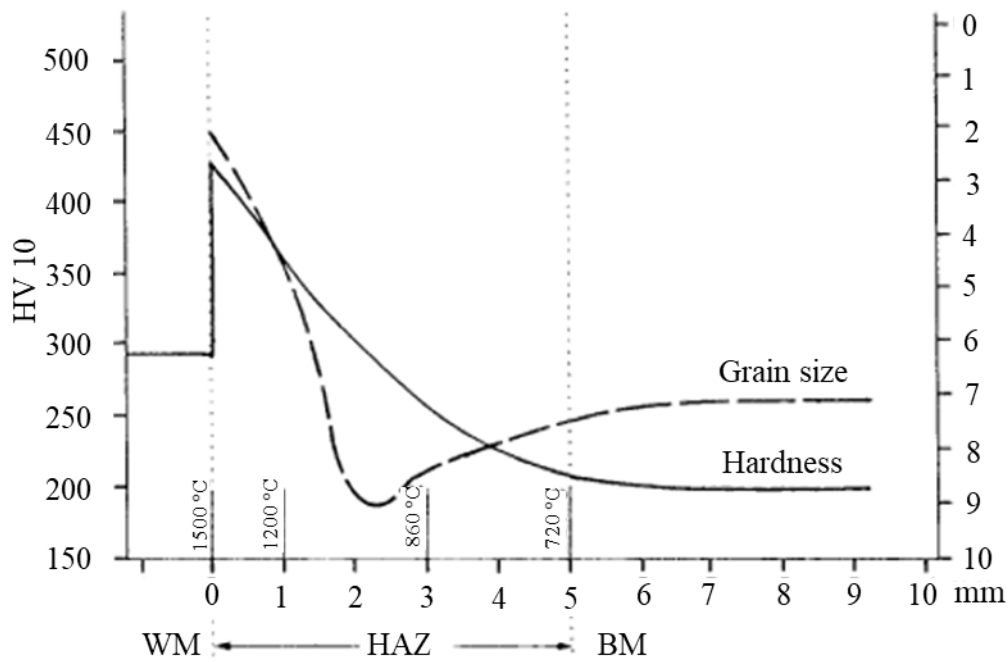


Figure 3.12 Vickers hardness values along the HAZ of structural steel, from Easterling (1992).

In Figure 3.12 it can be seen that the zone with maximum hardness value coincides with the zone with maximum grain size, close to the fusion line Easterling (1992).

The cooling rate is dependent on the welding process, the ambient temperature and the geometry of the welded joint. Thus it is possible to plot the maximum hardness close to the fusion line taking into account different cooling rates, of different welding processes. The relation between hardness value and cooling rate is presented in Figure 3.13 (Easterling, 1992).

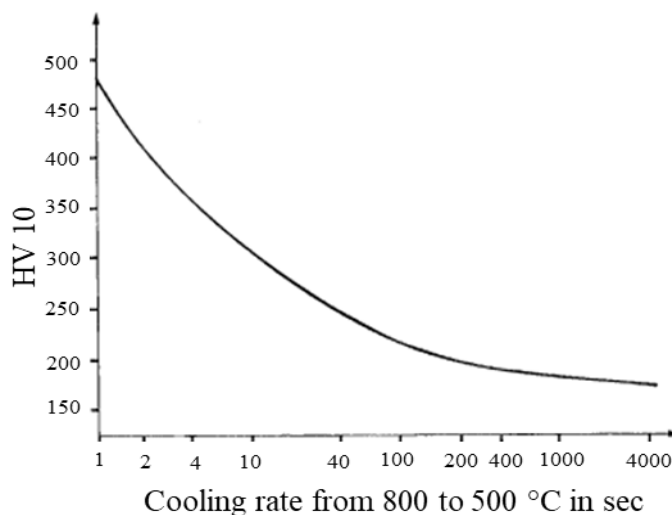


Figure 3.13 Mean vickers hardness values along the HAZ of medium strength 20 mm thick C-Mn steel based on several different welding processes, adapted from Easterling (1992).

4 High Frequency Mechanical Impact Treatment

4.1 Introduction

The fatigue strength of a welded joint is decreased because of three main reasons, namely the stress concentration due to geometry changes, the tensile residual stresses introduced by the welding process and the defects of the weld, like undercuts or porosity, which shorten the crack initiation period or in some cases even eliminates it altogether.

In order to increase the fatigue strength of welded joints, a number of post-weld treatment (PWT) methods were developed and divided in two categories, weld geometry improvement methods and residual stress improvement methods. An overview of existing improvement methods is presented in Figure 4.1 below.

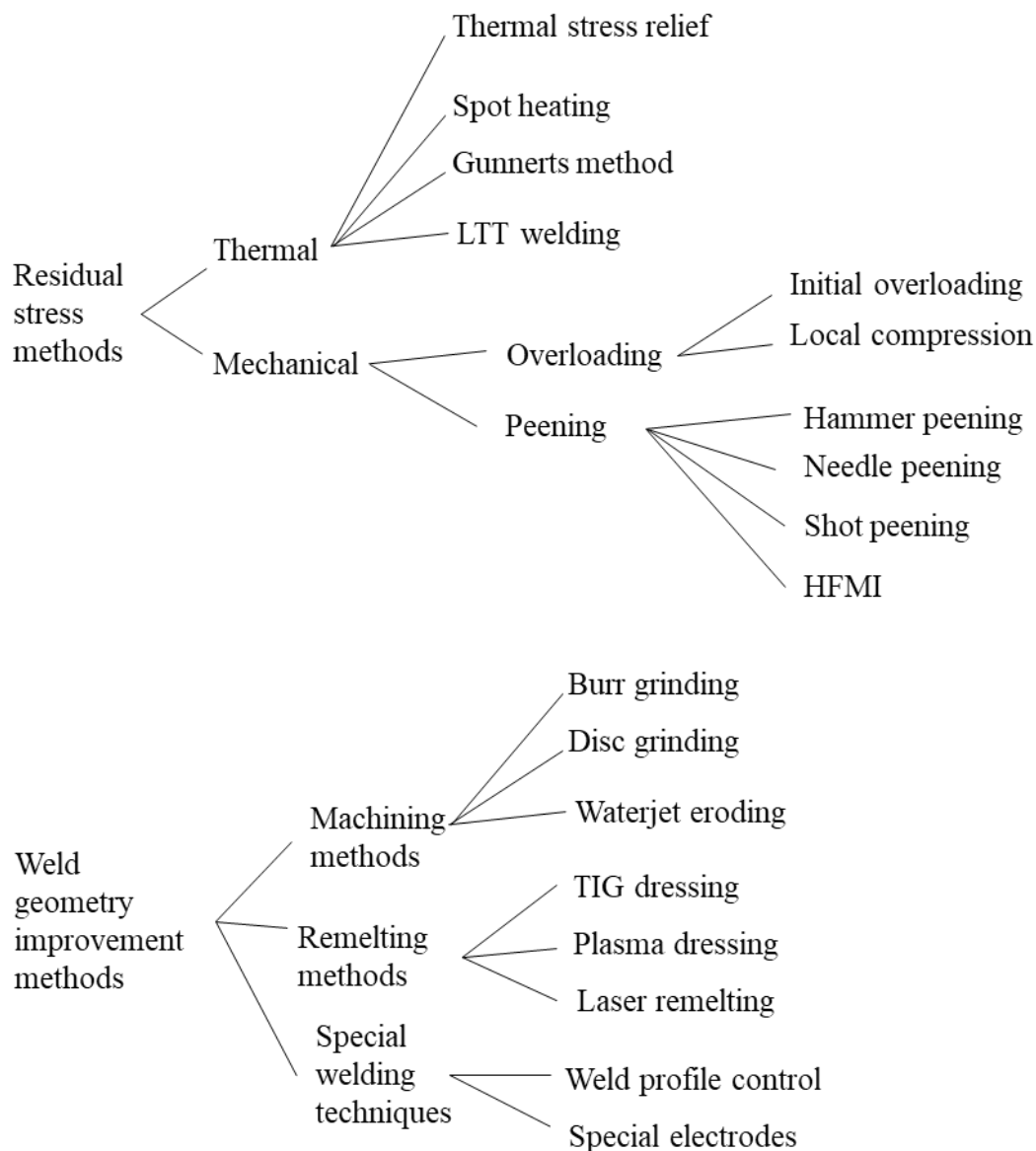


Figure 4.1 Overview of weld improvement techniques, adapted from Marquis and Barsoum (2016).

Some methods concentrate solely on geometry improvement, or the introduction of compressive residual stresses into the material, while others offer a combination of beneficial effects, which act together in order to increase the fatigue strength. Table 4.1 offers an overview of the manner in which certain methods are improving the overall performance of the welded joint.

Table 4.1 *Weld improvement methods and their effects, after Marquis and Barsoum (2016).*

Method	Geometry improvement	Introduce compressive residual stresses
Grinding	x	-
TIG-remelting	x	-
Shot peening (blasting)	-	x
Hammer/needle peening	x	x
HFMI	x	x

Since the different methods have different ways of enhancing the fatigue strength, it is understandable that some will have greater influence on the global behaviour of the joint than others. Figure 4.2 displays a comparison between PWT methods, with respect to their effect on the fatigue life of the joint.

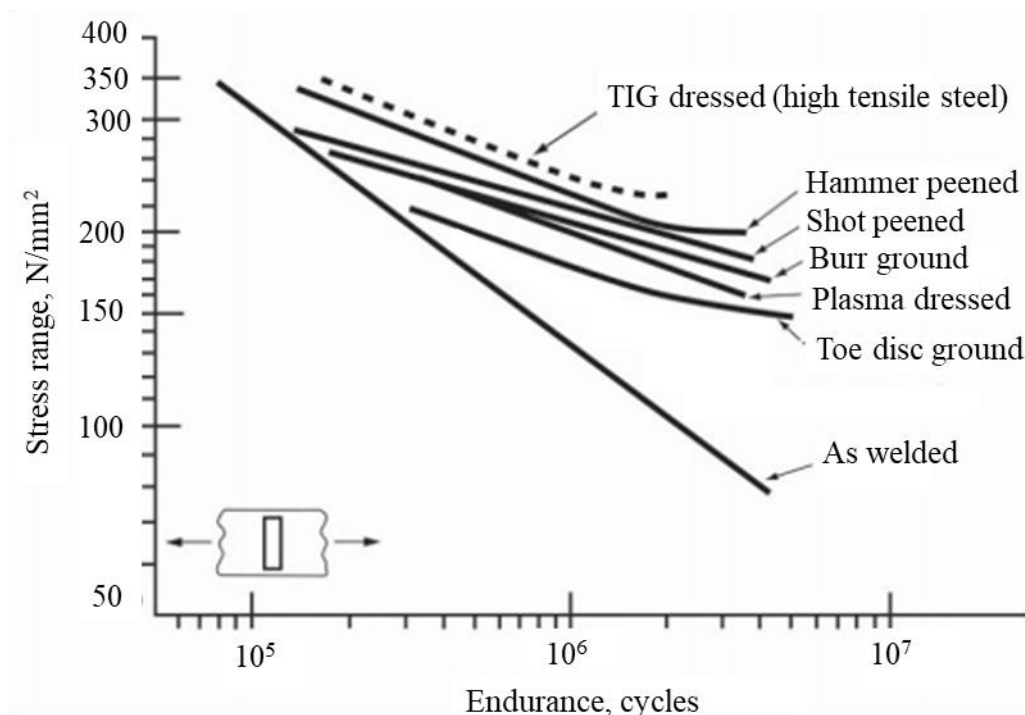


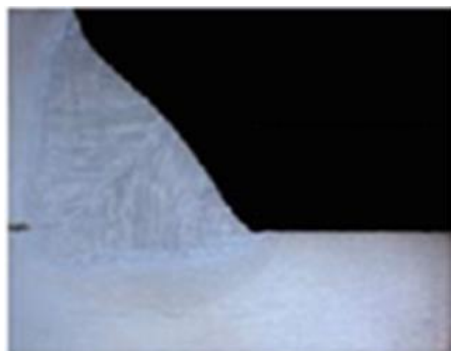
Figure 4.2 *Effect of weld improvement techniques, adapted from Johnson and ProcessBarron (-).*

In the current chapter the focus is set on one of the residual stress improvement methods, more exactly the high frequency mechanical impact treatment (HFMI), also referred to in relevant literature as ultrasonic peening treatment (UPT), pneumatic impact treatment (PIT) or high frequency impact treatment (HiFiT). It is regarded as having similar improvement capability as hammer peening or needle peening (Marquis, Barsoum, 2016).

4.2 HFMI treatment process

The high frequency mechanical impact (HFMI) treatment method is classified as a mechanical, residual stress method, belonging to the peening methods subcategory (see Figure 4.3). As the name suggests, the method is based on mechanical impact of a cylindrical indenter, using high frequency, of approximately 90 Hz. It has three main improvement effects, the insertion of compressive residual stresses, the reduction of stress concentrations by improving the weld toe geometry, and strain hardening of the material at the treatment surface. The treatment is applied to the weld toe, since it is considered a critical region, because of the stress concentration induced by sudden change in geometry. Thus the method will have a significant effect on all three material layers located in this region, namely the WM, the HAZ and BM.

a) As-welded state



b) After HFMI treatment



Figure 4.3 Weld toe profile before and after HFMI treatment, from Marquis and Barsoum (2016).

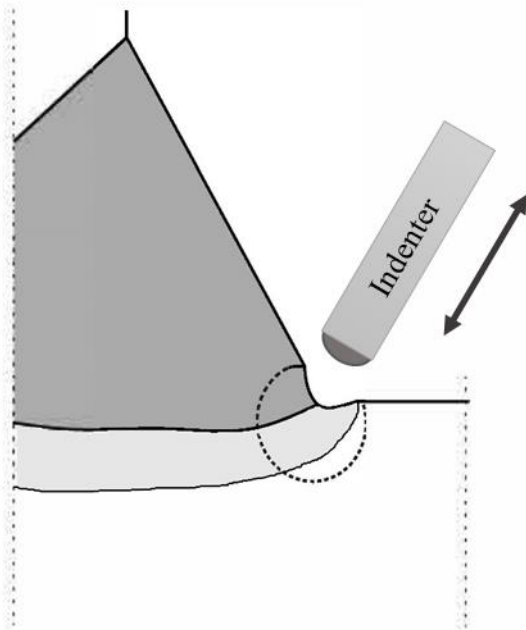


Figure 4.4 HFMI treatment process.

Schematic illustration of the HFMI treatment process can be seen in Figure 4.4. The areas that are affected by the treatment are presented in Figure 4.5. The red arrows, from the same figure, mark the extent of the strain hardening effect.

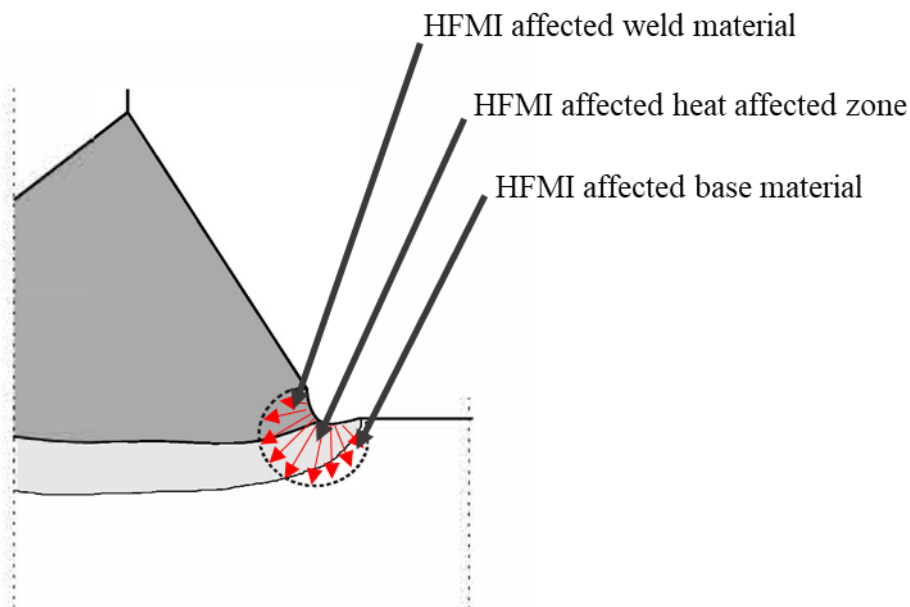


Figure 4.5 Areas affected by the HFMI treatment.

Various HFMI machines were developed during the last decade, which led to a large variety of indenter configurations. The machine is composed by two parts, a power unit and a tool with a high strength steel cylinder indenters.

Before applying HFMI treatment on the weld toe region, the area has to be cleaned from any traces of slag, oxide or other foreign materials. Grinding should be avoided, since it could reduce the visibility of the weld toe.

The International Institute of Welding (IIW) defines the typical values of the HFMI groove geometry as ranging between 0.2 and 0.6 mm considering the depth and between 2 and 5 mm for the width. In a study conducted by Ghahremani et al. (2014), regarding the quality assurance of HFMI treated welded steel, it was found that average between the depth of treatment in the base material (D_b) and weld material (D_w) has to be between 0.25 and 0.5 mm, anything above this value is considered as over-treated and anything below this value is considered as under-treated. These measurements are represented schematically in Figure 4.6.

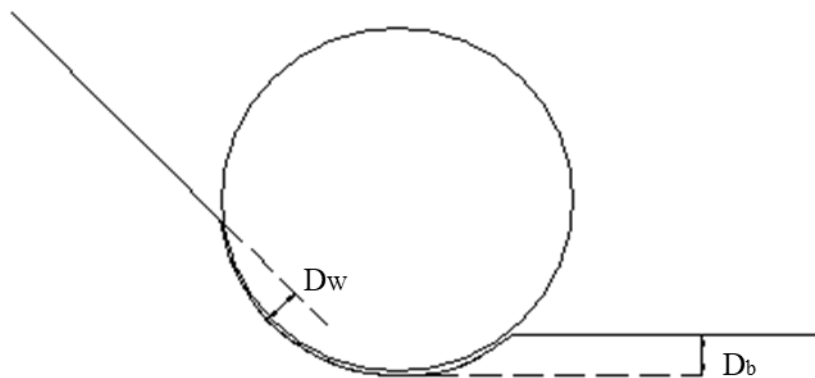


Figure 4.6 Measurements of the HFMI treatment.

It should be noted, that this treatment method is appropriate for joints that are likely to develop weld toe cracks. In the case of other welded joint types, where the occurrence of root cracking is expected, the improvement of the fatigue life is limited and special measures should be taken, as using full penetration welds or increasing the weld throat.

4.2.1 Treatment defects

If the treatment procedure is performed correctly, a smooth and shiny HFMI groove is created along the weld toe region. However, certain defects may appear, which are easily detectable during surface inspection. A dark crack-like line may appear in the HFMI groove, if the contact area between indenter and treated surface is inadequate or if the chosen indenter is inadequate. The schematic representation of this defect is presented in Figure 4.7 and a real life example of this type of defect is observable in Figure 4.8 below.

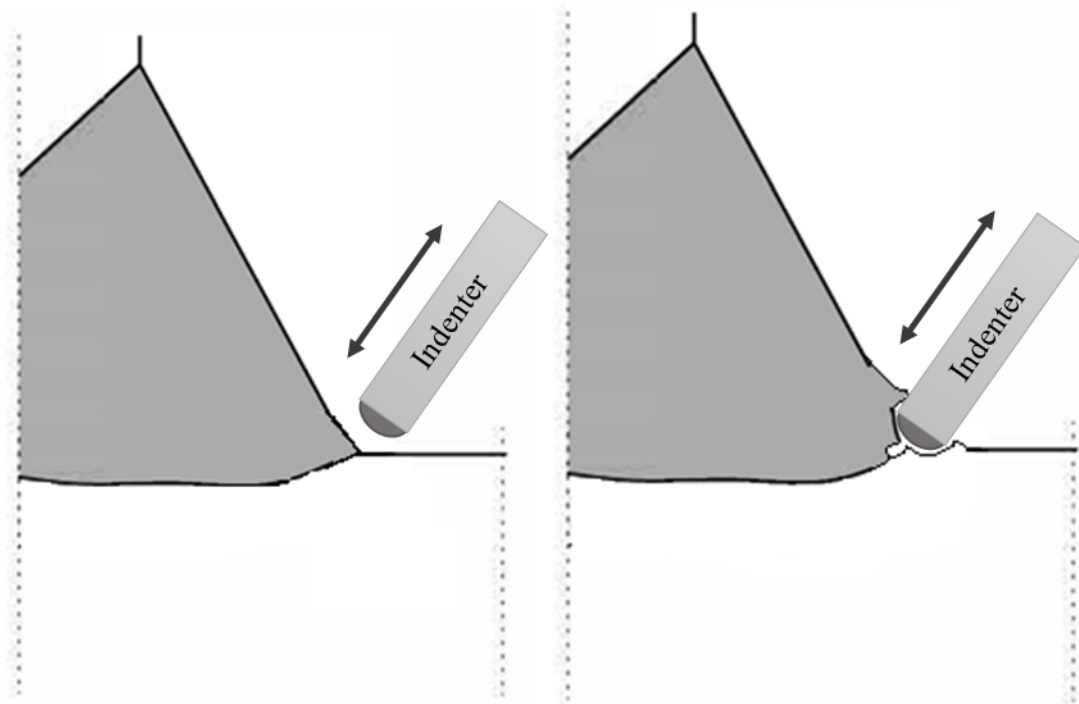


Figure 4.7 Potential crack like defect due to treatment carried out with a steep angle of the indenter or too large indenter, after Marquis and Barsoum (2016).

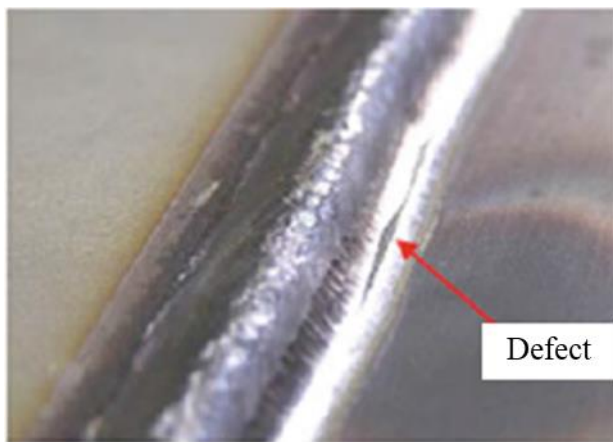


Figure 4.8 Example of improperly treated weld toe, from Marquis and Barsoum (2016).

Defects can appear in the case of under-treatment as well, implying that the number of applied passes are insufficient and the indenter strikes are observable along the treated surface. However, this defect is easily fixable by additional passes with the HFMI device. Figure 4.9 shows an example of under-treated weld toe with the individual indenter strikes still visible, adapted from Marquis and Barsoum (2016).

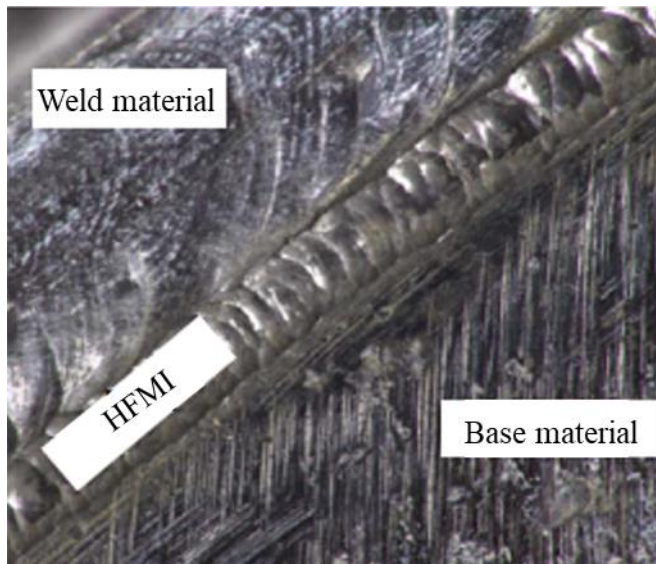


Figure 4.9 Example of under-treated weld toe, from Marquis and Barsoum (2016).

Another common defect is due to the cold working of the material, which induces plastic deformations. In this situation, a crack-like line may appear if a specific point is over treated. The schematic representation of a proper HFMI groove and one having a crack-like line is presented in Figure 4.10.

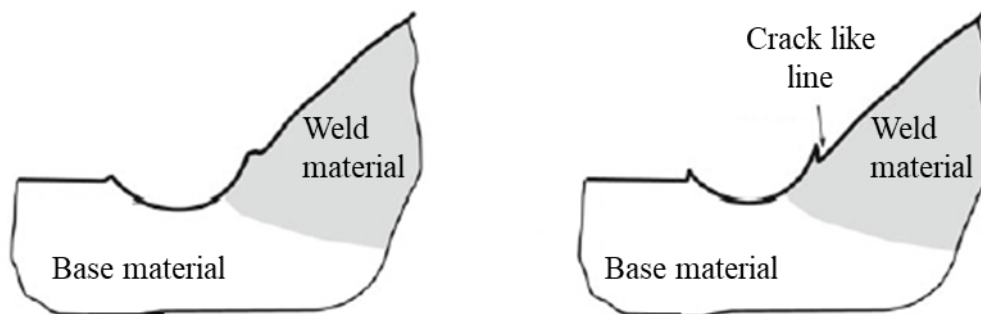


Figure 4.10 Proper HFMI groove (left) and HFMI groove having crack-like lines (right), from Marquis and Barsoum (2016).

4.3 Consequences of HFMI treatment

As mentioned in Chapter 3, the welding process produces tensile residual stresses in the metal, which have a negative influence on the fatigue life of the joint. However, these tensile residual stresses are counteracted by the compressive residual stresses resulted by the HFMI treatment.

Local stress concentrations appear when there is a sudden change in the geometry, as in the case of a weld toe. As a result of the HFMI treatment, the weld-toe region deforms plastically, creating a smooth transition between the weld and the base material, this way reducing the stress concentration at the weld toe.

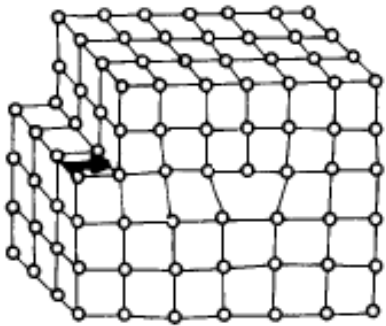
During the treatment process, the material undergoes strain hardening, thus increase in the local yield strength, hardness and fatigue strength is expected.

The most significant microstructural change induced by the HFMI treatment, is the decrease in average grain size. However, according to Mikkola (2016) this reduction occurs only in one direction, resulting in the elongation of the grains.

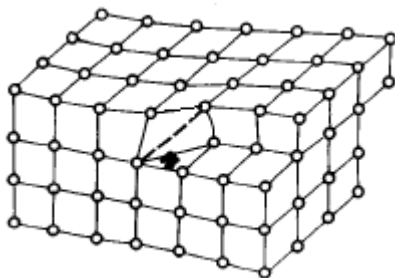
5 Plasticity Models

Ductile materials, like structural steel, exhibit large irreversible, plastic deformations, if they experience stresses beyond their yield strength. The crystal structure rearranges and due to shear stresses acting on the material, a slip displacement occurs, which leads to permanent strains. The plastic deformation is possible due to defects in the crystal lattice, like edge dislocation, screw dislocation or dislocation loop, which are presented in Figure 5.1 (Lemaitre, Chaboche, 1990).

a) Edge dislocation



b) Screw dislocation



c) Dislocation loop

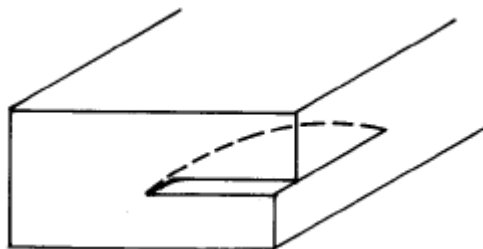


Figure 5.1 Defects in the crystal lattice, from Lemaitre and Chaboche, (1990).

5.1 Yield condition

The yielding strength of a material in a uniaxial stress state is easily determined by uniaxial testing. However, generally a structure experiences a multiaxial stress state, characterized by a stress tensor, having six stress components.

$$\sigma = \begin{bmatrix} \sigma_{xx} & \sigma_{xy} & \sigma_{xz} \\ \sigma_{xy} & \sigma_{yy} & \sigma_{yz} \\ \sigma_{xz} & \sigma_{yz} & \sigma_{zz} \end{bmatrix} = \begin{bmatrix} \sigma_x & \tau_{xy} & \tau_{xz} \\ \tau_{xy} & \sigma_y & \tau_{yz} \\ \tau_{xz} & \tau_{yz} & \sigma_z \end{bmatrix} \quad (5.1)$$

The yield condition relates the multiaxial stress state with the uniaxial one, in order to determine if the combined effect of the stress components induce yielding of the material or not. In other words, it determines the stress state, at which yielding starts.

It is represented by a yield surface in the stress state coordinate system delimiting the elastic region from the plastic region (Ottosen, Ristinmaa, 2005). Every point in the coordinate system marks a stress state. The stress states located inside the yield surface, induces elastic deformations in the material. Thus it can also be used, as a limit considering the state of stress in structures, if elastic analysis of the structure is desired.

The most commonly used yield criterion in the case of metals is the Tresca and the von Mises, the former being implemented in the finite element method (FEM) software, Abaqus.

5.1.1 The von Mises yield criterion

The general formula, of the equivalent von Mises stress, taking into account all the stress components is (Krenk, Høgsberg, 2013):

$$\sigma_e = \sqrt{\frac{1}{2} \left[(\sigma_{xx} - \sigma_{yy})^2 + (\sigma_{xx} - \sigma_{zz})^2 + (\sigma_{yy} - \sigma_{zz})^2 + 6(\sigma_{yz}^2 + \sigma_{xz}^2 + \sigma_{xy}^2) \right]} \quad (5.2)$$

Expressed in principal stresses, the formula can be rewritten as:

$$\sigma_e = \sqrt{\frac{1}{2} \left[(\sigma_x - \sigma_y)^2 + (\sigma_x - \sigma_z)^2 + (\sigma_y - \sigma_z)^2 \right]} \quad (5.3)$$

Yielding occurs, when the equivalent stress is equal to the yield strength (σ_Y), obtained by uniaxial testing. Thus the von Mises yield condition can be written in terms of the equivalent stress and the uniaxial yield strength (Ottosen, Ristinmaa, 2005):

$$\sigma_e = \sigma_Y \quad (5.4)$$

$$\sqrt{\frac{1}{2} \left[(\sigma_x - \sigma_y)^2 + (\sigma_x - \sigma_z)^2 + (\sigma_y - \sigma_z)^2 \right]} - \sigma_Y = 0 \quad (5.5)$$

$$(\sigma_x - \sigma_y)^2 + (\sigma_x - \sigma_z)^2 + (\sigma_y - \sigma_z)^2 = 2\sigma_Y^2 \quad (5.6)$$

By plotting the equation (5.6) in 3D principal stress space, the von Mises yield surface is obtained, in the form of a cylinder, aligned with the $\sigma_1 = \sigma_2 = \sigma_3$ axis (see Figure 5.2). Any stress state located inside the above defined cylinder is inducing elastic behaviour in the material. Stress states directly on the surface of the cylinder leads to yielding of the material (Krenk, Høgsberg, 2013). The Von Mises cylinder is graphically represented in Figure 5.2.

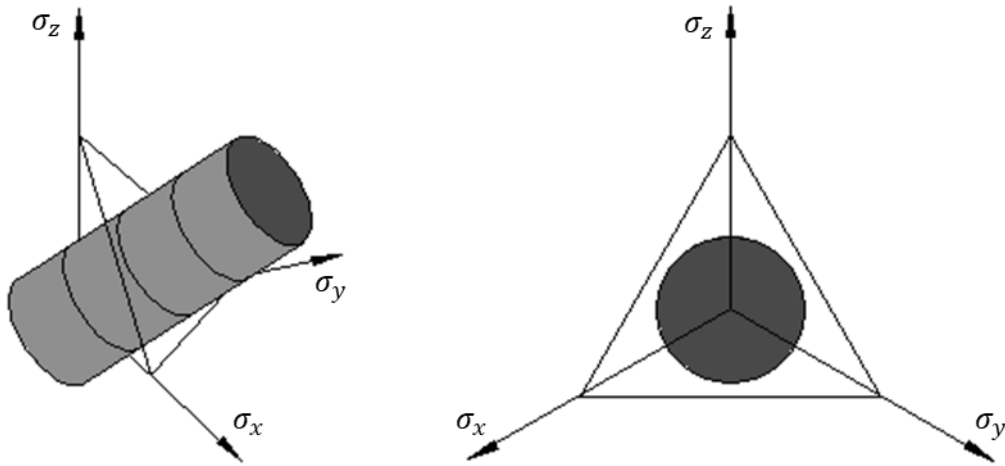


Figure 5.2 Von Mises stress cylinder in principal stress space, after Krenk and Høgsberg (2013).

5.1.2 The Tresca criterion

According to the Tresca criterion, the material is yielding, when the maximum shear stress is greater than a characteristic stress value, which is regarded as half of the yield stress (σ_Y) (Krenk, Høgsberg, 2013. Ottosen, Ristinmaa, 2005).

The maximum shear stress is defined as the radius of the Mohr's circle, expressed as half of the difference between the maximum and minimum principal stress. Thus the general expression for the Tresca yield criterion can be written as:

$$2\tau_{\max} = \sigma_{\max} - \sigma_{\min} = \sigma_Y \quad (5.7)$$

According to Krenk and Høgsberg (2013), the Tresca yield surface can be obtained in a simple way by considering three situations in the $\sigma_x\sigma_y$ - plane, when $\sigma_z = 0$.

Therefore, when σ_x and σ_y are of different signs, the yield equation will be:

$$2\tau_{\max} = |\sigma_x - \sigma_y| = \sigma_Y \quad (5.8)$$

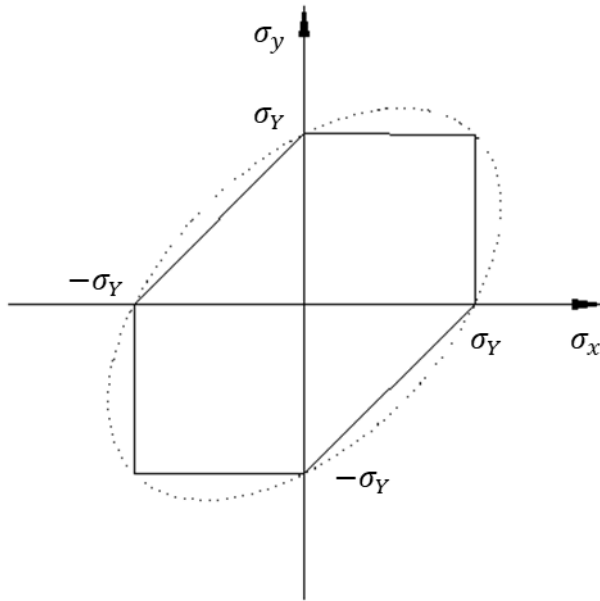


Figure 5.3 Tresca stress polygon in plane stress, after Krenk and Høgsberg (2013).

Equation (5.8) will mark the inclined lines of the yield surface trace in the $\sigma_x\sigma_y$ - plane, as shown in Figure 5.3. The horizontal and vertical lines are provided by the case, when σ_x and σ_y have the same sign, the yield criterion being defined by the largest stress.

$$2\tau_{\max} = |\sigma_x - 0| = \sigma_Y \quad (5.9)$$

$$2\tau_{\max} = |\sigma_y - 0| = \sigma_Y \quad (5.10)$$

As seen in Figure 5.4, the Tresca yield surface has the shape of a hexagon, which is inscribed in the von Mises ellipse, having the same intersections with the axes. Thus for stress states located in the apexes of the hexagon, the two yield conditions, predict the same yield limit. However in some cases, the Tresca criterion predicts lower yield stresses with up to 13.4%, compared to those predicted by the von Mises (Ottosen, Ristinmaa, 2005).

In the 3D principal stress space, the Tresca yield surface will have the shape of a hexagonal prism, aligned with the $\sigma_1 = \sigma_2 = \sigma_3$ axis.

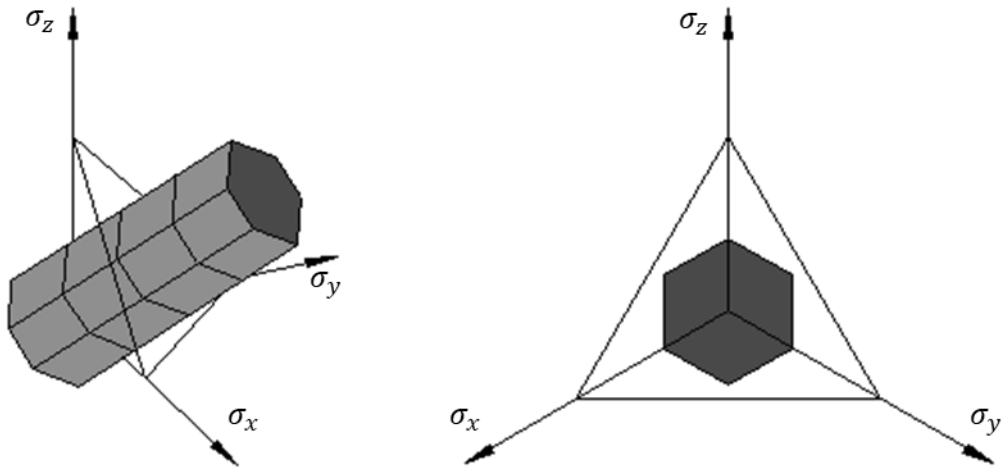


Figure 5.4 Tresca stress surface in principal stress space, after Krenk and Høgsberg (2013).

A study conducted by Taylor and Quinney (1931), comparing the von Mises yield condition and Tresca yield condition to experimental results is presented by Ottosen and Ristinmaa (2005) and Chakrabarty (2006). The experiment was realized considering copper, aluminium and mild steel thin walled tubes subjected to combined tension and torsion. The study clearly showed, that the von Mises yield condition has a better concordance with the experimental results, than the Tresca yield condition. This comparison can be seen in Figure 5.5.

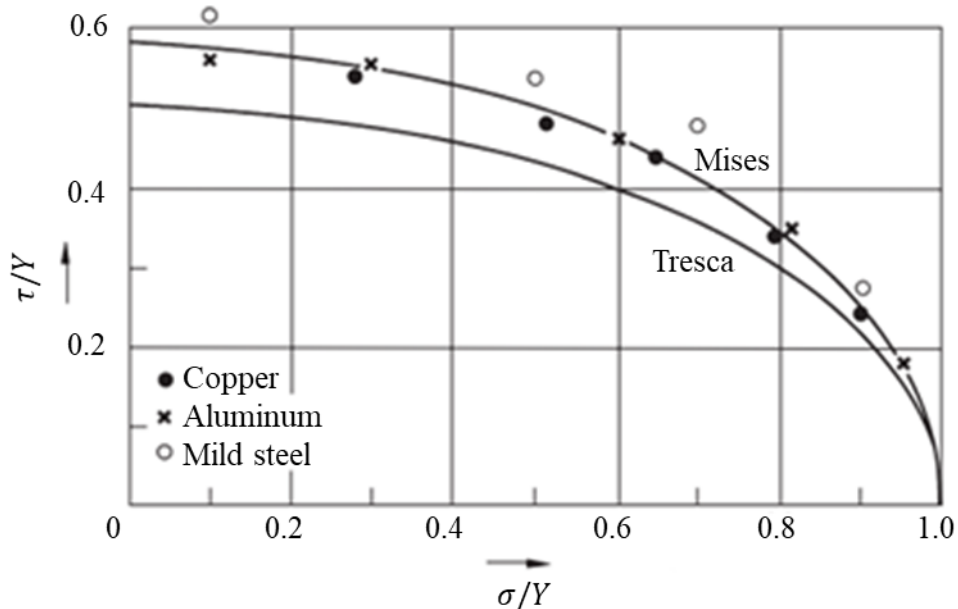


Figure 5.5 Tresca and Mises ellipses on the (σ, τ) plane together with the experimental results of Taylor and Quinney, from Chakrabarty (2006).

5.1.3 The Hill criterion

The Hill criterion is an extension of the von Mises yield condition, which is used to model anisotropic plasticity. It can be expressed with the following formula (Lemaitre, Chaboche, 1990):

$$F(\sigma_x - \sigma_y)^2 + G(\sigma_y - \sigma_z)^2 + H(\sigma_x - \sigma_z)^2 + 2L\sigma_{xy}^2 + 2M\sigma_{yz}^2 + 2N\sigma_{xz}^2 = 1 \quad (5.11)$$

where the parameters F, G, H, L, M and N are scalar numbers representing the state of anisotropic hardening. These can be determined from pure tension and pure shear tests.

An example concerning Hill criterion can be observed in Figure 5.6.

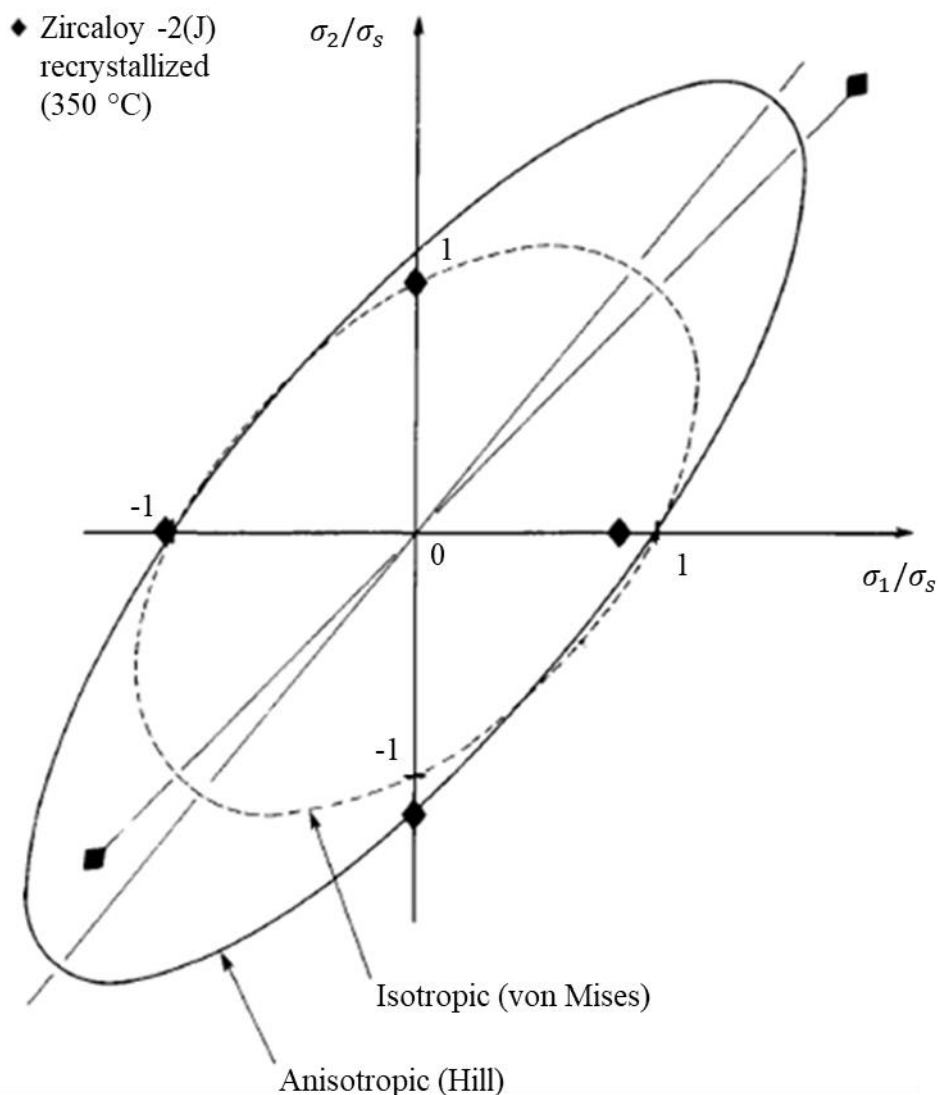


Figure 5.6 Example of plastically anisotropic material, Hill criterion, from Lemaitre and Chaboche (1990).

In the FEM software, Abaqus, Hill's yield criterion can be introduced in the sub option 'Potential', by defining the stress ratios (equation (5.12)), between the given stress and

the reference yield stress (σ_Y), which was defined using Mises plasticity (Abaqus Analysis User's Guide, 2013).

$$R_{ij} = \frac{\bar{\sigma}_{ij}}{\sigma_Y} \quad (5.12)$$

5.2 Hardening rules - overview

According to Ottosen and Ristinmaa (2005), the hardening rule is defined as the rule governing the way in which the yield surface modifies as a consequence of plastic loading, since the yield stress generally changes its value according to the plastic deformation.

In the case of perfectly plastic materials, the yield surface stays the same during loading, thus keeping its initial yield strength even after the yield stress is reached. However, when the material shows signs of strain hardening, as in the case of structural steel, at stresses above the initial yield stress, the yield surface changes as guided by the chosen hardening rule (Araújo, 2002).

Three types of hardening rules may come into effect after plasticity takes place: isotropic, kinematic or a combination of these two. Over the years, a large number of models were developed in order to simulate the different hardening rules, making it possible to include various effects that may appear. Table 5.1. offers an overview of the different hardening models and their validity concerning the inclusion of certain phenomena, which were observed during experiments.

Table 5.1 *Hardening rules and their validity, after Lemaitre and Chaboche (1990).*

Models	Monotonic hardening	Bauschinger effect	Cyclic hardening / softening	Ratcheting effect
Isotropic	x	-	x	-
Linear kinematic	x	x	-	-
Multilinear kinematic	x	x	x	-
Nonlinear kinematic	x	x	-	x
Mixed (isotropic + kinematic)	x	x	x	x

Monotonic hardening appears, when the material is subjected to static loading. This can be simulated by all of the above presented hardening rules. However, these are significantly different, when we consider effects due to cyclic loading.

A so called, Bauschinger effect, is observable, when tensile loading is followed by compressive loading. According to which, the yield stress in compression is much lower than the maximum reached stress in tension. Thus the yield stress in compression is inversely proportional to the yield stress increase in tension. This phenomenon is presented in Figure 5.7.

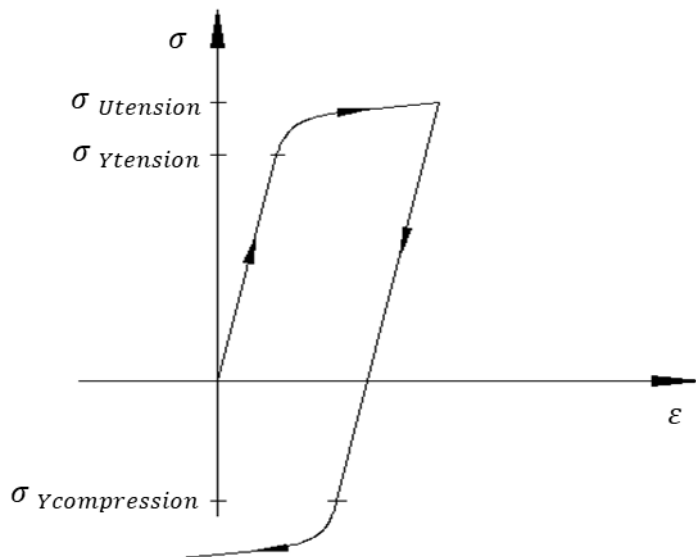


Figure 5.7 Bauschinger effect, after Ottosen and Ristinmaa (2005).

Depending on the analyzed material, either cyclic hardening or cyclic softening can be detected, when subjected to cycling between fixed and symmetrical strain or stress values. This phenomenon, is depicted in Figure 5.8 and 5.9.

a) Cyclic hardening

b) Cyclic softening

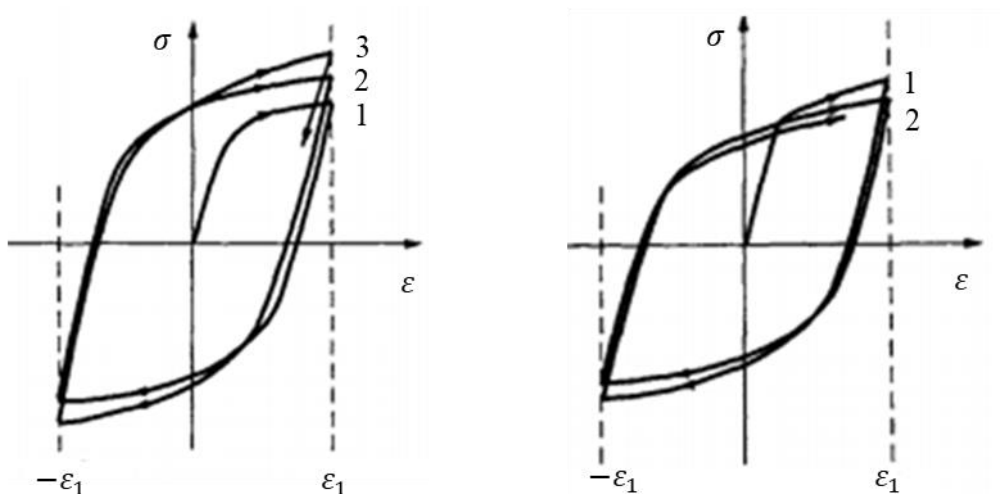
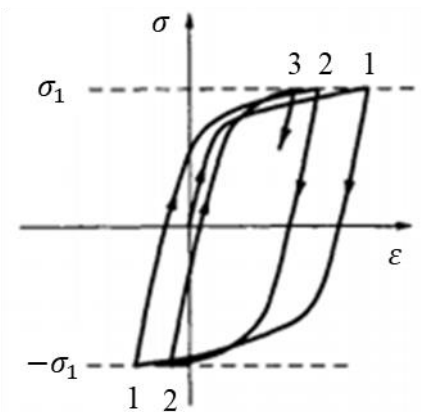


Figure 5.8 Strain cycling between $\pm \epsilon_1$, after Ottosen and Ristinmaa (2005).

a) Cyclic hardening



b) Cyclic softening

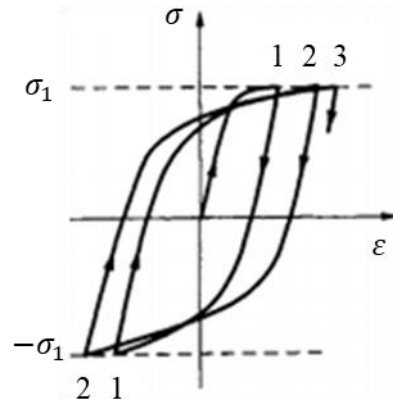


Figure 5.9 Stress cycling between , after Ottosen and Ristinmaa (2005).

If the cycling is performed between fixed stress values, which are not symmetrical about zero, the observed phenomenon is called ratcheting effect. This is characterized by a strain increase, after each cycle, if the mean stress is positive, as shown in Figure 5.10.

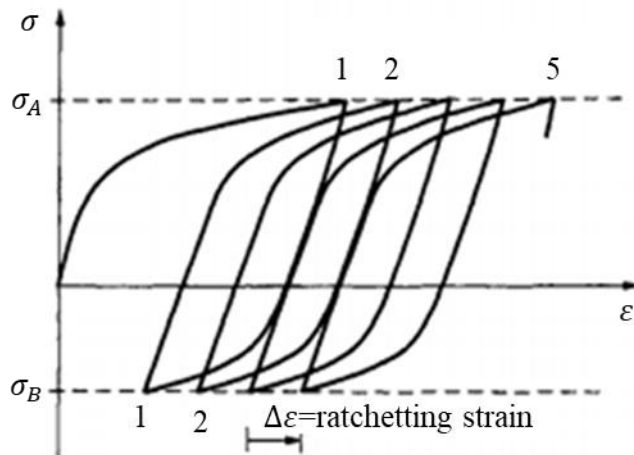


Figure 5.10 Stress cycling between unsymmetric stress values with ratcheting, after Ottosen and Ristinmaa (2005).

When modeling the plastic behavior of the material in a FEM software, special attention should be accorded to the input stress-strain data. The regularly used engineering stress-strain data is no longer adequate input data, thus the true stress vs. logarithmic plastic strain data must be provided. These can be calculated using the engineering stress-strain values. Until twice the yielding strain, the true stress and true plastic strain values are equal to the engineering values. Between this point and the point when necking initializes, the following formula can be used:

$$\sigma_{true} = \sigma(1 + \epsilon) \tag{5.13}$$

$$\varepsilon_{true}^p = \ln(1 + \varepsilon^p) = \ln\left[1 + \left(\varepsilon - \frac{\sigma}{E}\right)\right] \quad (5.14)$$

Figure 5.11 shows the difference between engineering stress-strain curve and true stress and true strain curve.

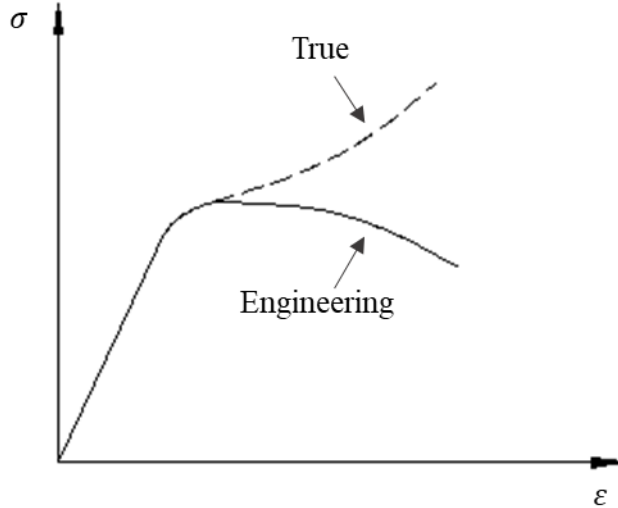


Figure 5.11 Engineering stress-strain curve and true stress-strain curve.

In the current chapter the focus is fixed on plasticity models that can be implemented in the FEM software Abaqus.

5.3 Isotropic hardening

Isotropic hardening is characterised by a uniform increase or decrease of the yield surface, while sustaining its centre point in the same position throughout the change, as well as maintaining its initial shape. Depending on the exhibited behaviour, in the case of softening, the yield surface shrinks in size, while during hardening, it expands. The rate of expansion is governed by the increase of equivalent plastic strain during loading or the dissipated plastic work.

The isotropic hardening of a yield function can be generally expressed as (Ottosen and Ristinmaa, 2005):

$$f(\sigma_{ij}, K_\alpha) = F(\sigma_{ij}) - K = 0 \quad (5.15)$$

$$K_\alpha = \{K\} \quad (5.16)$$

, where $F(\sigma_{ij})$ is the initial yield surface. K_α represents the hardening parameter, in the form of K , as a function of equivalent plastic strain (ε_{eff}^p), which increases with the increase of plastic strain.

The effective plastic strain can be calculated as presented in equation (5.17), where $\dot{\varepsilon}_{ij}^p$ stands for plastic strain rate (Ottosen and Ristinmaa, 2005).

$$\dot{\varepsilon}_{eff}^p = \sqrt{\frac{2}{3} \dot{\varepsilon}_{ij}^p \dot{\varepsilon}_{ij}^p} \quad (5.17)$$

In the case of von Mises yielding criterion, experiencing isotropic hardening, equation (5.18.) can be rewritten as:

$$f(\sigma_{ij}, K_\alpha) = \sqrt{\frac{1}{2} [(\sigma_x - \sigma_y)^2 + (\sigma_x - \sigma_z)^2 + (\sigma_y - \sigma_z)^2]} - \sigma_Y - K = 0 \quad (5.18)$$

The yield surface translation in isotropic hardening is depicted in Figure 5.12.

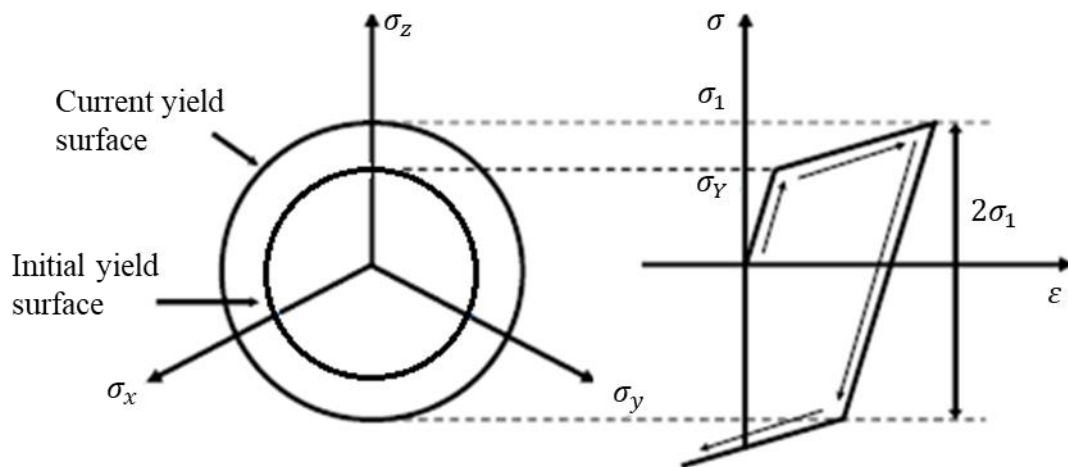


Figure 5.12 Yield surface translation in isotropic hardening, after Ottosen and Ristinmaa (2005).

This hardening model is most commonly used in the case of modelling large strains or proportional loading. It cannot describe cyclic behaviour of the material on its own, thus in case of cyclic loading it is usually combined with the kinematic hardening model.

According to the isotropic hardening rule, when the material experiences tensile loading, followed by compressive loading, the yielding stress in compression will be equal to the highest stress reached during the tensile loading. Meaning, that the isotropic hardening model of the von Mises criterion leads to equal yield stresses in compression as in tension, this being in contradiction with experimental results carried out on steel, concerning the Bauschinger effect (Ottosen and Ristinmaa, 2005).

5.3.1 Johnson-Cook isotropic hardening

It is considered a type of isotropic hardening, which utilizes an analytical function. The equation is composed of three parts, taking into account the equivalent plastic strain,

strain rate and thermal softening. It is most often used in the case of modelling high-strain-rate deformation (Abaqus Analysis User's Guide, 2013).

According to Johnson-Cook hardening, the yield stress has the following equation (Johnson and Cook, 1983):

$$\sigma_Y^{J-C} = \left[A + B(\varepsilon_{eff}^p)^n \right] \left[1 + C \ln \left(\frac{\dot{\varepsilon}_{eff}^p}{\dot{\varepsilon}_0} \right) \right] (1 - \hat{T}^m) \quad (5.19)$$

, where A is a constant, equal to the yield stress, B and n are constants representing strain hardening and C is the strain rate constant. The exponent m is the thermal softening constant and \hat{T} is the homologous temperature, defined as in equation (5.20). In order to determine the homologous temperature, the reference temperature (T_r), the melting temperature (T_m) and the current temperature (T) has to be defined (Dorogoy and Rittel, 2009).

$$\hat{T} = \begin{cases} 0 & \text{for } T < T_r \\ \frac{T - T_r}{T_m - T} & \text{for } T_r < T < T_m \\ 1 & \text{for } T > T_m \end{cases} \quad (5.20)$$

The constants can be obtained by using a least square method curve fitting of the experimental data.

5.4 Kinematic hardening

Considering the kinematic hardening rule, the yield surface will not change its size or shape after the occurrence of plasticity, but it translates in the direction of yielding.

The kinematic hardening of a yield function can be generally expressed as (Ottosen and Ristinmaa, 2005):

$$f(\sigma_{ij}, K_\alpha) = F(\sigma_{ij} - \alpha_{ij}) = 0 \quad (5.21)$$

The translation is induced by the tensor α_{ij} , also referred to as back-stress, which marks the centre of the von Mises surface in the stress space and has an initial value of 0. Thus in the case of von Mises yield criteria, the generalised formula becomes:

$$f(\sigma_{ij}, K_\alpha) = \left[\frac{3}{2} (s_{ij} - \alpha_{ij}^d)(s_{ij} - \alpha_{ij}^d) \right]^{1/2} - \sigma_Y = 0 \quad (5.22)$$

$$K_\alpha = \{\alpha_{ij}^d\} \quad (5.23)$$

, where K_α is the hardening parameter, in the form of the deviatoric back-stress (α_{ij}^d) and s_{ij} is the deviatoric stress tensor.

$$s_{ij} = \begin{bmatrix} s_x & s_{xy} & s_{xz} \\ s_{xy} & s_y & s_{yz} \\ s_{xz} & s_{yz} & s_z \end{bmatrix} = \begin{bmatrix} (\sigma_x - \sigma_0) & \tau_{xy} & \tau_{xz} \\ \tau_{xy} & (\sigma_y - \sigma_0) & \tau_{yz} \\ \tau_{xz} & \tau_{yz} & (\sigma_z - \sigma_0) \end{bmatrix} \quad (5.24)$$

$$\sigma_0 = \frac{\sigma_x + \sigma_y + \sigma_z}{3} \quad (5.25)$$

The yield surface translation in kinematic hardening is depicted in Figure 5.13.

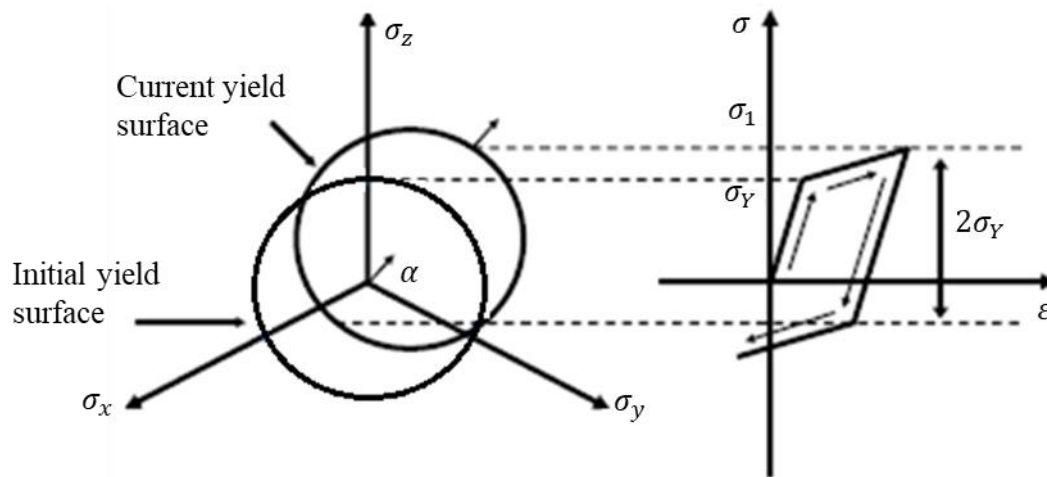


Figure 5.13 Yield surface translation in kinematic hardening, after Ottosen and Ristinmaa (2005).

In order to approximate the Bauschinger effect, in the case of tensile loading followed by compressive loading, the yield stress in compression is decreased with the same amount as the tensile yield stress is increased. Leading to a constant difference between the two yield stresses of two times the initial yield stress in tension (σ_Y).

The kinematic hardening models can be divided into three main groups: linear kinematic, multilinear kinematic and nonlinear kinematic hardening models, a few of which being presented in the current sub-chapter.

Table 5.2 presents an overview of the availability of certain kinematic hardening models in a few finite element analysis software (Halama, Sedlák and Šofer, 2012).

Table 5.2 Availability of kinematic hardening models in certain FE software, after Halama, Sedláč and Šofer, (2012).

Kinematic hardening	Ansys 13	Abaqus	MSC.Marc	MSC.Nastran
Bilinear	x	x	x	x
Multilinear	x	-	-	-
Armstrong-Frederick	x	x	x	x
Chaboche	x	x	-	-

5.4.1 Bi-linear kinematic hardening (Melan-Prager)

This is the simplest kinematic hardening model, which assumes that the back-stress varies linearly with the plastic strain.

The back-stress expressed by the Melan-Prager's evolution law (Ottosen and Ristinmaa, 2005):

$$\dot{\alpha}_{ij} = c \dot{\epsilon}_{ij}^p \quad (5.26)$$

, where $\dot{\epsilon}_{ij}^p$ denotes the plastic strain rate and c is the constant material parameter, obtained from uniaxial stress-strain curve, equal with two-thirds of the plastic modulus H . The interpretation of the plastic modulus is presented in Figure 5.14.

$$c = \frac{2}{3} H \quad (5.27)$$

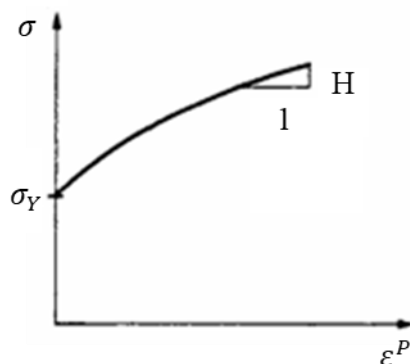


Figure 5.14 Interpretation of plastic modulus H , from Ottosen and Ristinmaa (2005).

The linear kinematic hardening model is presented in Figure 5.15.

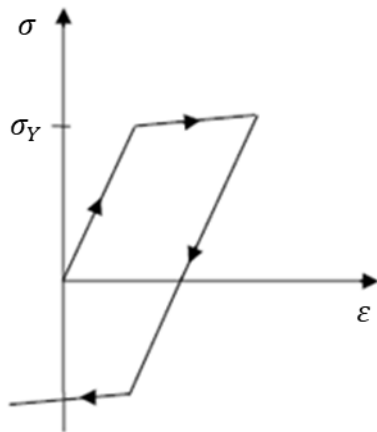


Figure 5.15 Linear kinematic hardening, from Dahlberg and Segle (2010).

Due to the assumed linearity, the consideration of the Bauschinger effect becomes rather rudimentary, which makes the linear kinematic hardening model unsuitable for very large strain simulations. Thus most often being utilised in the modelling of low cycle fatigue, with small strains.

5.4.2 Multilinear kinematic hardening (Mroz)

The multilinear kinematic hardening model, considers several linear segments, having different hardening modulus values. Thus every linear segment considered, is described by a different yield function, and different yield surface. Elastic response is only possible, when the stress state is within the smallest yield surface. This concept is depicted in Figure 5.16.

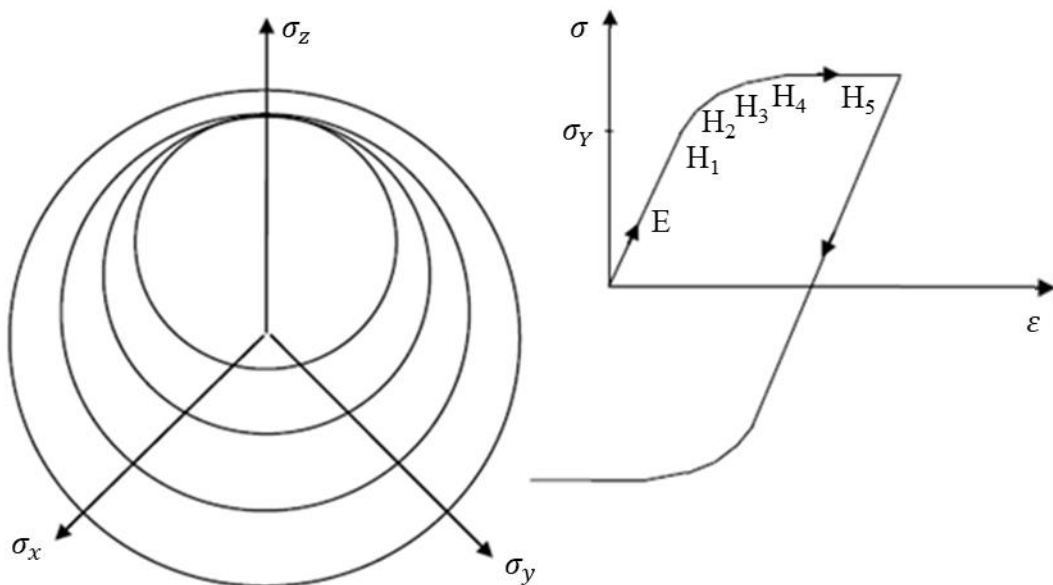


Figure 5.16 The Mroz concept of several yield surfaces, from Dahlberg and Segle (2010).

The back-stress is defined by the Mroz evolution law in the following manner (Ottosen and Ristinmaa, 2005):

$$\dot{\alpha}_{ij} = \dot{\lambda}q(\sigma_{ij}^M - \sigma_{ij}) \quad (5.28)$$

, where σ_{ij}^M is the mapping stress point, σ_{ij} is the current stress point and $\dot{\lambda}$ is a plastic multiplier. The positive quantity q can be calculated as:

$$q = \frac{2\sigma_y H}{3(s_{ij} - \alpha_{ij}^d)(s_{ij}^M - s_{ij})} \quad (5.29)$$

The Bauschinger effect is simulated in a correct manner in this model. However, the obtained loops are always symmetrical, thus material ratcheting is not possible to be described (Dahlberg and Segle, 2010).

5.4.3 Nonlinear kinematic hardening (AF and Chaboche)

The main advantage of this model is that it can simulate the ratcheting effect, due to asymmetric stress cycling, while introducing the Bauschinger effect in an accurate manner. However, it has a clear disadvantage when describing the shape of the hysteresis loop (Halama R., Sedlák J., Šofer M., 2012).

One of the most well-known nonlinear kinematic hardening model, is the Armstrong and Frederick (AF). The constants appearing in the evolution law of the back-stress tensor can be determined from uniaxial tests (Araújo, 2002).

Armstrong-Frederick evolution law (Ottosen and Ristinmaa, 2005):

$$\dot{\alpha}_{ij} = h \left(\frac{2}{3} \dot{\epsilon}_{ij}^p - \frac{\alpha_{ij}}{\alpha_\infty} \dot{\epsilon}_{eff}^p \right) \quad (5.30)$$

, where $\dot{\epsilon}_{ij}^p$ is the plastic strain rate, $\dot{\epsilon}_{eff}^p$ is the effective plastic strain rate, h and α_∞ are constant.

The last term in the Armstrong-Frederick back-stress evolution law can be regarded as a recall term, since if the second constant (α_∞) tends to infinity, the evolution law becomes the same as the Melan-Prager linear kinematic evolution law (Ottosen and Ristinmaa, 2005). This implies, that the second term is responsible for the introduction of nonlinearity in the evolution law.

As seen in Figure 5.17, the yield surface is limited by a bounding surface, which is fixed in the stress space. When the yield surface comes in contact with the bounding surface, the hardening modulus becomes zero, simulating an ideally plastic material. In all other cases, the hardening modulus will have a variable value, while loading (Halama R., Sedlák J., Šofer M., 2012).

In some literature, the constants from the Armstrong-Frederick evolution law are marked as C and γ . Thus the evolution law is written as:

$$\dot{\alpha}_{ij} = \frac{2}{3} C \dot{\epsilon}_{ij}^p - \gamma \alpha_{ij} \dot{\epsilon}_{eff}^p \quad (5.31)$$

Using this expression, the yield surface can be represented in the following way:

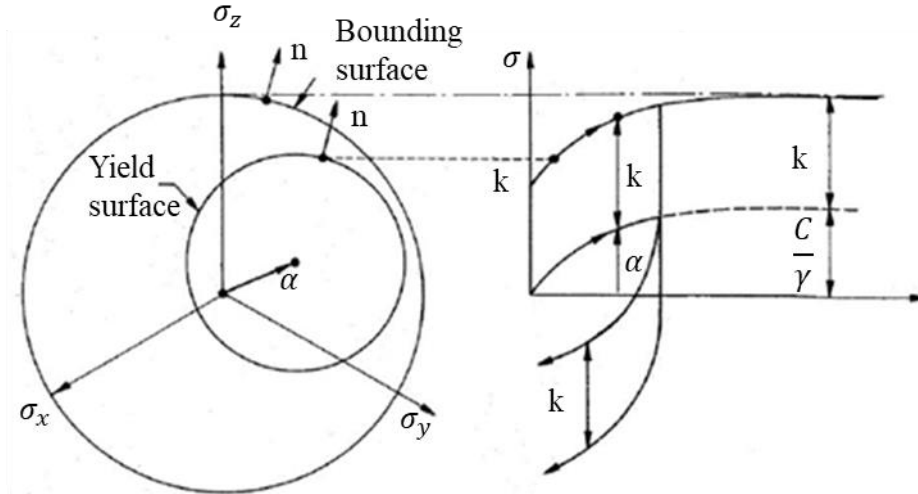


Figure 5.17 The yield surface and bounding for the AF-model, from Dahlberg and Segle (2010).

The Chaboche model is an improvement of the Armstrong-Frederick hardening model, by summing multiple nonlinear kinematic models. The improvement is observable in the simulation of the ratcheting effect, making it possible to describe ratcheting decay. It should be noted, that with the superimposition of a higher number of nonlinear kinematic models, the capability of the model is increased, and while choosing the number of superimposed models as 1, it will return to the Armstrong-Frederick model (Dahlberg and Segle, 2010).

Chaboche evolution law:

$$\dot{\alpha}_{ij} = \sum_{i=1}^n \left[h_i \left(\frac{2}{3} \dot{\epsilon}_i^p - \frac{\alpha_i}{\alpha_{\infty i}} \dot{\epsilon}_{eff}^p \right) \right] \quad (5.32)$$

$$\dot{\alpha}_{ij} = \sum_{i=1}^n \left[\frac{2}{3} C_i \dot{\epsilon}_i^p - \gamma_i \alpha_i \dot{\epsilon}_{eff}^p \right] \quad (5.33)$$

5.5 Mixed hardening

The mixed hardening model is obtained by combining the isotropic hardening model with the kinematic hardening model. The yield surface keeps a constant shape, while modifying its size and position during plastic deformation.

The mixed hardening is generally expressed as (Ottosen and Ristinmaa, 2005):

$$f(\sigma_{ij}, K_\alpha) = F(\sigma_{ij} - \alpha_{ij}) - K = 0 \quad (5.34)$$

By rewriting the generalised formula for the von Mises yield criterion, we obtain:

$$f(\sigma_{ij}, K_\alpha) = \left[\frac{3}{2} (s_{ij} - \alpha_{ij}^d)(s_{ij} - \alpha_{ij}^d) \right]^{1/2} - \sigma_Y - K = 0 \quad (5.35)$$

$$K_\alpha = \{\alpha_{ij}^d, K\} \quad (5.36)$$

Setting the hardening parameter K to 0, will result in a kinematic hardening model, while setting the back-stress hardening parameter to 0, we obtain an isotropic hardening model.

This model is used in the case of cyclic loading, when the cyclic hardening or softening is of interest. It also approximates the Bauschinger effect accurately, as well as the ratcheting effect.

The deviatoric plane and the uniaxial loading of mixed hardening von Mises material can be seen in Figure 5.18.

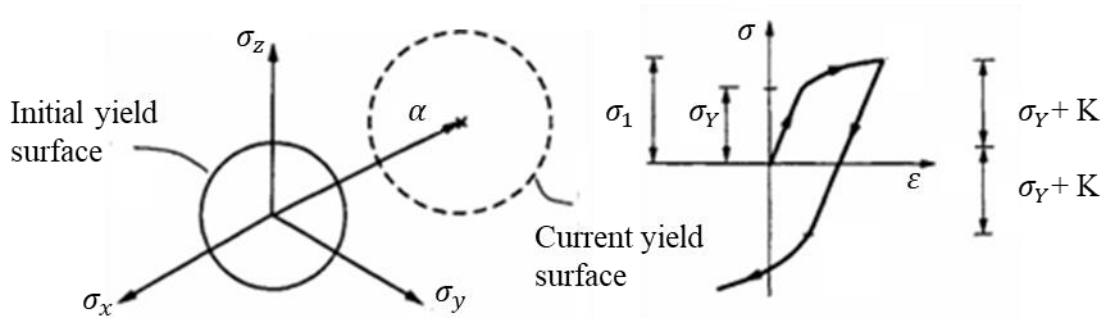


Figure 5.18 Mixed hardening of von Mises material, after Ottosen and Ristinmaa (2005).

In order to obtain a mixed hardening model between isotropic hardening and Armstrong-Frederick hardening, the isotropic hardening parameter is expressed in a similar manner as the back-stress tensor for Armstrong-Frederick hardening. By introducing a mixed hardening parameter (m), determining the amount of mixing between the two hardening models, the following hardening parameters are obtained (Ottosen and Ristinmaa, 2005):

$$\dot{\alpha}_{ij} = (1 - m)h \left(\frac{2}{3} \dot{\epsilon}_{ij}^p - \frac{\alpha_{ij}}{\alpha_\infty} \dot{\epsilon}_{eff}^p \right) \quad (5.37)$$

$$\dot{K} = mh \left(1 - \frac{K}{K_\infty} \right) \dot{\epsilon}_{eff}^p \quad (5.38)$$

, where m represents the mixed hardening parameter and K_∞ is a constant.

The deviatoric plane and the uniaxial loading of mixed AF hardening material can be seen in Figure 5.19.

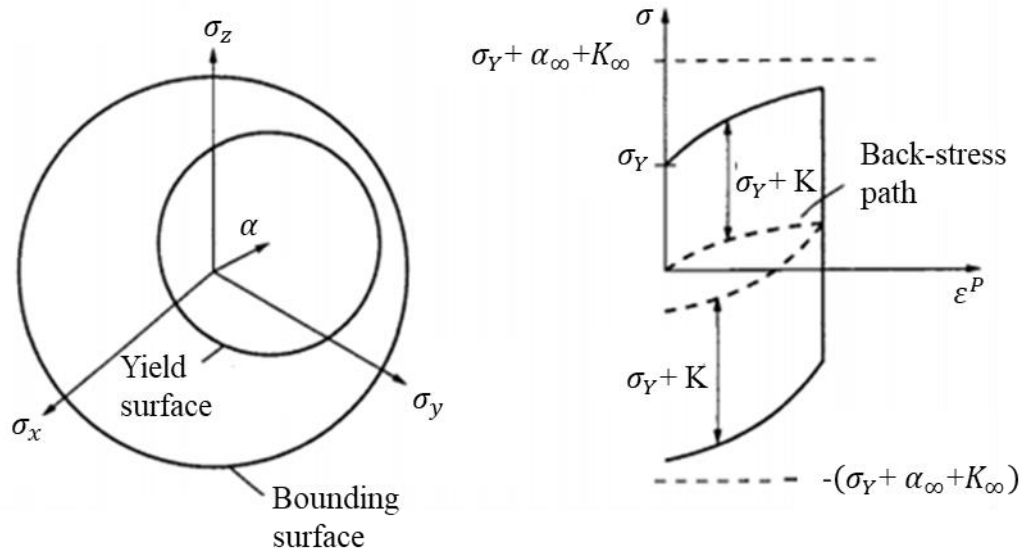


Figure 5.19 Mixed AF hardening model, after Ottosen and Ristinmaa (2005).

6 Experimental Procedures

6.1 Test specimens

The tested specimens are “slices” of two full-size weld details, one with and one without HFMI-treatment. The weld details consist of a base plate, having a perpendicular plate welded to it, using fillet welding, as seen in the figure below.

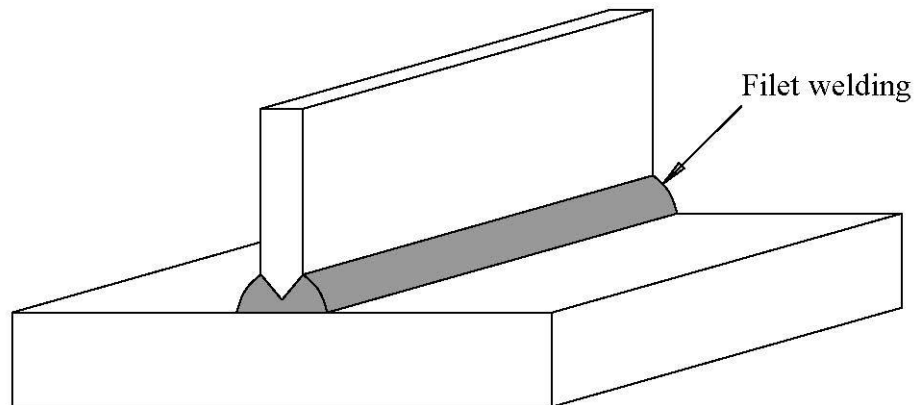


Figure 6.1 Analyzed weld detail.

A total of 4 test specimens were analyzed during the thesis work, two of them were loaded statically, while the other two have been subjected to cyclic loading. The specifications of the specimens are presented in the table below, together with the test specimen ID, which are used throughout the thesis work.

Table 1.1 Test specimen specifications.

Test specimen ID	Loading type	Treatment	Max. load [kN]	Steel grade
SAW	Static	No treatment (AW)	25	S460
SHFMI	Static	HFMI	25	S460
C18	Cyclic	HFMI	± 18	S460

6.1.1 Geometry

Two different testing specimen geometries were adopted for two different loading conditions, namely static and cyclic loading.

In both cases, in order to maintain symmetry, the base material was water jet cut on the opposite side of the weld, imitating the outline of the welding as seen in Figure 6.2.

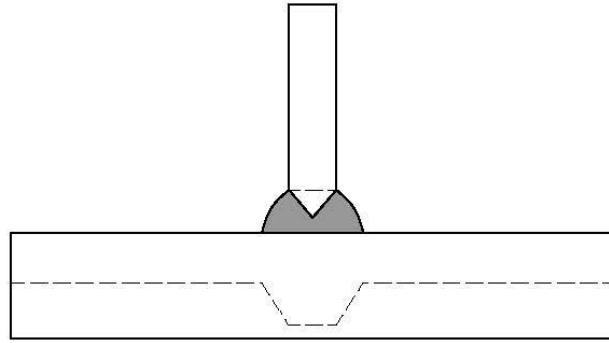
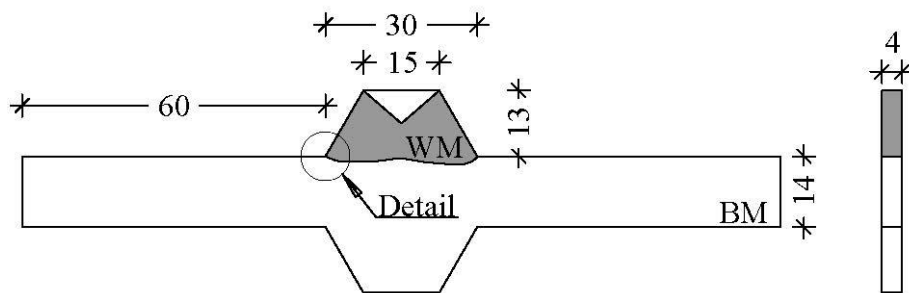


Figure 6.2 Symmetric cut of base material.

The specimen used for static testing are presented in Figure 6.3. It had a thickness of 4 mm and was flat on both sides. This enabled fine grinding of the two surfaces, exposing the micro-structure of the specimen. Due to the change in geometry and the presence of welding, stress concentration is expected to localise at the weld toe.

a) Specimen geometry



b) Detail of monitored area

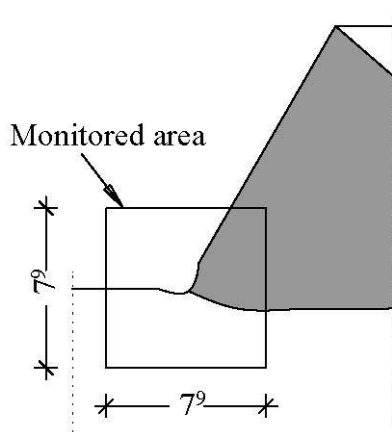


Figure 6.3 Specimen used in the case of static loading.

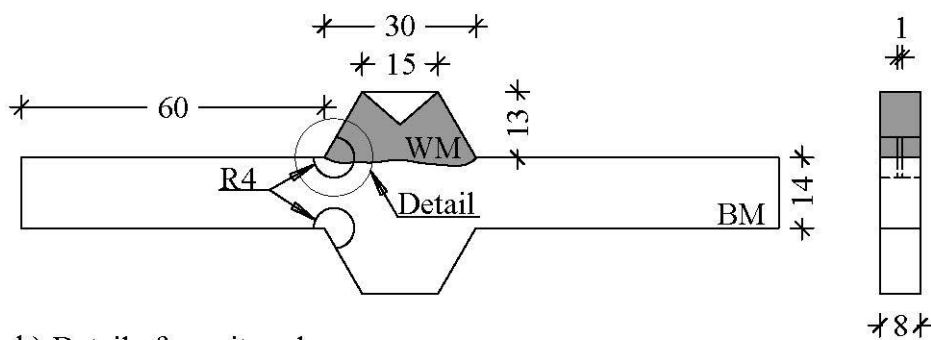
In the case of cyclic testing, the specimen having 4 mm thickness is no longer adequate, because of the risk of buckling of the specimen in compression. Thus in order to eliminate the buckling possibility during cyclic loading, the thickness of the specimen

used for cyclic testing was increased to 8 mm and a circular cut-out, with a radius of 4 mm and depth of 3.5 mm was made around the area of interest from both sides, leaving a thickness of 1 mm in this specific area. This circular cut-out was performed in order to ensure that the highest stresses will appear in the area of interest.

To maintain symmetry of the test specimen, the circular cut-out was made in the other side of the specimen as well, as seen in Figure 6.4.

Due to slicing of the test specimens the residual stresses from welding and HFMI disappear, thus the only effect due to HFMI treatment left behind is the strain hardening of the material in the vicinity of the treatment zone and the geometry improvement at the weld toe.

a) Specimen geometry



b) Detail of monitored area

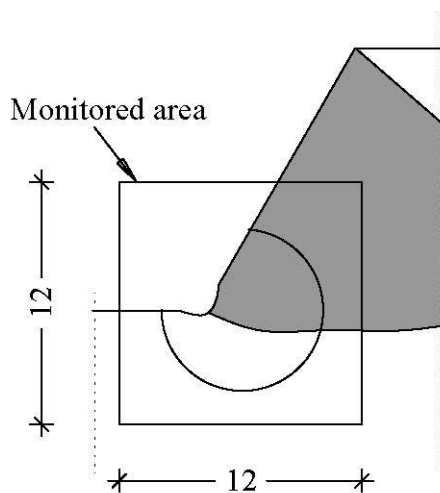


Figure 6.4 Specimen used in the case of cyclic loading.

6.1.2 Material

Only one structural steel type was chosen as base material, namely S460, because of the time limitation of the thesis project. Table 6.1 lists the steel properties of the used steel, provided by the manufacturer.

Table 6.1 Steel properties provided by manufacturer.

State	t [mm]	Steel	fy [MPa]	fu [MPa]
As-welded (AW)	60	S460	494	597
HFMI treated	40	S460	566	639

Table 6.2 gives an overview of the welding parameters used for the welding of the specimens. The welding method used was flux-cored arc welding.

Table 6.2 Welding parameters.

Method	Voltage	Current	Average welding speed	No. of weld passes
FCAW 136	27.5 V	260 A	370 mm/min	3 on each side of attachment

As described in Chapter 3, three different materials can be found at the weld toe region. These areas, can be seen in the pictures from Figure 6.5, which were taken on both the as-welded and the HFMI treated weld detail, using a scanning electron microscope (SEM). Due to the difference in micro-structure, these three regions can be easily distinguished between each other.

a) As-welded (AW)

b) HFMI treated

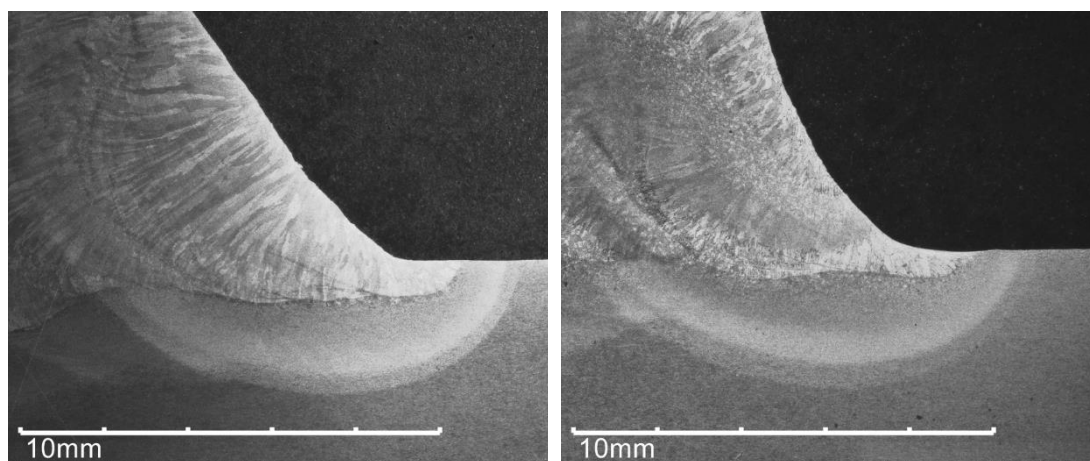


Figure 6.5 SEM pictures of the two welded details.

More in-depth pictures were taken on the HFMI treated weld detail, showing the micro-structure of the different regions, these are presented in Figure 6.6.

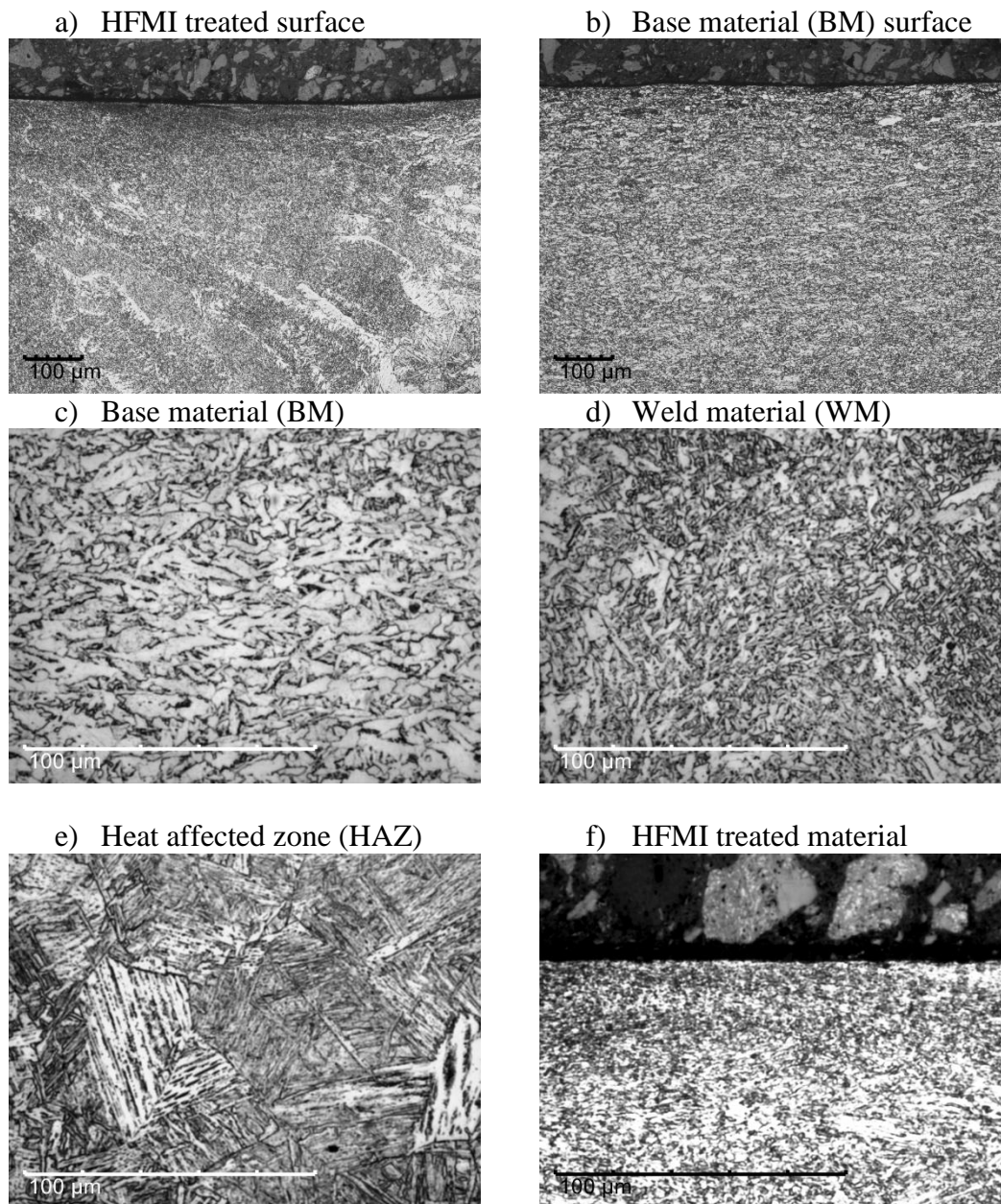


Figure 6.6 SEM pictures of the HFMI treated welded detail.

6.2 Testing

The tensile testing was performed at room temperature, with steadily increasing load, reaching a maximum load of 25 kN. The load increase speed was 4 kN per minute.

The cyclic testing was performed at a loading rate of 60 seconds per cycle, having a total of 25 cycles. The two specimens tested cyclically were subjected to different cycle loads. Specimen C18 was subjected to a load of ± 18 .

6.3 Digital image correlation

6.3.1 Introduction

The deformation behavior of the specimens, during the static and cyclic testing was monitored using the Aramis 4M measuring system. This provides a non-contact and material independent measuring procedure, which consists of high resolution image capturing, during the experiment. Subsequent images are then analyzed, using Digital Image Correlation (DIC) techniques.

The DIC, returns the strain field over the area of interest, by comparing the acquired images. More exactly, the area of interest is divided in square zones, of a specified size, called facets. These are identified by the software, in every image, considering the stochastic pattern of the specimen. The position of the facet is searched in the images, by means of minimizing the quadratic difference between the observed patterns inside the facets. The location changes of the facets, throughout the image series, gives possibility of calculating the local strain field for the tested specimen. The first image can be considered as the reference frame, i.e. when strain is considered to be equal to 0 in every point. If desired, an initial strain value can be introduced, calculating the strain field of upcoming images based on the applied, fix reference strain value of the first image.

The facet size is specified by the software user as a number of pixels, marking the edge length of the square facet. This should be chosen as small as possible, in order to reduce computation time and increase the acquisition of local effects within the facet, while being also large enough to enable the computation of the facet (GOM mbH, 2015).

The accuracy of the result can be increased by overlapping the facets, both in vertical and horizontal direction. This can be achieved by the point distance parameter in the software, describing the distance between two contiguous facets. With a smaller point distance, the measurement point density is increased, creating a finer mesh, which also influences the computation time. Thus, with smaller point distance, the mesh is finer, but the computation time is longer. The recommended overlapping percentage interval is considered to be between 20 % and 50 % (GOM mbH, 2015).

The DIC was performed using the software GOM Correlate 2016, in the current study. An area of 7.9 x 7.9 mm was monitored, right at the weld toe in the case of static loading, using a digital camera (2048 x 2048 pixel). Since the analyzed area was very small, the camera was equipped with a magnification device. By trial and error, a facet size of 39 x 39 pixels was considered adequate in this case, with an overlap of 33 %. Thus the point distance was set to 26 pixels, this corresponding to 0.1 mm.

In the case of cyclic loading, the monitored area was increased to 12 x 12 mm, thus magnification was no longer necessary.

In both cases, i.e. static loading and cyclic loading, the image acquisition rate was 1Hz.

6.3.2 Specimen preparation

In order to obtain better results, the specimens had to undergo certain preparations, consisting in surface pattern enhancements, to improve the facet creation. Two different methods were used for the static, respectively cyclic testing, prior testing.

In the case of static loading, the specimens were polished, to expose the crystalline structure of the 3 material regions (BM, WM and HAZ). This enabled the use of microstructure pattern, as reference points for the facets. The polished test specimen, the monitored area and the location of the monitored area can be seen in Figures 6.7, 6.8 and 6.9.

On the other hand, the cyclic test specimens were painted with a speckle pattern before testing, as seen in Figure 6.10. The monitored area and the location of the monitored area is presented in Figure 6.11 and 6.12.



Figure 6.7 Polished test specimen for static testing.

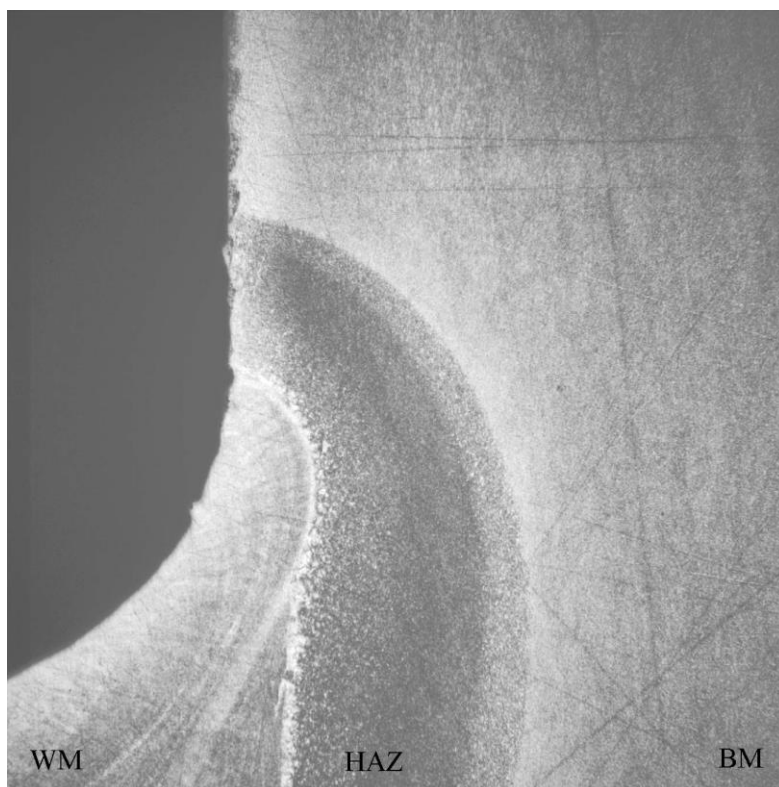


Figure 6.8 Monitored area (7.9 x 7.9 mm) for DIC, of static test specimen.

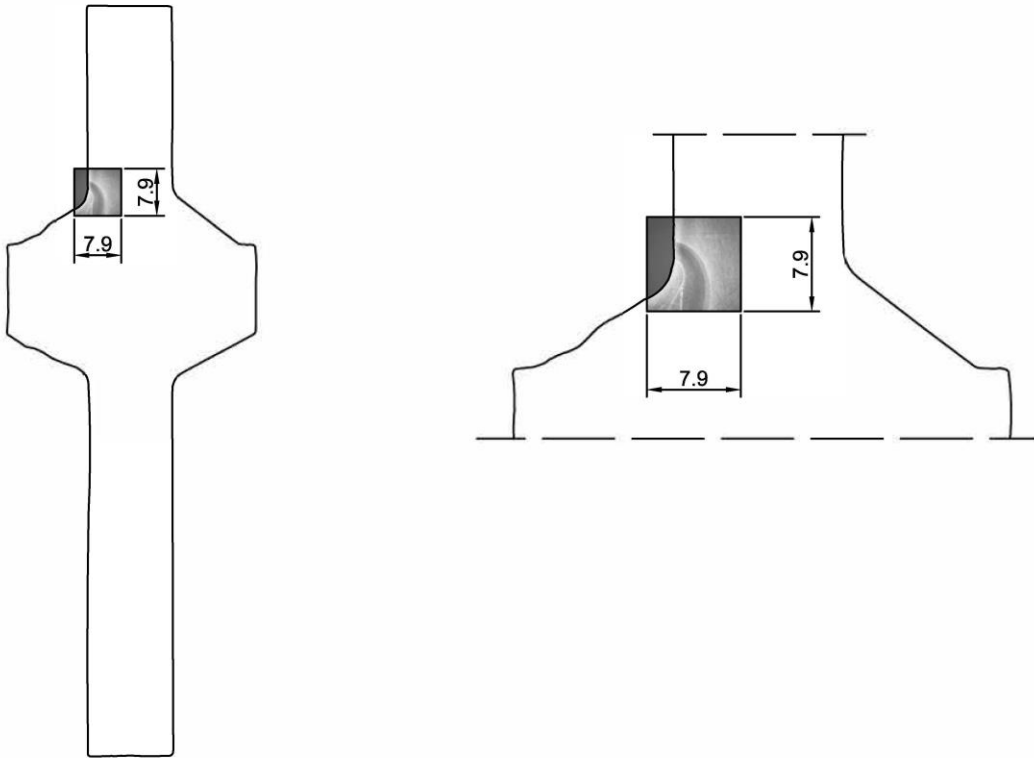


Figure 6.9 Location of monitored area (7.9 x 7.9 mm) for DIC, of static test specimen.



Figure 6.10 Painted test specimen for cyclic testing.

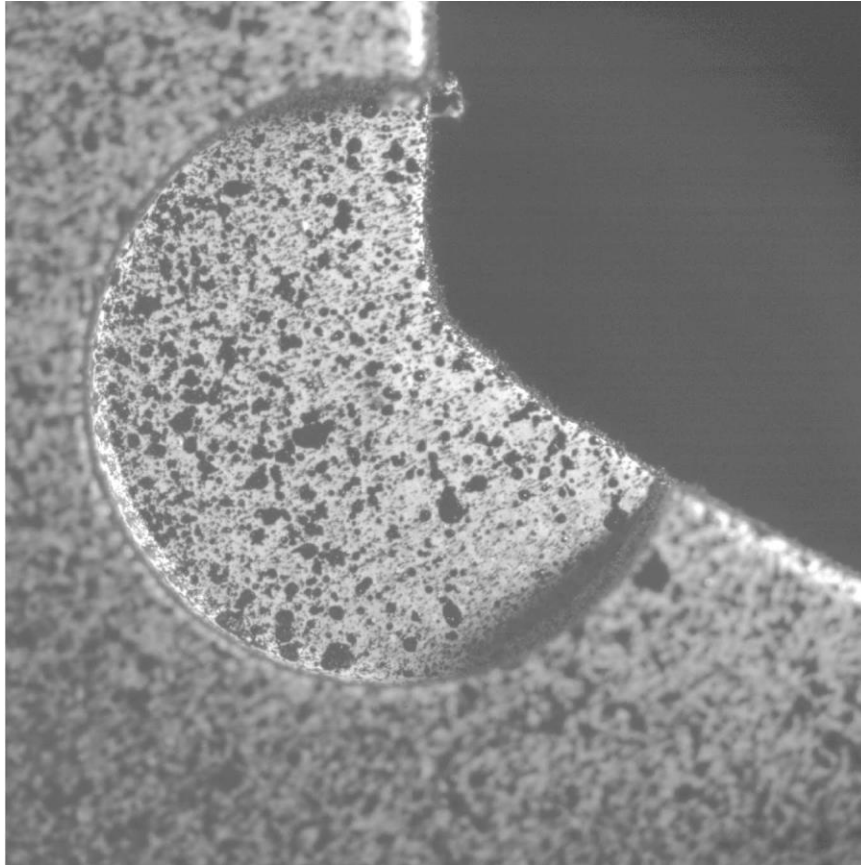


Figure 6.11 Monitored area (12 x 12 mm) for DIC, of cyclic test specimen.

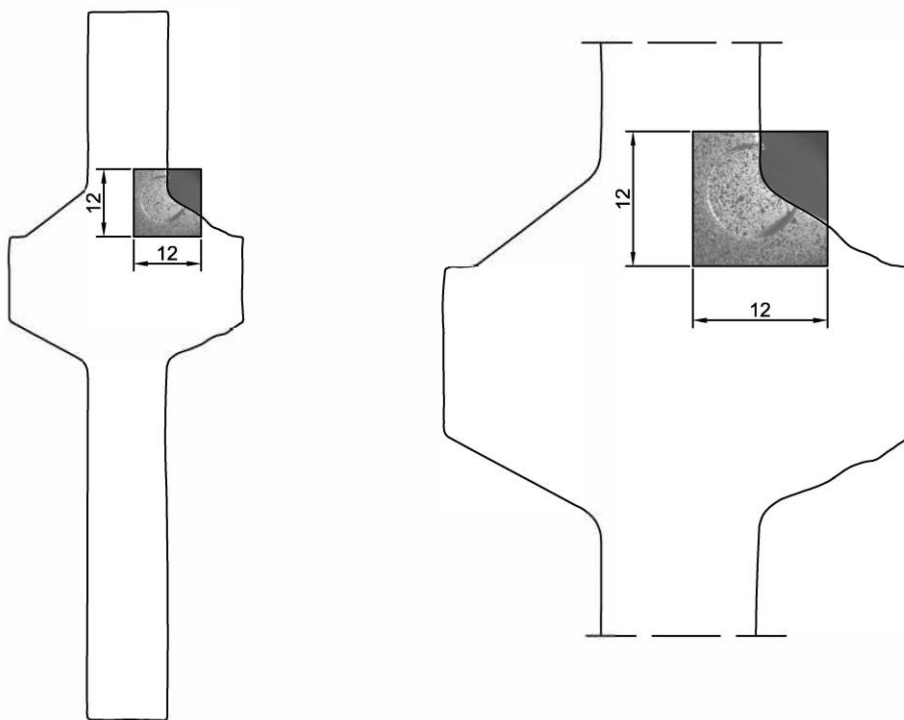


Figure 6.12 Location of monitored area (12 x 12 mm) for DIC, of cyclic test specimen.

6.3.3 Convergence study – Analyzed area size

The strain field in the area of interest was obtained by means of DIC. In order to reduce the noise from the strain measurements, the strain values were averaged over a specific area, and a convergence study was carried out to examine the used area size.

Two locations were chosen to analyze the influence of the chosen area size, one right at the weld toe where high stress concentrations are found, and one in the base material, which is located far from the stress concentration zone. In both locations, six different area sizes were selected over which the averaged strain values were determined. As seen in Figure 6.13, the selected area sizes were ranging between 0.2 x 0.2 mm and 1 x 1 mm.

Figure 6.14 and Figure 6.15 shows the variation of strain in the two locations for the different area sizes during loading. It is observable that in both graphs, the smallest area size (0.2 x 0.2 mm) shows significant fluctuation, while with the increase of the area size the fluctuation is reduced. The fluctuation appears due to the noise of the experimental results, and it has as consequence the loss of accuracy in the measured data. Since the monitored area is very small (7.9 mm x 7.9 mm for static loading and 12 mm x 12 mm for cyclic loading), accuracy on a local scale is very important. Thus a balance has to be reached between localized data and accurate data.

It was concluded that an area size of 0.6 x 0.6 mm is sufficiently small in order to capture the important localized strain data, while also being sufficiently large to reduce the noise of the experimental values and obtain converging strain data.

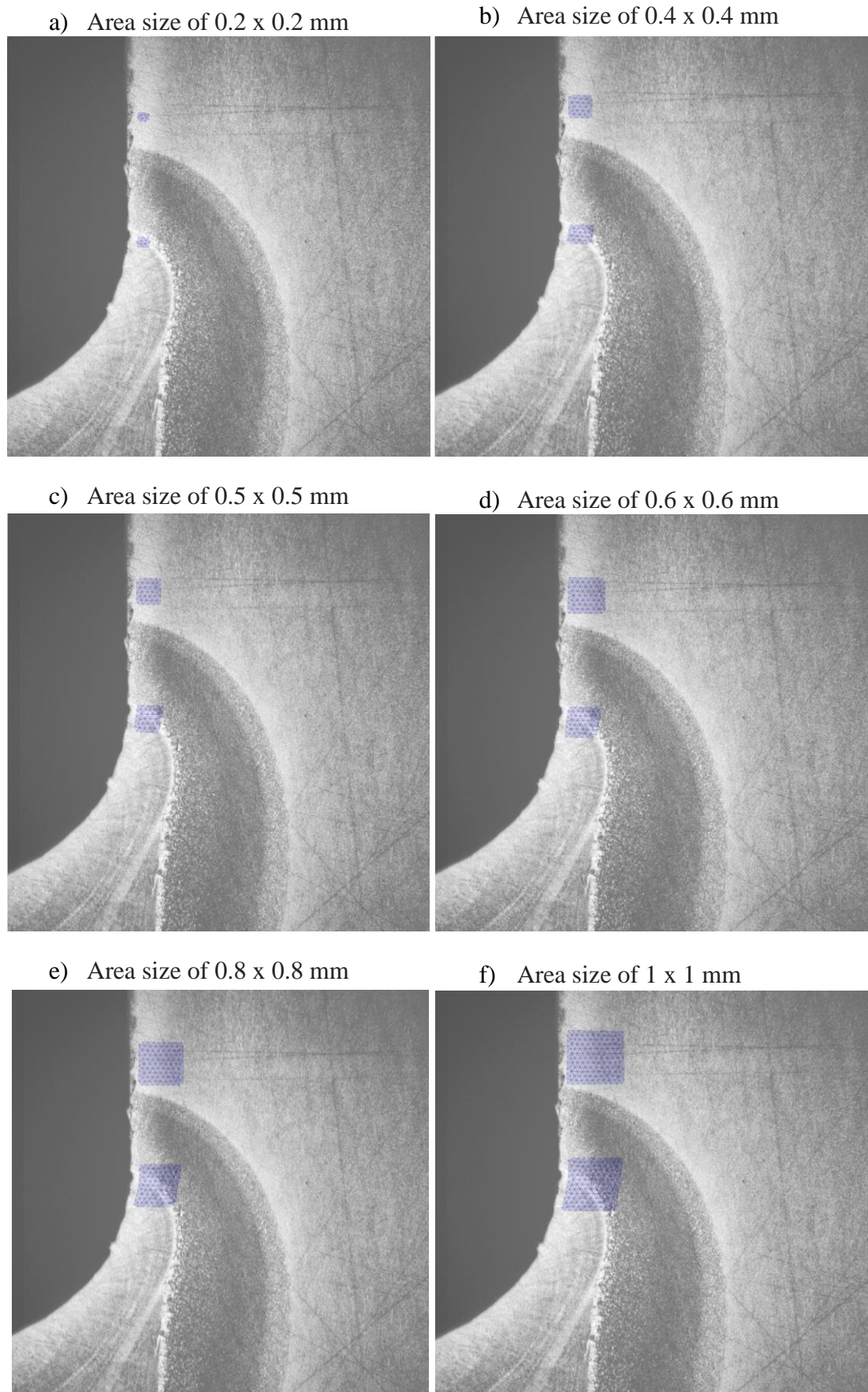


Figure 6.13 Area sizes for convergence study.

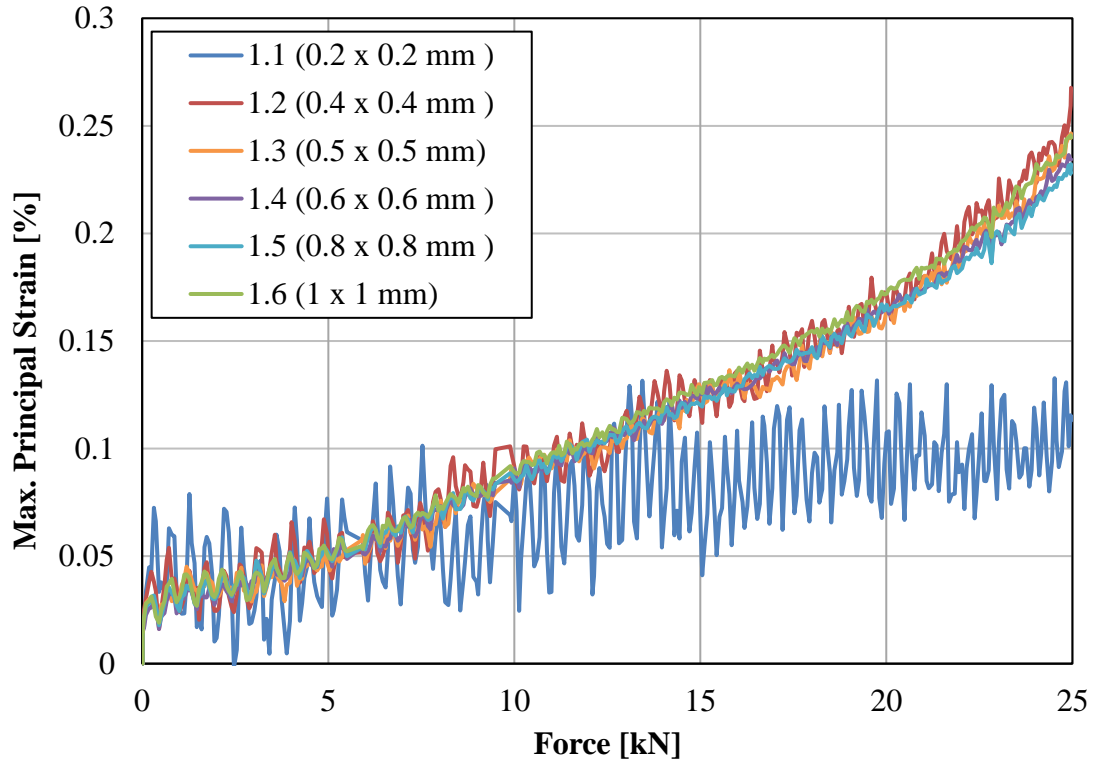


Figure 6.14 Maximum principal strain during loading in base material, averaged over different area sizes.

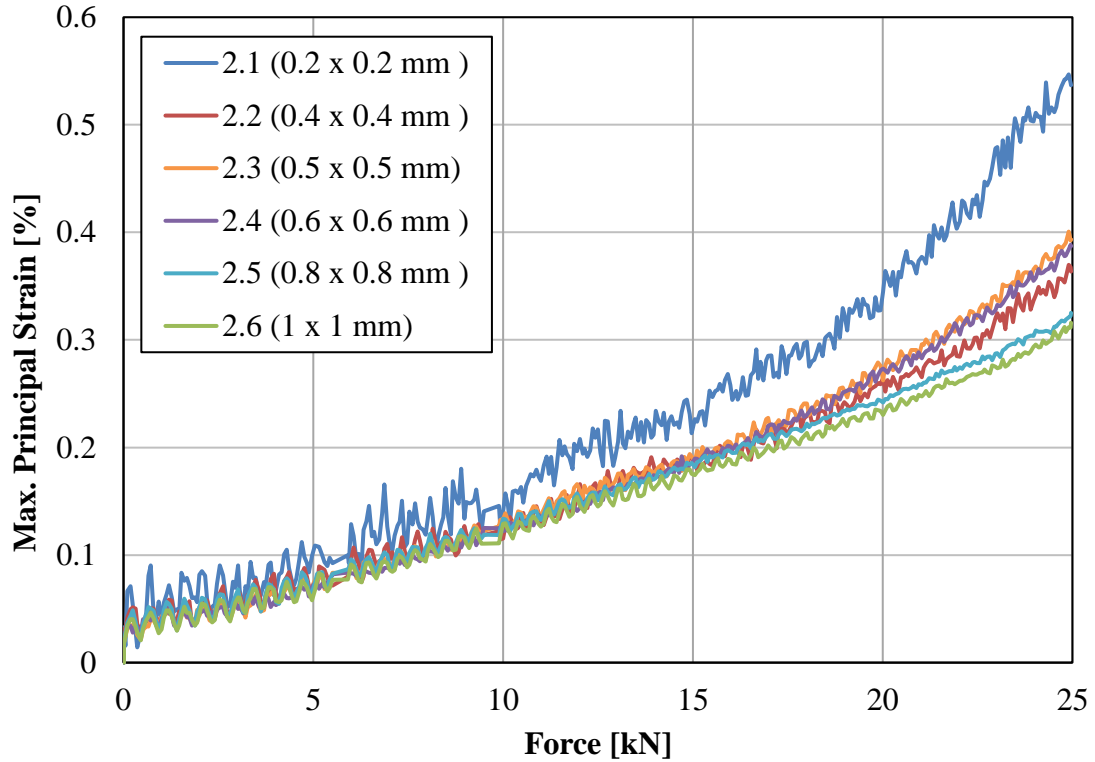


Figure 6.15 Maximum principal strain during loading at the weld toe, averaged over different area sizes.

6.4 Results

6.4.1 Static test results – As welded specimen

Figure 6.16 displays the maximum principal strain color plot of the specimen, at different load levels. The figures show that stress concentration appears at the weld toe region, as expected.

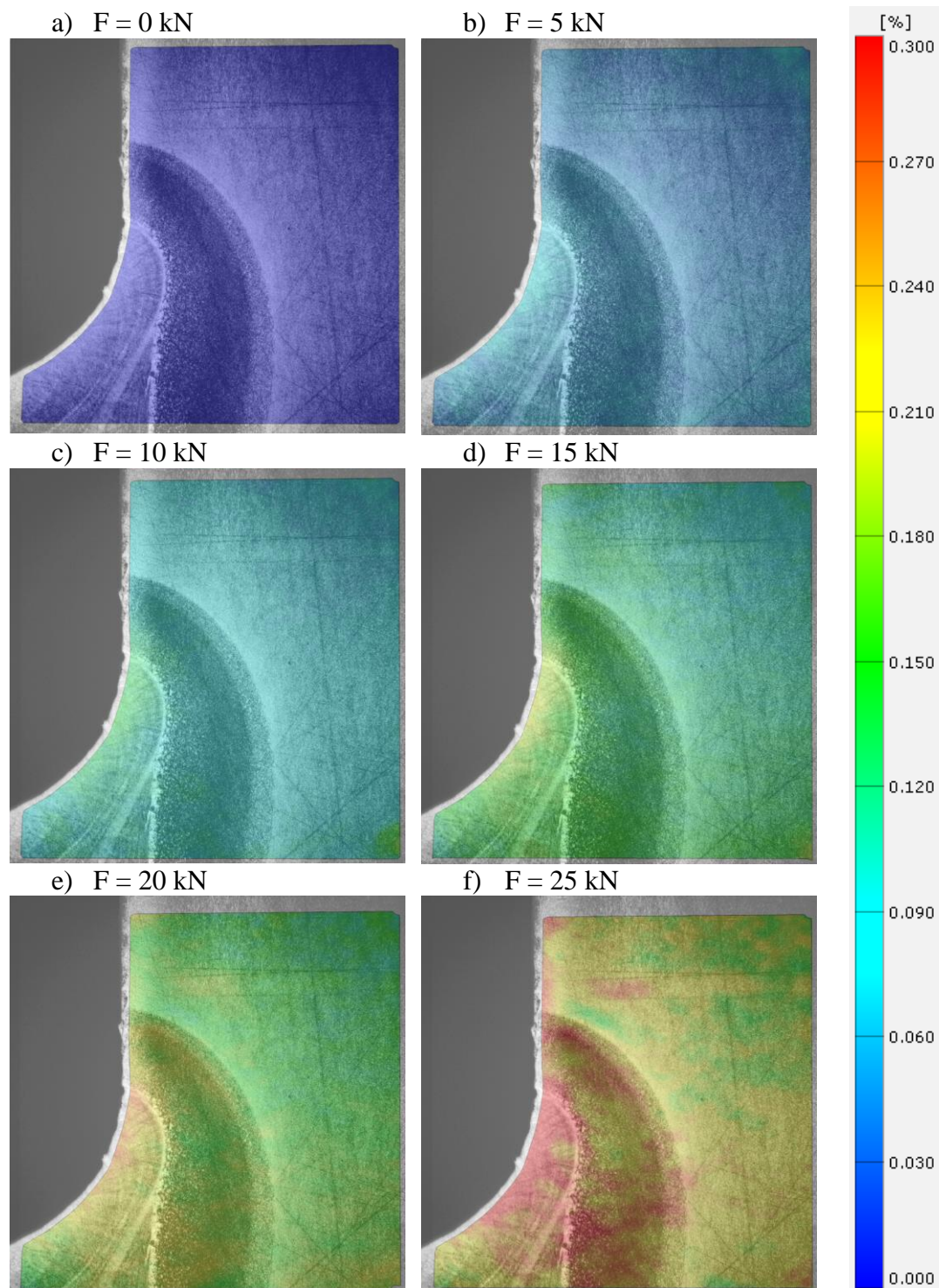


Figure 6.16 Maximum principle strain [%] color plots of statically tested as-welded test specimen, at different load levels.

In order to analyze the strain data in different material regions, areas of 0.6 x 0.6 mm were placed along the area of interest, as shown in Figure 6.17 and the E11 strain value was averaged over these areas.

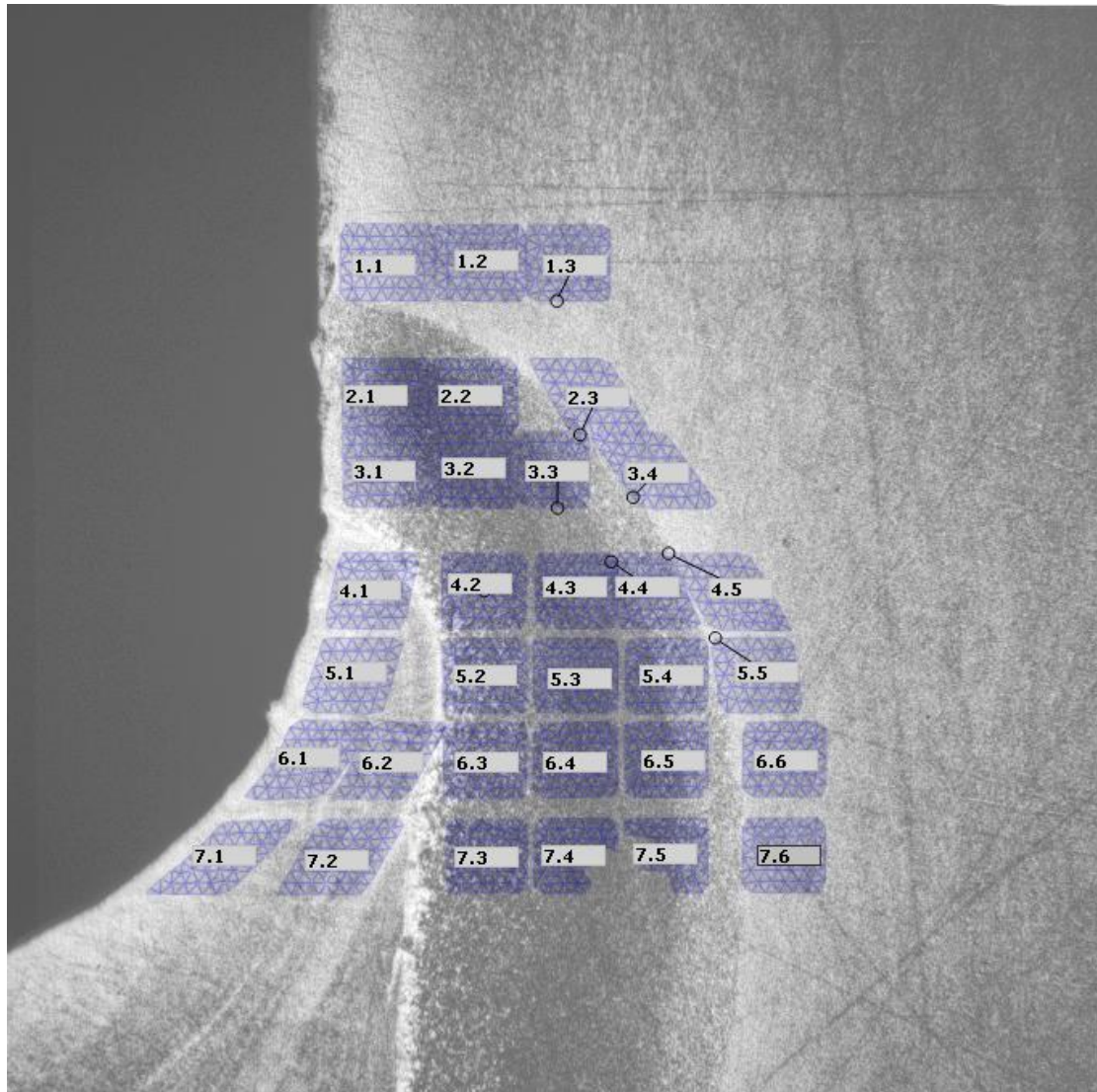


Figure 6.17 Displacement of analyzed areas on the SAW specimen.

The area with the highest strain value was area 4.1, located in the weld material, right at the weld toe. The strain concentration factor (K_ϵ) of this area was calculated at the load level of 15 kN, by dividing the strain value obtained from DIC with a calculated nominal strain value (ϵ_{nom}), using the equations below.

$$\epsilon_{nom} = \frac{\sigma_{nom}}{E} = \frac{F}{EA} \quad (6.1)$$

$$K_\epsilon = \frac{\epsilon}{\epsilon_{nom}} = \frac{0.0017505}{0.0012755} = 1.372 \quad (6.2)$$

The obtained strain concentration factor at 15 kN, at the weld toe was 1.372 and the strain – force diagram of this area is presented in Figure 6.18.

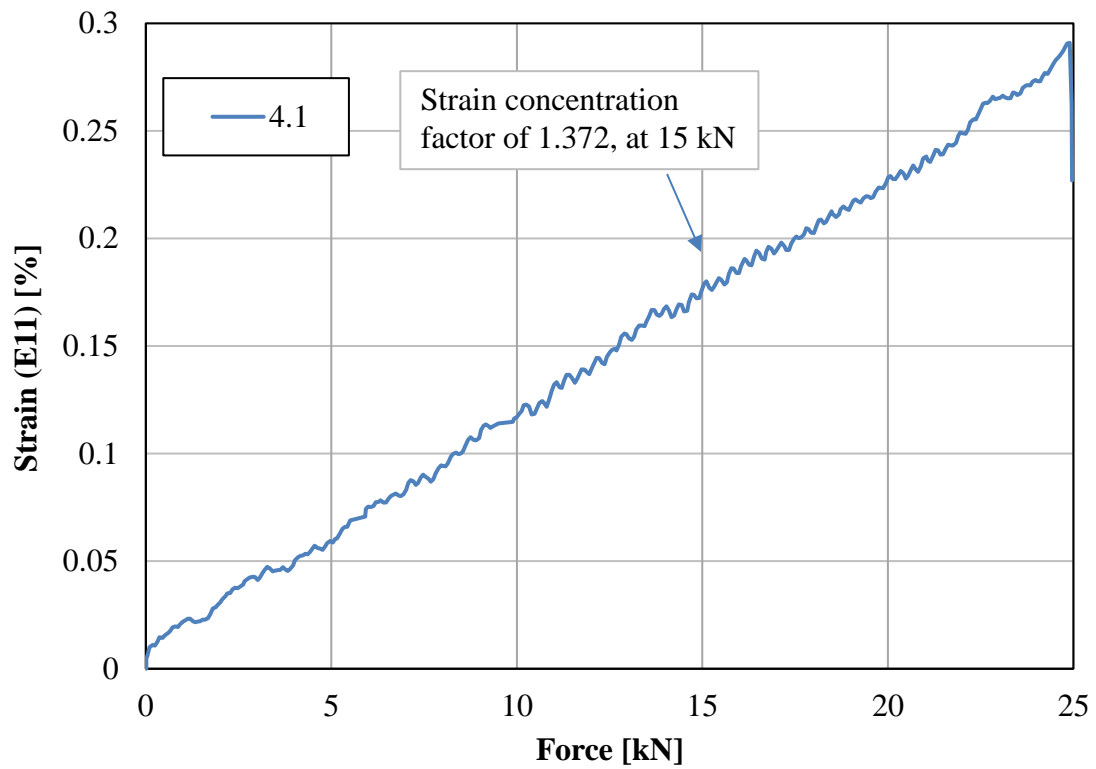


Figure 6.18 E11 strain [%] – Force [kN] diagram of area 4.1.

6.4.2 Static test results – HFMI treated specimen

Figure 6.19 displays the maximum principal strain color plot of the HFMI treated and statically tested specimen, at different load levels. The figures show that stress concentration appears at the weld toe region, as expected and that the area having strain above 0.3 % at maximum load is smaller than in the case of the untreated specimen.

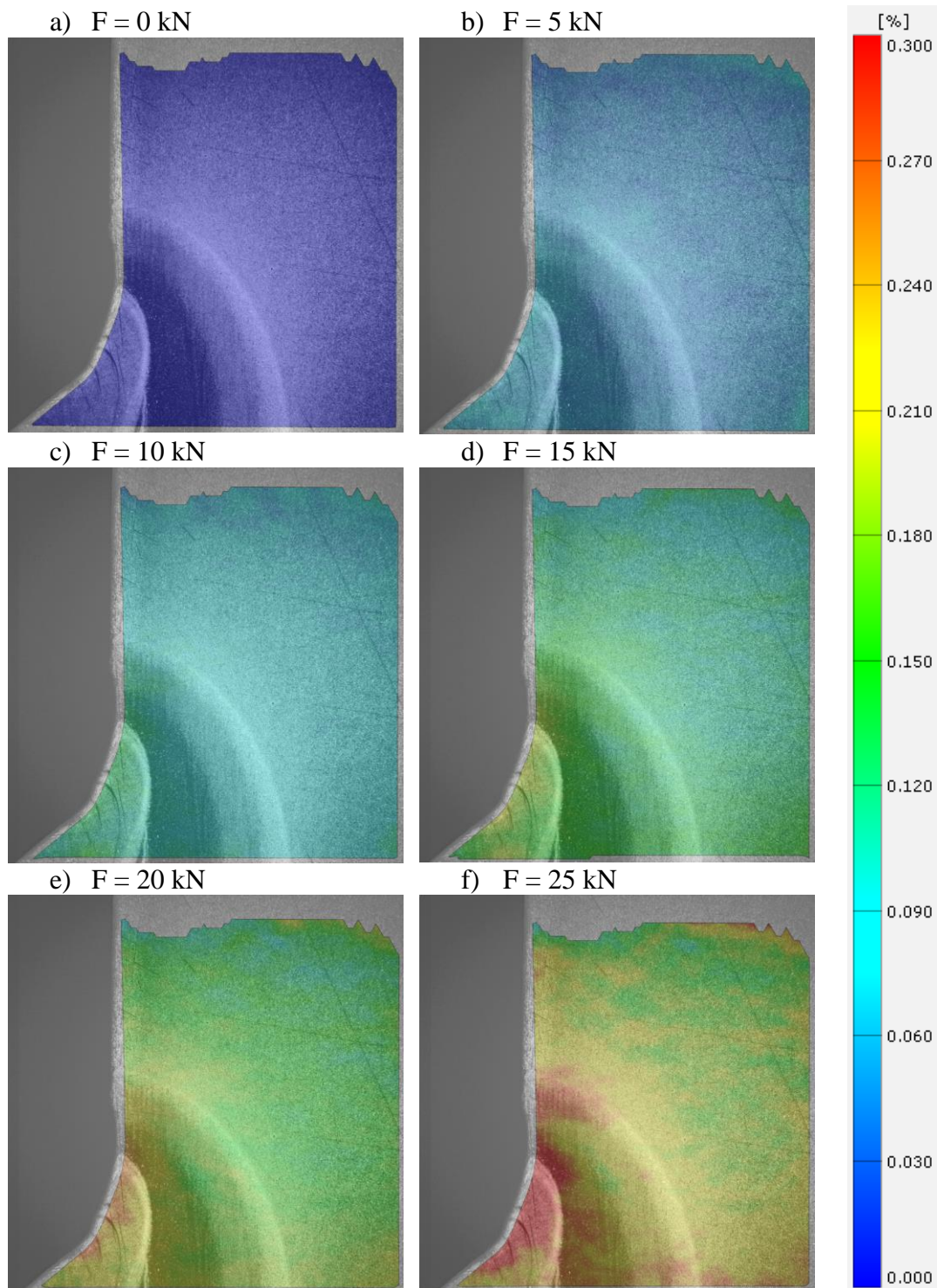


Figure 6.19 Maximum principle strain [%] color plots of statically tested HFMI treated test specimen, at different load levels.

Areas of 0.6 x 0.6 mm were positioned in the different material regions, in order to establish the area with highest strain concentration, as shown in Figure 6.20 and the E11 strain value was averaged over these areas.

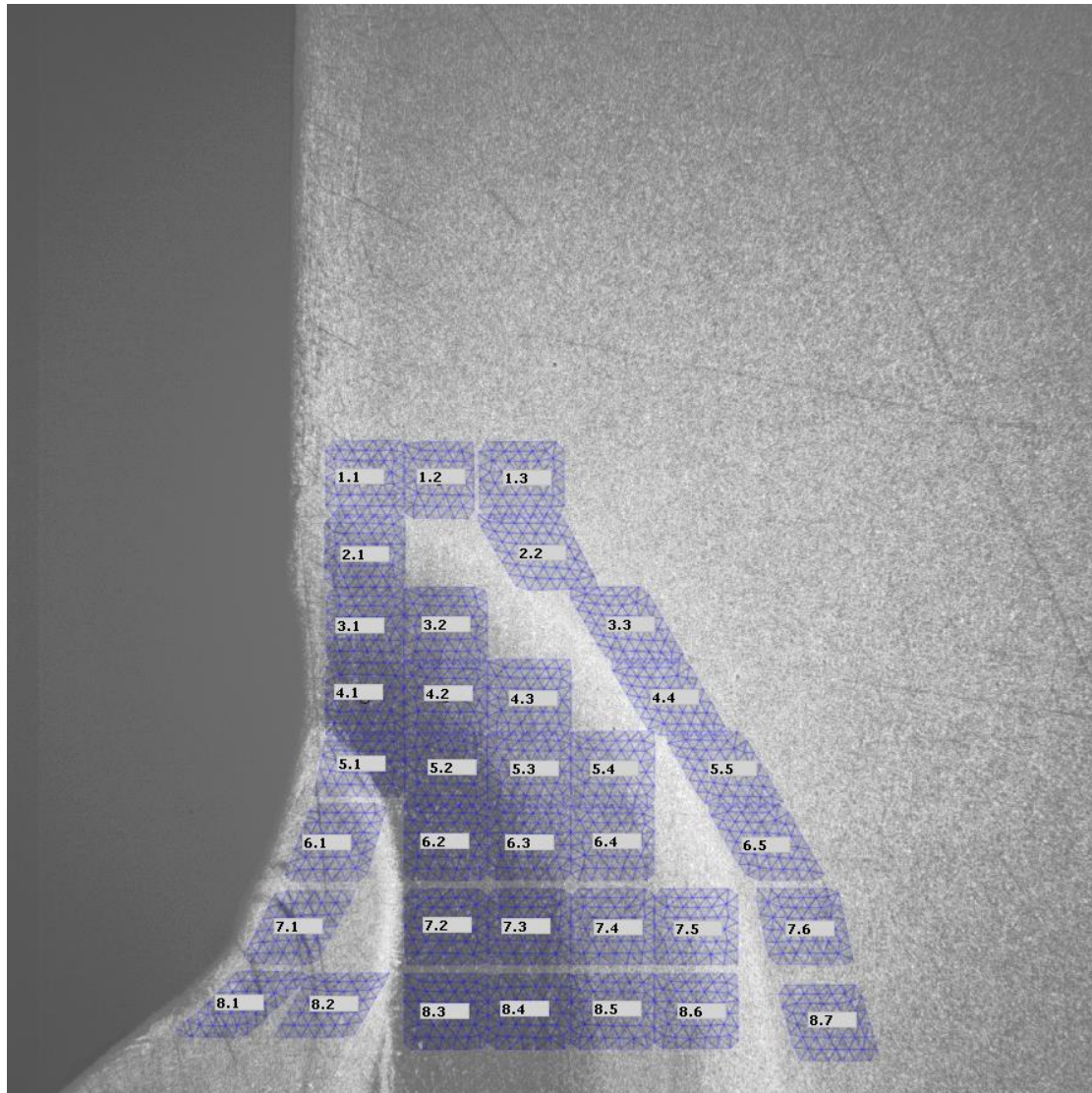


Figure 6.20 Displacement of analyzed areas on the SHFMI specimen.

The strain concentration factor was calculated using the equation (6.1) and equation (6.3), obtaining 1.417.

$$K_{\varepsilon} = \frac{\varepsilon}{\varepsilon_{nom}} = \frac{0.0018078}{0.0012755} = 1.417 \quad (6.3)$$

Under normal circumstances, the stress concentration factor for the HFMI treated specimen should have been smaller than the one for the untreated specimen, which was equal to 1.372. This was expected due to the geometry improvement induced by the HFMI treatment. However, this was not the case concerning the analyzed test specimens in the current thesis project. This can be explained by the fact that the radius at the weld toe was smaller for the HFMI treated test specimen than for the untreated test specimen and smaller radius causes higher strain concentration.

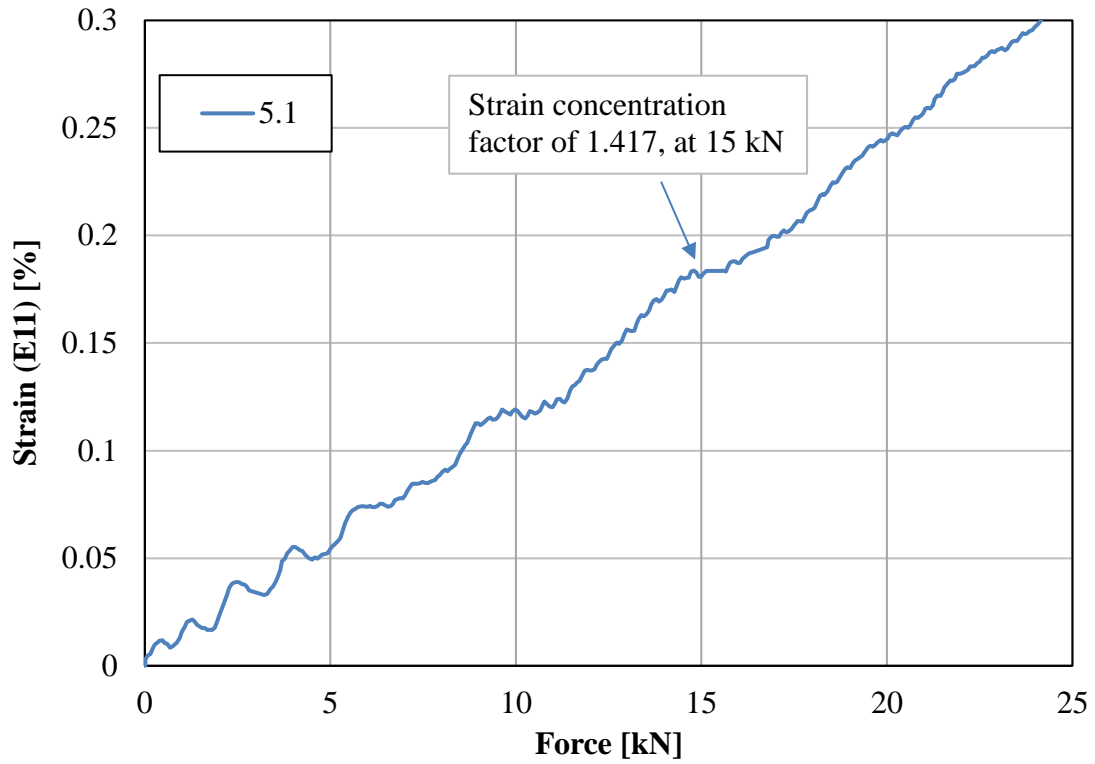


Figure 6.21 E11 strain [%] – Force [kN] diagram of area 5.1.

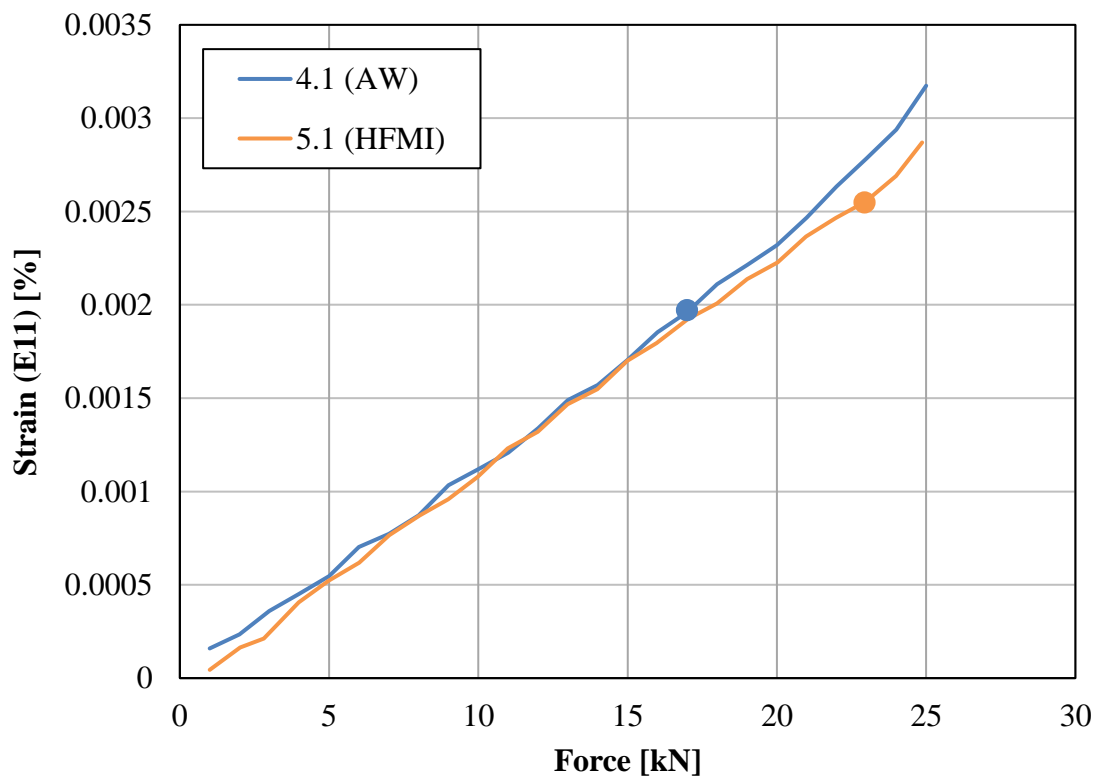


Figure 6.22 Comparison of maximum E11 strain areas of statically tested as-welded and HFMI treated specimens.

Figure 6.22 shows the strain – force curves of the areas with highest strain from the as-welded specimen, respectively the HFMI treated specimen, when loaded statically, both areas being located in the weld material, right at the weld toe. The circular marks on the curves have the purpose of showing the point when the curves start to deviate from a linear behavior. These can be associated in a qualitative manner to the point when yielding occurs in the specific area. Taking this into account, it can be observed, that yielding occurs much later (at higher load level) in the HFMI treated specimen, at the specific area location, than in the as-welded specimen. This coincides with the behavior expected due to the HFMI treatment of the weld toe.

6.4.3 Cyclic test results

A grid of areas was established in order to analyze the extent of the plastic zone. The areas were deemed to deform plastically if they exhibit a substantially larger strain in the first compressive cycle than in the previous tension cycle. Thus after analyzing every area separately, it was concluded that the areas marked with red, in Figure 6.23 are experiencing plastic deformation and the stress – strain loops are stabilized after 5 to 10 cycles. The areas marked with green, show stable cycles even after the first cycle, without any plastic deformation. The two areas marked with yellow, showed smaller strain in the first compressive cycle than in the previous tension cycle, which would indicate shrinking. However, the observed strain difference between the two cycles was small enough, to consider it as a result of noise in the experimental data and regard these areas as zones having elastic behavior.

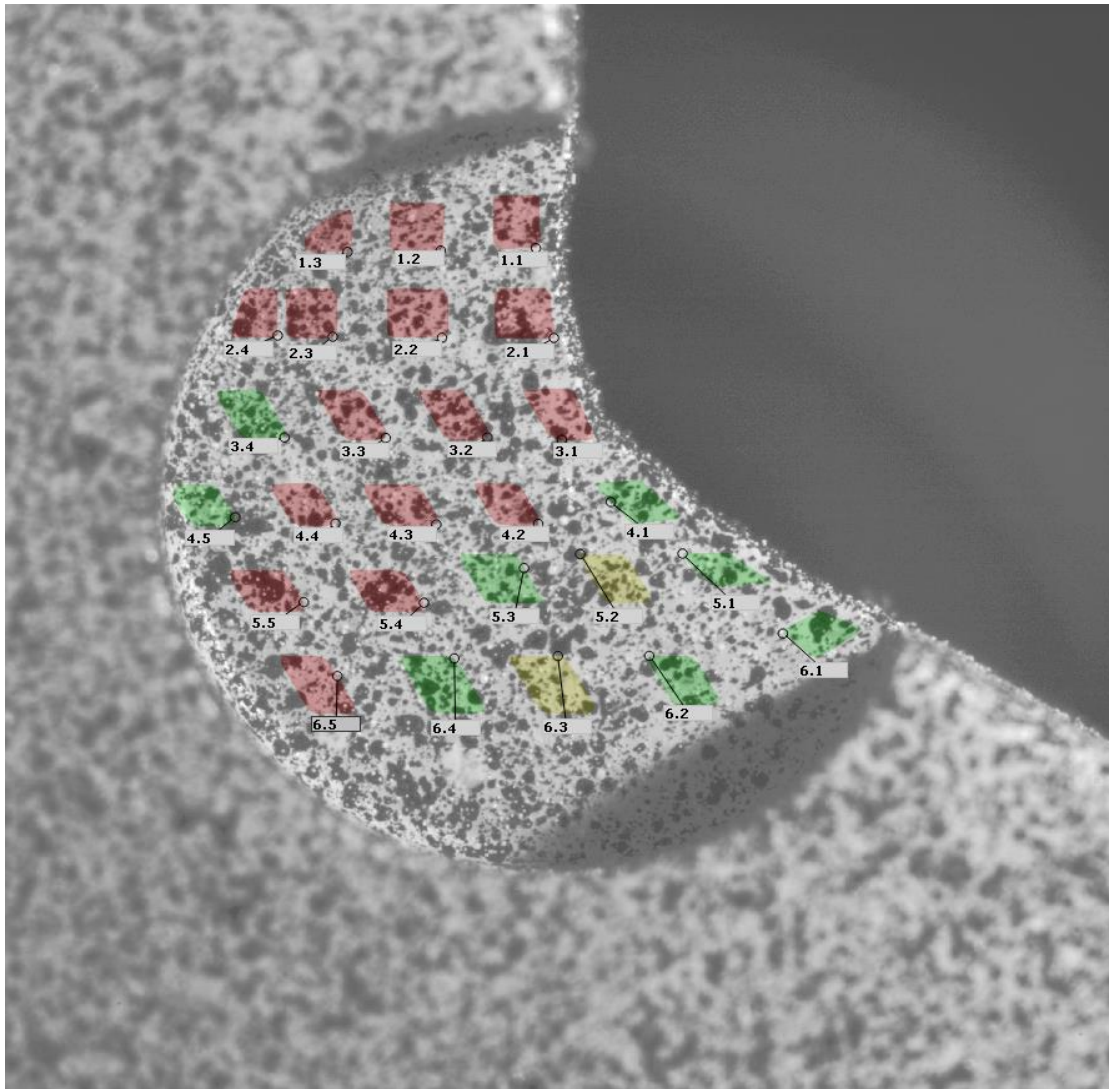


Figure 6.23 Displacement of analyzed areas on the C18 specimen. Areas marked with red experience plastic deformation, while the other areas remain in the elastic regions during testing.

The force-strain diagram and frame-strain diagram of a plastically deformed area (3.1) and an elastic area (5.1) are presented in the figures below. Figure 6.24 and Figure 6.25 are referring to area 3.1, which has deformed plastically during cyclic testing and was stabilized after 7 cycles, showing large strain value differences between the tension and compression cycles. On the other hand, Figure 6.26 and Figure 6.27 shows the behavior of the elastically deformed area 5.1, being stabilized already after the first cycle.

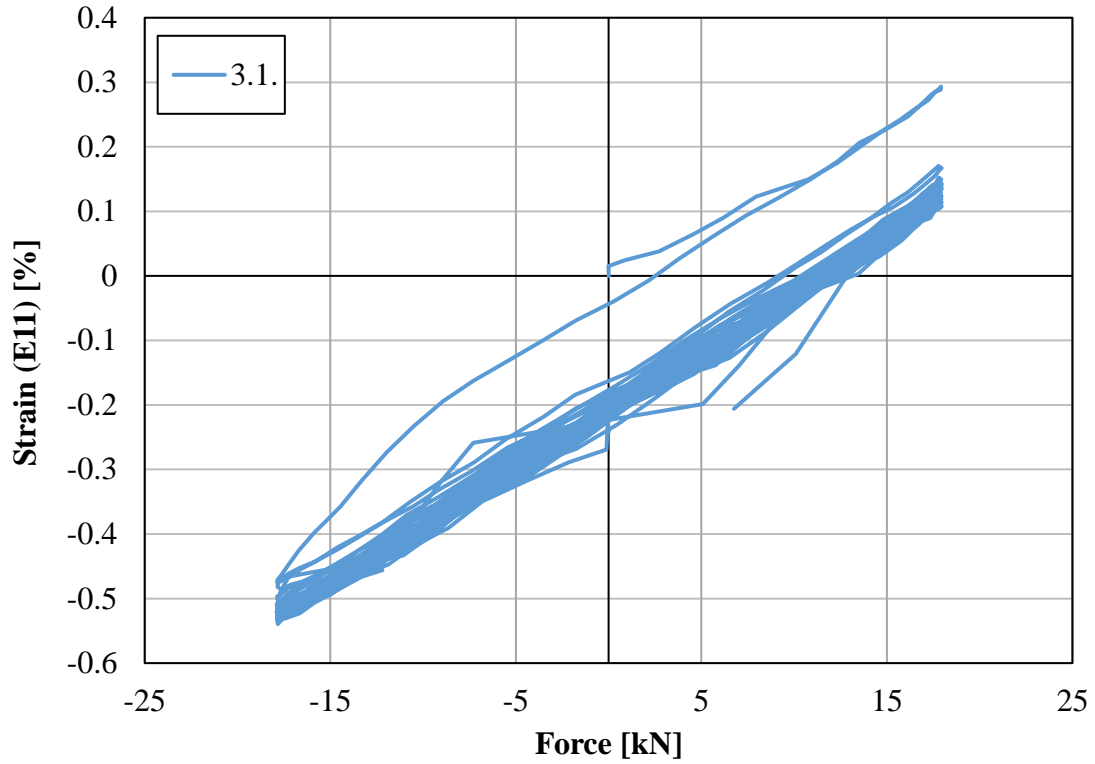


Figure 6.24 *E11 strain [%] – Force [kN] diagram of area 3.1.*

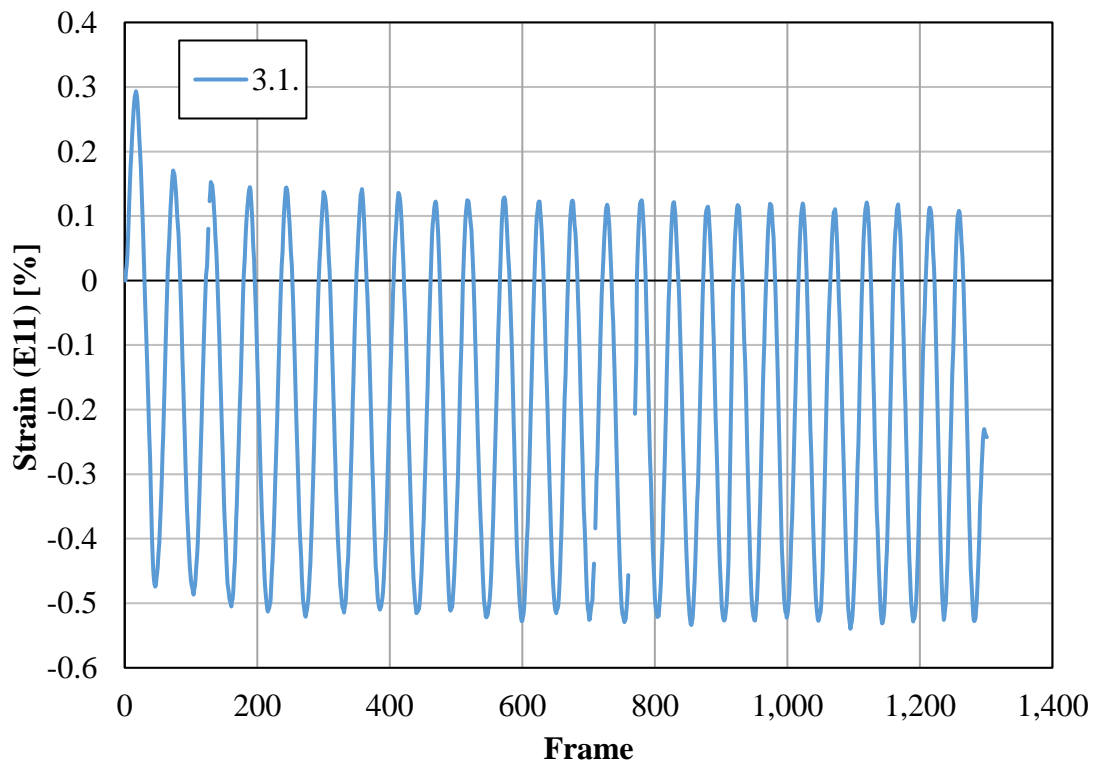


Figure 6.25 *E11 strain [%] – Frame [-] diagram of area 3.1.*

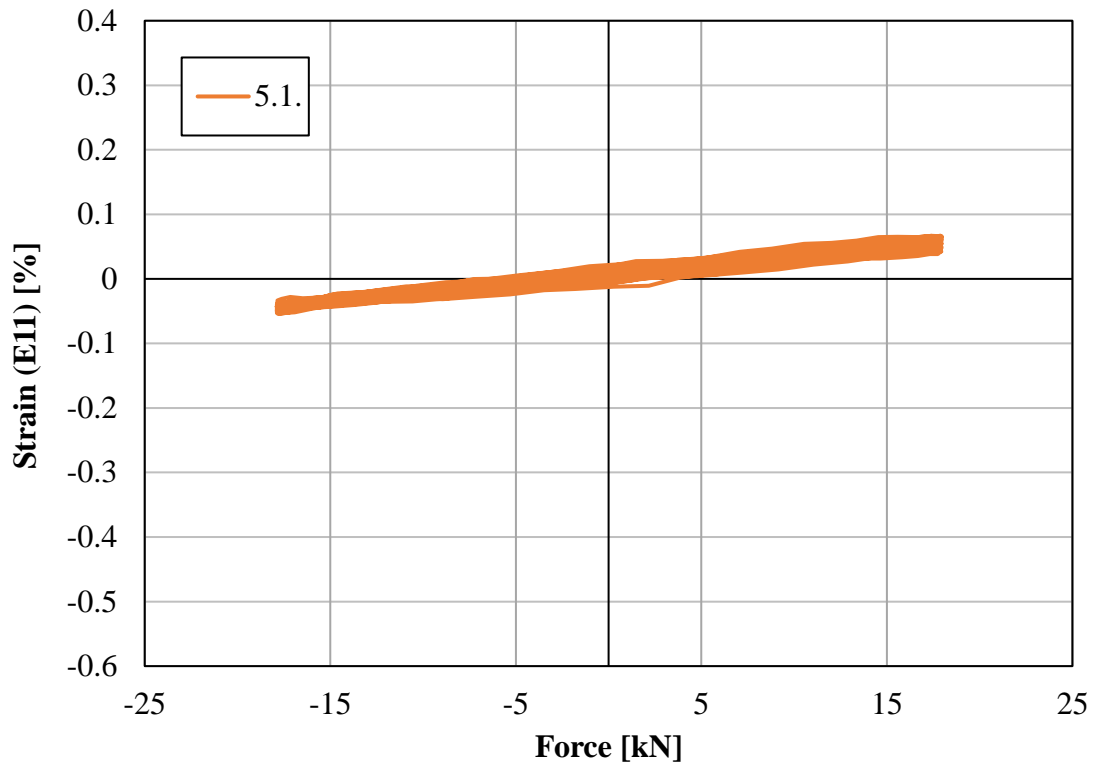


Figure 6.26 *E11 strain [%] – Force [kN] diagram of area 5.1.*

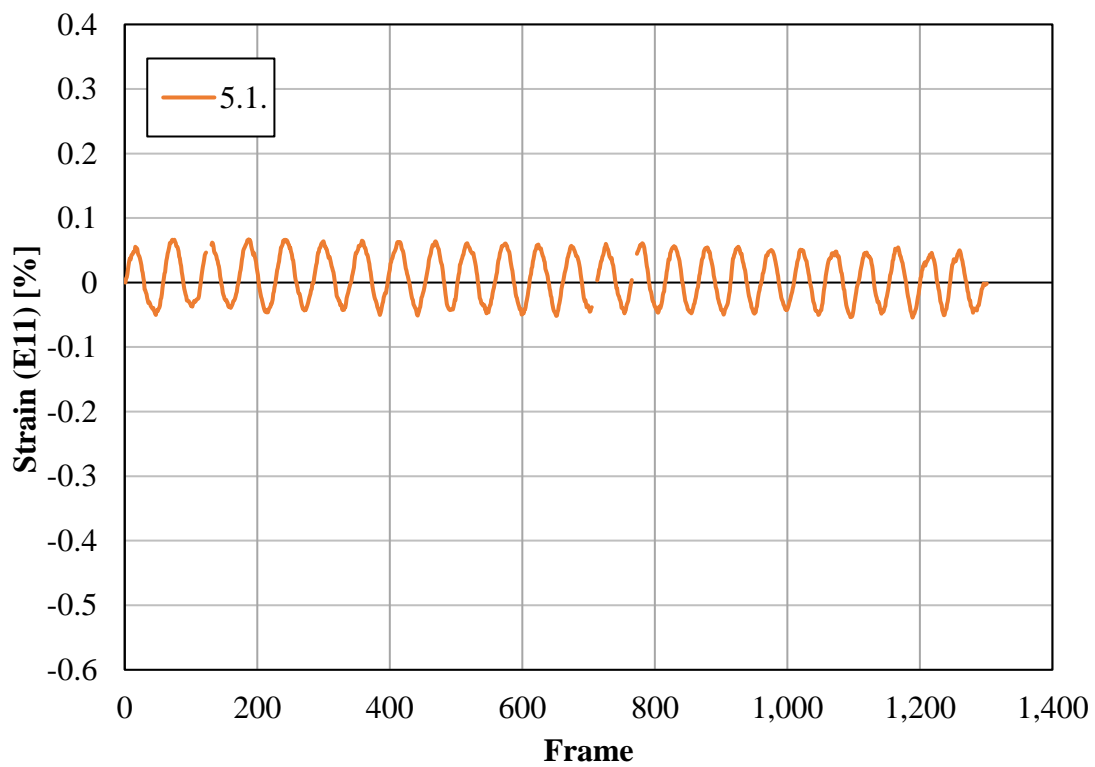


Figure 6.27 *E11 strain [%] – Frame [-] diagram of area 5.1.*

7 Modelling Procedures (Abaqus + 3D scan)

7.1 3D scanning of test specimen

The geometry of the tested specimens was obtained by 3D scanning. Prior to the scanning procedure, the specimens were treated by applying a thin layer of white powder on the surface of the specimen. This was necessary, because of the smooth and glossy surface of the testing specimens, which would have made it difficult for the laser of the 3D scanner to capture the proper geometry.

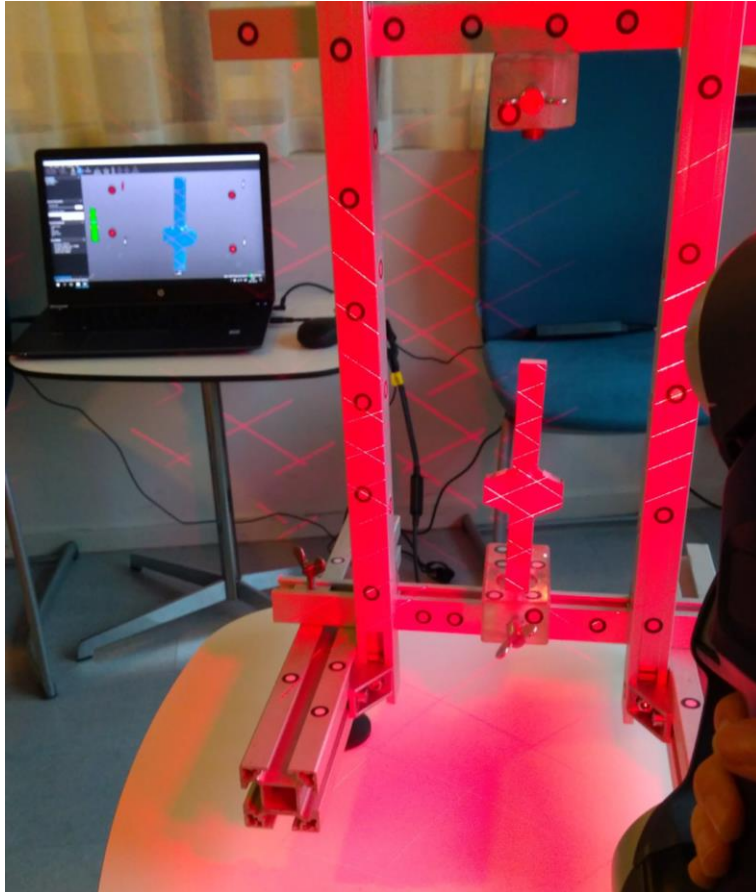


Figure 7.1 3D scanning procedure of the test specimen.

Using the software VXELEMENTS, the accurate contour line of the analyzed specimens was obtained from the 3D scan of the specimens, which further on was used in order to create the Abaqus model of the specimens. The contour line was used, rather than the full 3D scan, in order to reduce the Abaqus model size, and consequently the computation time, while also facilitate a desired mesh creation.

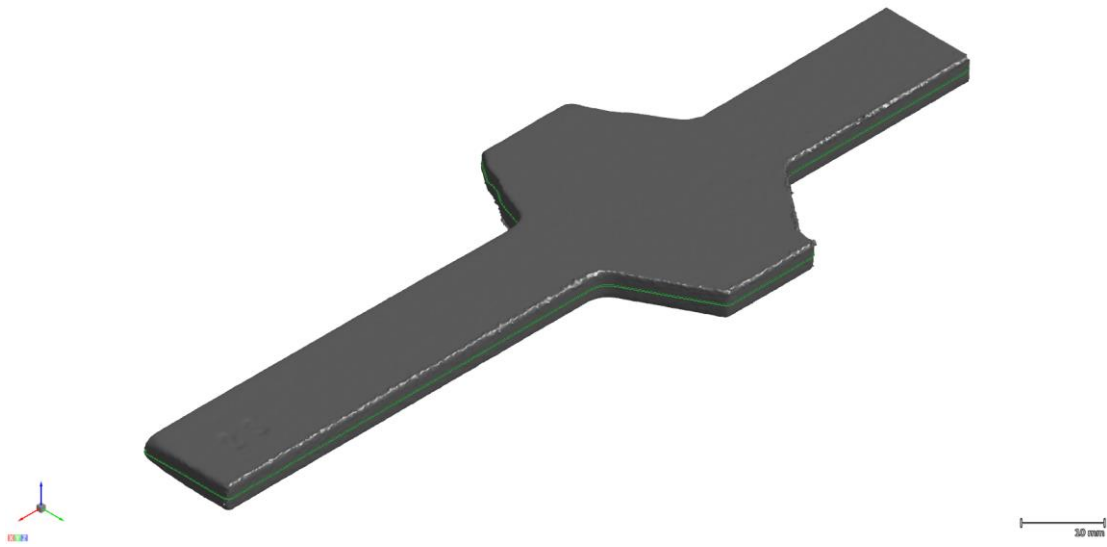


Figure 7.2 Isometric view of 3D scanned SAW test specimen.

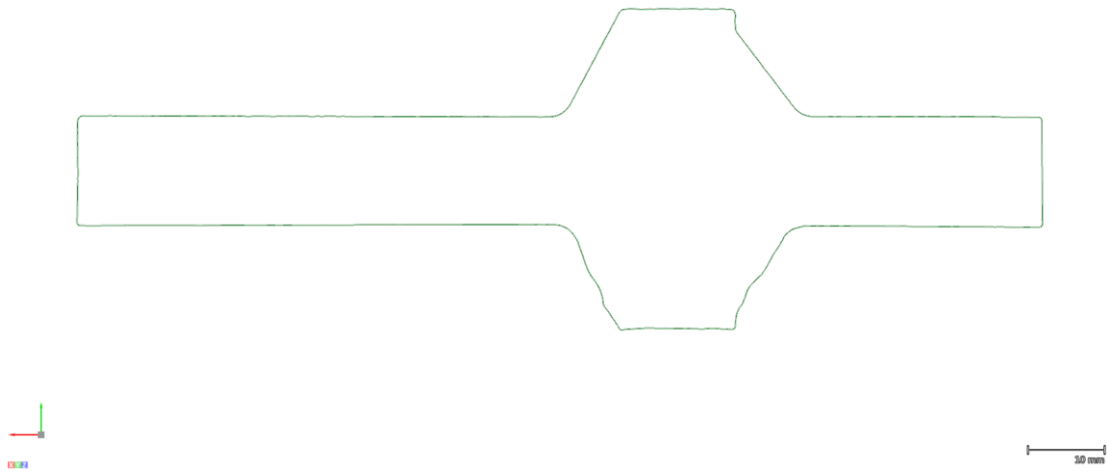


Figure 7.3 Contour line of 3D scanned SAW test specimen.

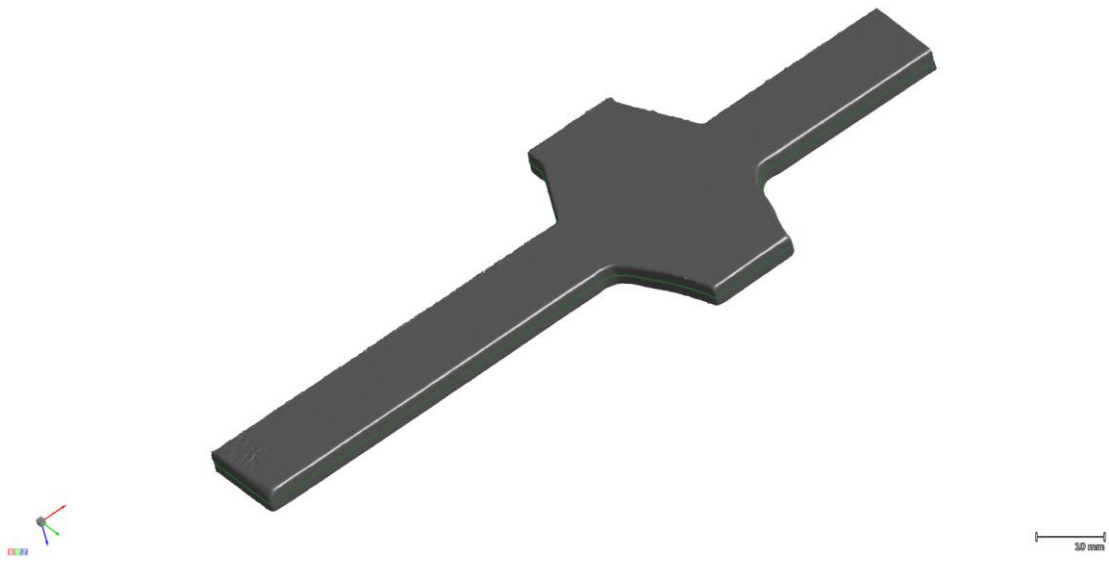


Figure 7.4 Isometric view of 3D scanned SHFMI test specimen.

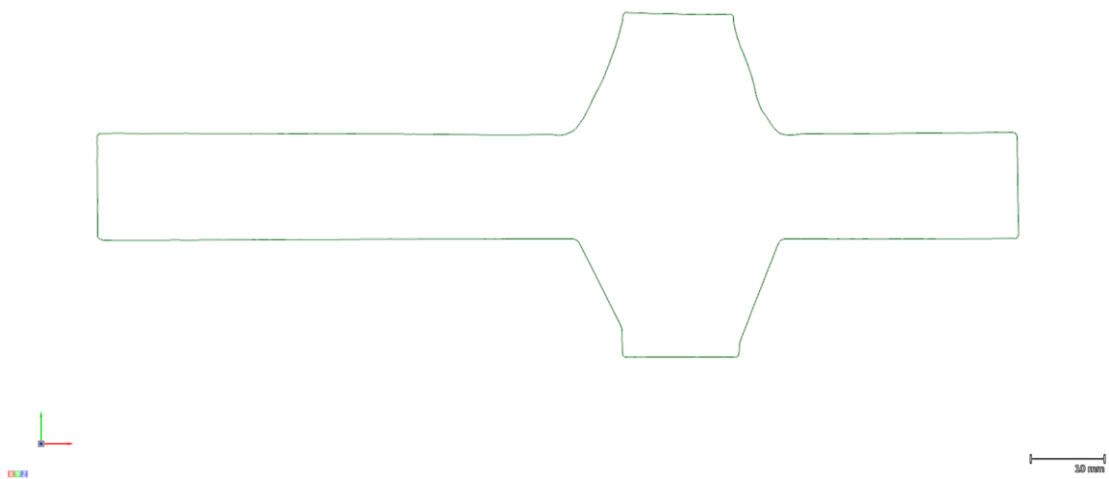


Figure 7.5 Contour line of 3D scanned SHFMI test specimen.

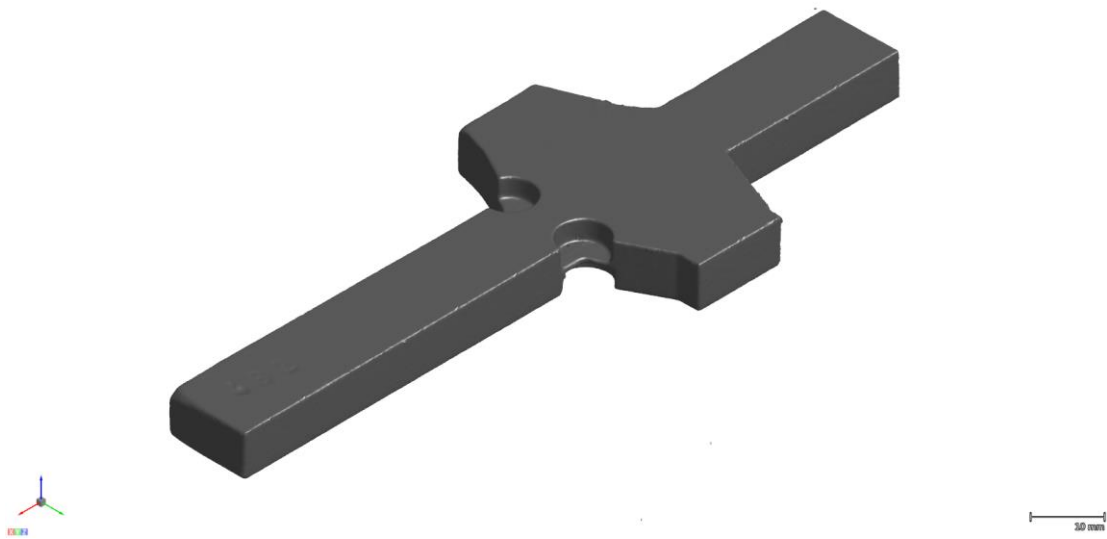


Figure 7.6 Isometric view of 3D scanned C18 test specimen.

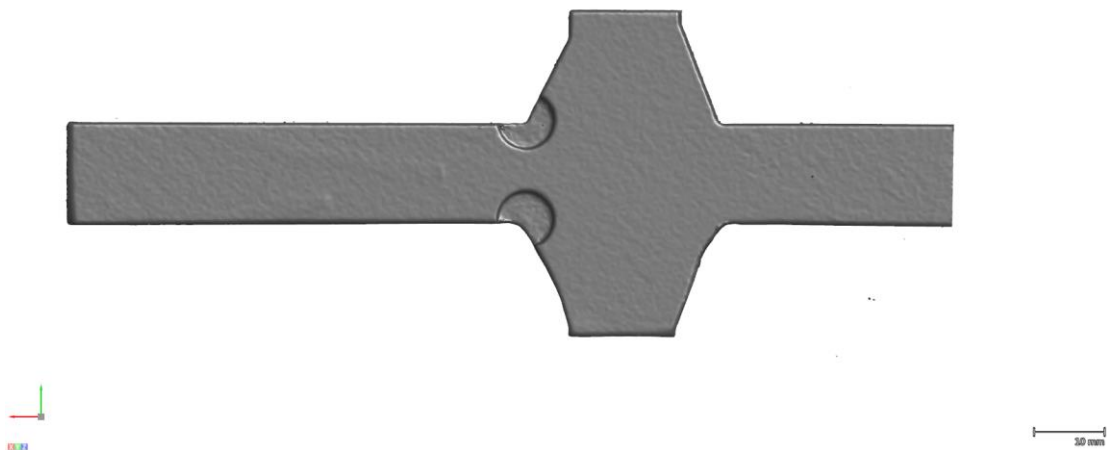


Figure 7.7 Side view of 3D scanned C18 test specimen.

7.2 Abaqus model

The contour line obtained as a result of the 3D scanning of the specimens, was introduced into the finite element analysis software Abaqus as a sketch and then extruded to the desired thickness of 4 mm. The partitioning lines of the three material regions, were traced by overlaying the image captured on the polished specimen on the 3D scanned contour line. This procedure can be seen in Figure 7.8. The partitioning lines were also introduced in Abaqus as a sketch and used to partition the Abaqus model according to the real material regions.

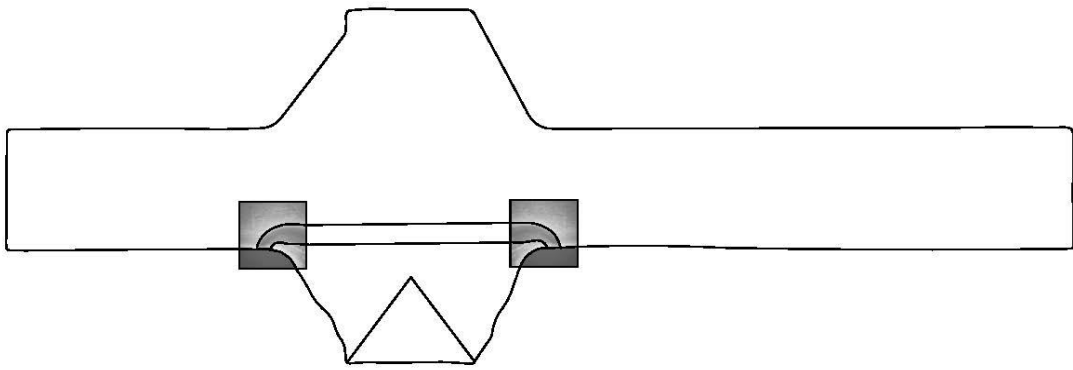


Figure 7.8 Determination of the different material region location on the SAW specimen.

The impression left by the grips on the specimen after testing made it possible to measure the clamping length directly on the tested specimen. Thus for a better representation of reality, the length on which the specimen was clamped at the two ends during testing was removed in the Abaqus model of the specimen. A circular partitioning was performed in the area of interest, having the purpose of allowing a finer mesh assignment in that region. The final geometry considered in the Abaqus model can be seen in Figure 7.9, while the material assignment of different regions is presented in Figure 7.10.

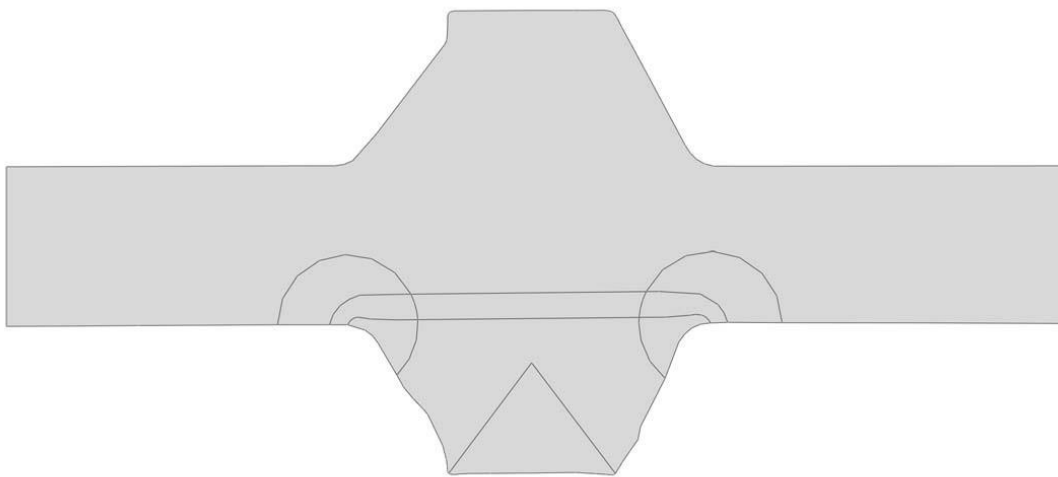


Figure 7.9 Considered geometry for the material calibration of the SAW specimen.

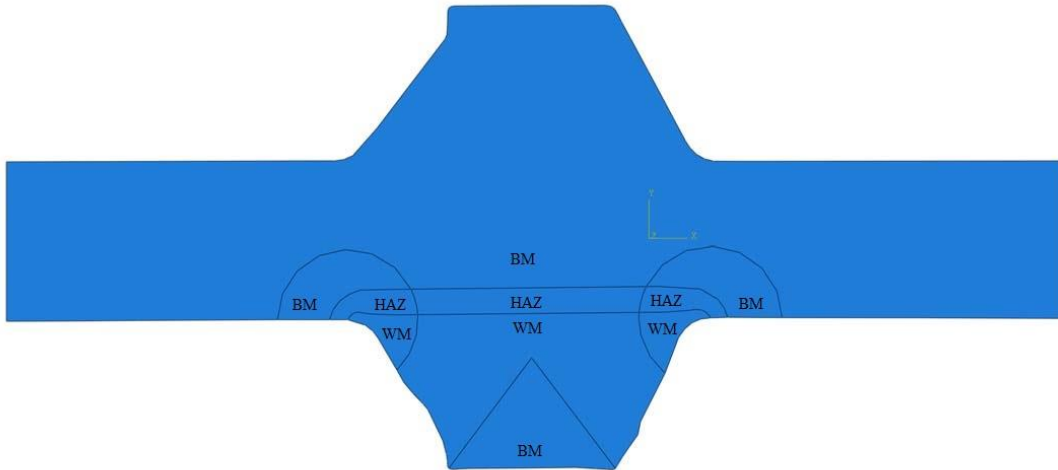


Figure 7.10 Considered material assignment for the material calibration of the SAW specimen.

The assigned mesh size in the area of interest, inside the defined circles was 0.6 mm. In order to reduce the Abaqus computation time, the mesh size was increased to 1.5 mm everywhere outside the area of interest, as illustrated in Figure 7.11.

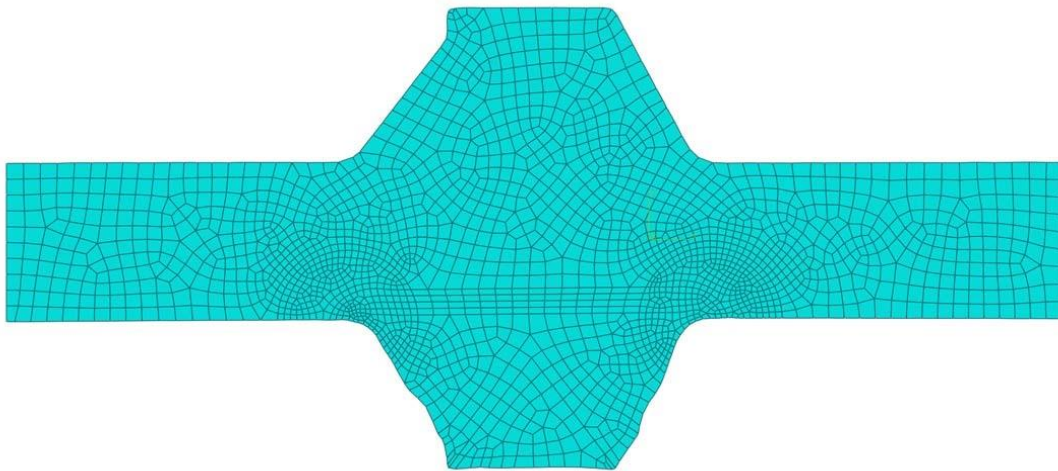


Figure 7.11 Considered mesh for the material calibration of the SAW specimen.

Similar to the testing conditions, a load of 25 kN was applied on the right hand side of the model and necessary boundary conditions were introduced in order for the model to be adequately restrained in all three directions, mimicking the laboratory testing conditions.

8 Material Calibration Procedure

For the calibration process the Abaqus2Matlab toolbox was used in order to create a connection between the finite element software Abaqus and the commercial software Matlab. This was necessary in order to utilize the optimization function of Matlab for the introduction of the material data in Abaqus.

The toolbox is written in MATLAB programming language and it enables the running of Abaqus analysis through Matlab, without starting the software. It requires the Abaqus Input file, containing the geometry, and boundary condition definitions.

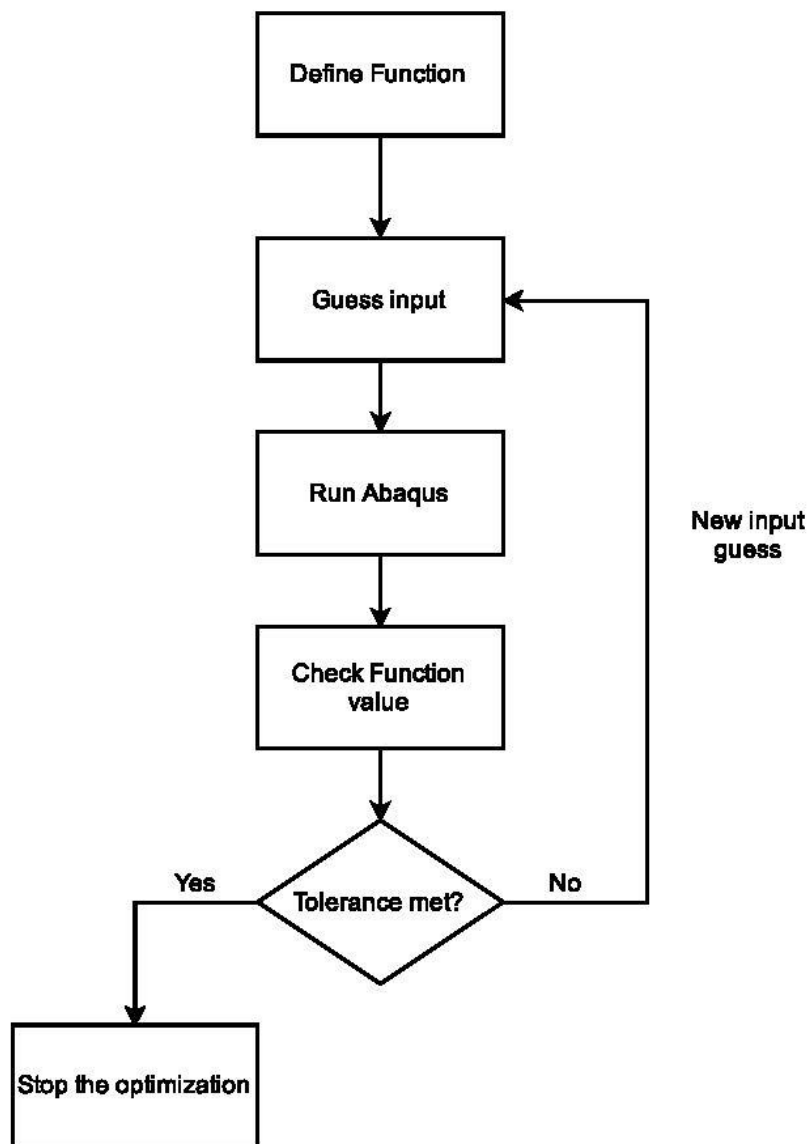


Figure 8.1 Simplified flow chart of the material calibration procedure.

The material calibration procedure was performed according to the flow chart presented in Figure 8.1. The defined function in this case is the relative error between the experimental strain value in a given point, obtained from the DIC and the strain value in the same point obtained by means of Abaqus modeling (equation (8.1)).

$$Function = \frac{\varepsilon_{exp} - \varepsilon_{Abaqus}}{\varepsilon_{exp}} \quad (8.1)$$

The strain value extracted from Abaqus is in function of the defined material parameters, which are changed in the Abaqus Input file during the optimization procedure. Throughout the material calibrations, the improved material input is guessed by the “fminsearch” optimization function, which is inbuilt in Matlab. Thus the material calibration starts out with a guess material input in the Abaqus model, which is continuously improved until the defined relative error function is equal to the assigned tolerance value. When the optimization is stopped, the modelled strain value is regarded as equal to the experimental strain value. Therefore, the introduced material model in Abaqus at the end of the optimization, should coincide with the real material model.

The difficulty of the material calibration of a welded detail, is due to the influence which every introduced material parameter of one material has on the other materials.

8.1 Simple case study

During the material calibration of a welded detail, certain problematics might arise due to the stress concentration at the weld toe and the presence of multiple materials. Thus the material calibration procedure was carried out initially on a simple case, considering a statically loaded plate with a hole in the middle and consisting of two different materials.

This enabled the creation of a calibration procedure, which takes into account the presence of multiple materials, as well as the presence of stress concentrations, while being able to test the accuracy of the results.

Two material models were considered and introduced into the Abaqus model. The resulting maximum principle stresses in two elements were used later on as experimental data, in the process of material calibration.

8.1.1 Abaqus model

The plate with a hole was modelled using shell elements, having a length of 300 mm, height of 100 mm and a radius of 12 mm for the hole.

In order to have a better control over the mesh size, the face of the shell element was partitioned at the edge of the hole, forcing the software to assign a mesh with smaller size in the desired region. The global assigned mesh size was 10 mm.

The load was applied on the right hand side as uniform traction force, while being fixed in the direction of the load on the left hand side. A second boundary condition was introduced to the two bottom corners; these being fixed in the direction perpendicular to the load. Figures 8.2 – 8.5 below show the considered geometry, the assigned mesh, the considered material assignment and the two elements used for the material calibration procedure.

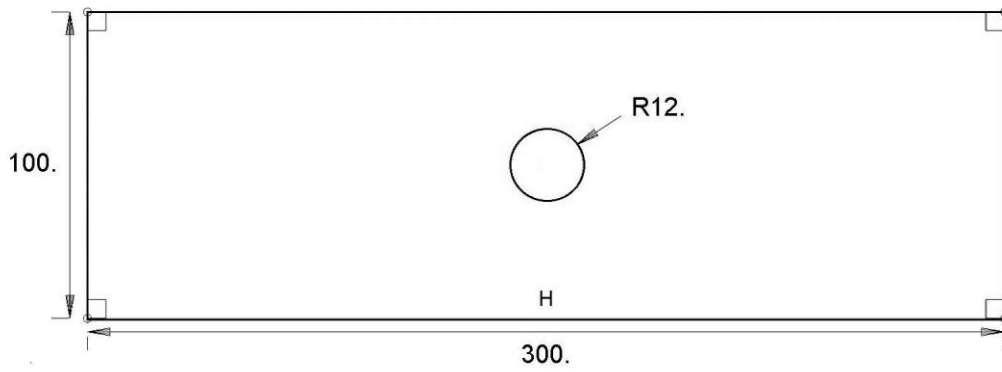


Figure 8.2 Considered geometry for the material calibration of a plate with a hole.

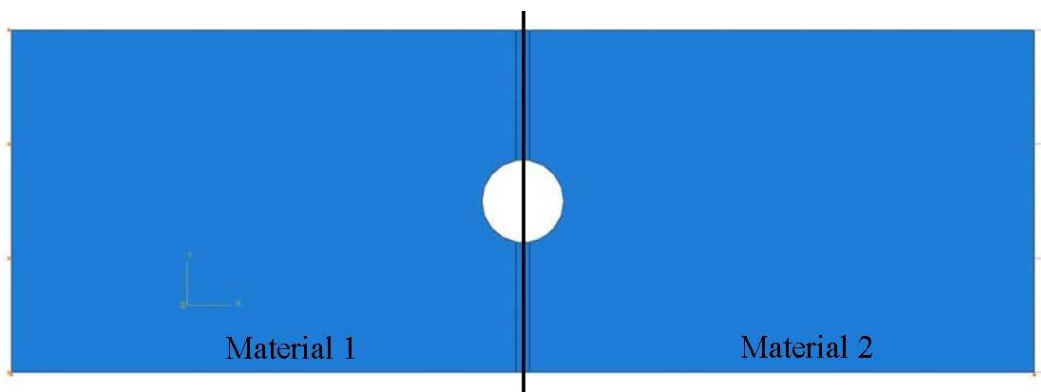


Figure 8.3 Considered material assignment for the material calibration of a plate with a hole.

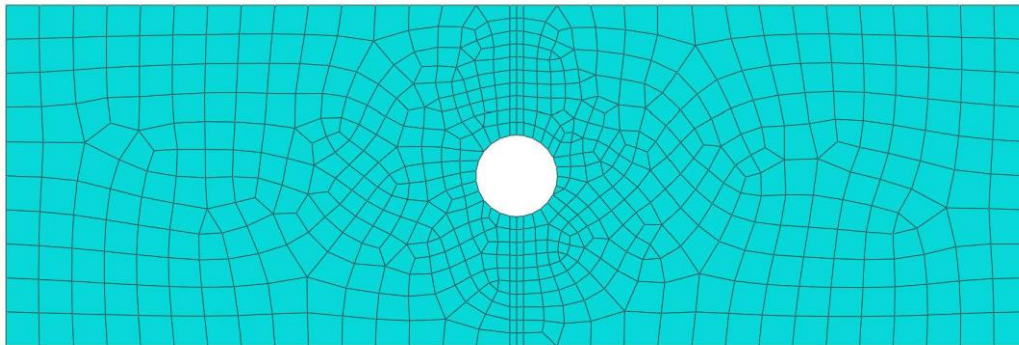


Figure 8.4 Considered mesh for the material calibration of a plate with a hole.

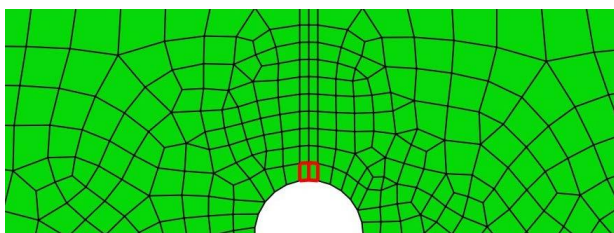


Figure 8.5 Considered elements for the material calibration of a plate with a hole.

The considered two isotropic elastic and plastic material models are presented in the Tables 8.1 and 8.2 below and were introduced into the Abaqus model. Isotropic plasticity model was chosen, since the model is loaded statically, and there is no need for a more complex plasticity model.

Table 8.1 Isotropic elastic material models.

Material 1		Material 2	
E-modulus (GPa)	250	E-modulus (GPa)	270
Poisson's Ratio	0.3	Poisson's Ratio	0.3

Table 8.2 Isotropic plastic material models.

Material 1		Material 2	
Stress (MPa)	Strain	Stress (MPa)	Strain
300	0	460	0
340	0.005	525	0.005
385	0.01	597	0.01
415	0.015	644	0.015
445	0.02	679	0.02
470	0.025	732	0.025
490	0.03	-	-
500	0.035	-	-
510	0.04	-	-

The obtained E11 strain values in two of the elements of the model, one in each material considered, were regarded as the experimental values that are used for the calibration procedure. After saving the desired maximum principal strain values, the input material parameters were deleted and the Abaqus Input file was saved, without any material input data.

8.1.2 Calibration procedure

The Abaqus Input file for the plate with a hole was introduced to Matlab, together with the specification of the requested output and the link was created between Abaqus and Matlab using the Abaqus2Matlab toolbox. The material calibration was performed by an iterative process, which focused on matching the “experimental” strain values to the strain values obtained in the Abaqus analysis. During the whole material calibration,

the strain values were extracted from two elements of the Abaqus model, one from each material, right at the stress concentration zone, as marked with red in Figure 8.5.

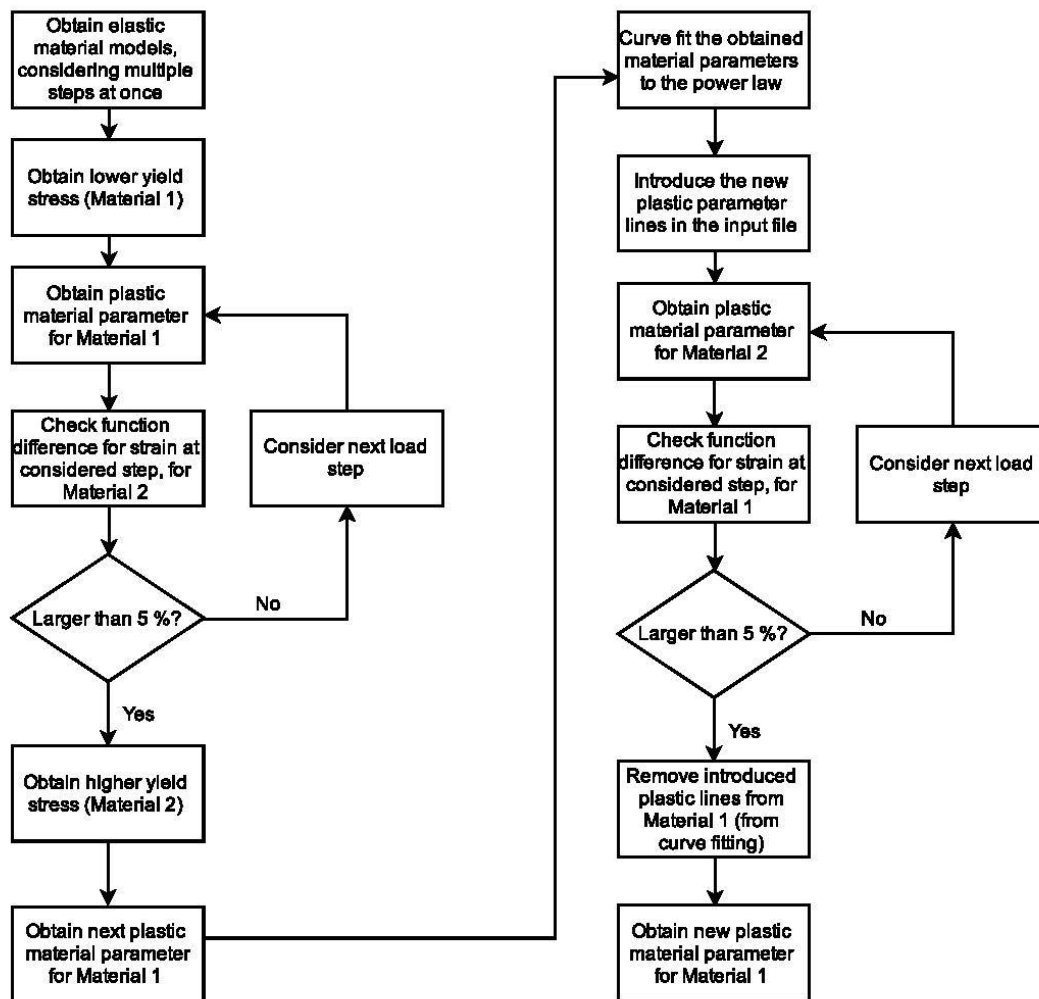


Figure 8.6 Flow chart of the material calibration procedure for the plate with a hole.

Figure 8.6 presents the flow chart of the case study, showing all the steps of the iterative process. The expression plastic parameters refer to the pair of stress-strain values which are introduced in the Abaqus material definition windows in order to describe the material isotropic plasticity model. In a very simplified step wise manner, this can be presented as follows:

- Step 1:** Obtaining the elastic material model, consisting of the E-modulus values for the two material regions. The Poisson's ratio of each material was considered to be equal to 0.3.
- Step 2:** Obtaining the yield stress and plastic material parameters of the material having the lowest yield stress value from the analyzed model, in this case Material 1.
- Step 3:** Obtaining the yield stress of Material 2.

- Step 4:** Performing a curve fitting to the power law of the plastic parameters of Material 1, obtained up to this point and using the power law parameters to predict a new line in the plastic material definition.
- Step 5:** Obtaining plastic material parameters of Material 2.
- Step 6:** Removing the predicted plastic material parameters of Material 1, which were introduced in Step 4 and obtaining further, more accurate plastic material parameters of this material.

The input elastic material model was obtained by creating a function script, which changes the E-modulus values in the Input file as specified by the optimization function and runs the Abaqus analysis with the new E-modulus input. After each Abaqus analysis run the maximum principal strain values in the requested elements are obtained as output, for the first few number of steps. In order for the material calibration to work, it is crucial to make sure that all the considered steps are located in the elastic region. In this specific case, the data of the first 5 steps was used simultaneously, from a total of 20 steps. By increasing the number of steps being calibrated simultaneously, the accuracy of the obtained elastic material model is increased, while increasing the computation time of the calibration procedure. The above mentioned function script is used in the definition of a function, having as variable the input E-modulus values, which is further on used by the optimization function in order to minimize the chosen function value, described by equation (8.1).

The plastic material model was obtained similarly to the elastic material model, considering only one load step for each calibration procedure and making a clear distinction between the first line of the plastic material definition, which describes the yield stress value and the rest of the stress-plastic strain pair lines.

8.1.3 Results

As a result of the iterative process presented in the flow chart in Figure 8.6, the obtained material parameters are presented in this subchapter, in direct comparison to the considered “real” material models.

Table 8.3 shows the predicted elastic material model of the two materials next to the reference models, the difference between them being of 0 %.

Table 8.3 Comparison between reference elastic material models and predicted elastic material models.

	Material 1			Material 2		
	Reference values	Predicted values	Dif. (%)	Reference values	Predicted values	Dif. (%)
E-modulus (GPa)	250	249.999	0	270	269.999	0
Poisson's Ratio	0.3	0.3	0	0.3	0.3	0

When analysing the plastic material model obtained for Material 1 in comparison to the reference material model, which is presented in Table 8.4 and Figure 8.7, a good correlation can be seen between the two, having a maximum difference of under 5 %.

Table 8.4 Comparison between reference plastic material model and predicted elastic material model for Material 1.

Reference Material 1		Predicted Material 1		Difference (%) in input stress values
Stress (MPa)	Strain	Stress (MPa)	Strain	
300	0	302.938	0	0.98
340	0.005	339.418	0.005	0.17
385	0.01	380.585	0.01	1.15
415	0.015	415.814	0.015	0.20
445	0.02	448.873	0.02	0.87
470	0.025	483.306	0.025	2.83
490	0.03	510.74	0.03	4.23
500	0.035	-	-	-
510	0.04	-	-	-

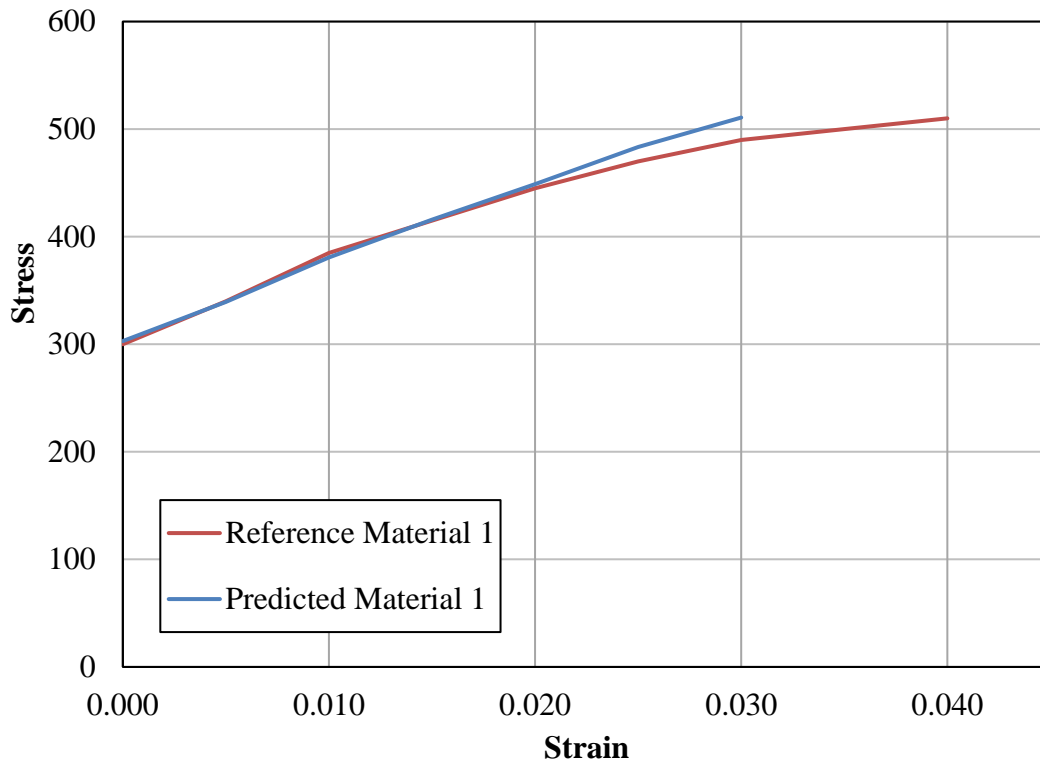


Figure 8.7 Comparison between the stress-strain curves of the reference plastic material model and predicted plastic material model for Material 1.

In the case of Material 2, the difference between the predicted material and the reference material model is even lower, reaching a maximum of 3.5 %, as seen in Table 8.5 and Figure 8.8.

Table 8.5 Comparison between reference plastic material model and predicted plastic material model for Material 2.

Reference Material 2		Predicted Material 2		Difference (%) in input stress values
Stress (MPa)	Strain	Stress (MPa)	Strain	
460	0	462.082	0	0.45
525	0.005	519.117	0.005	1.18
597	0.01	576.519	0.01	3.46
644	0.015	624.444	0.015	2.99
679	0.02	-	-	-
732	0.025	-	-	-

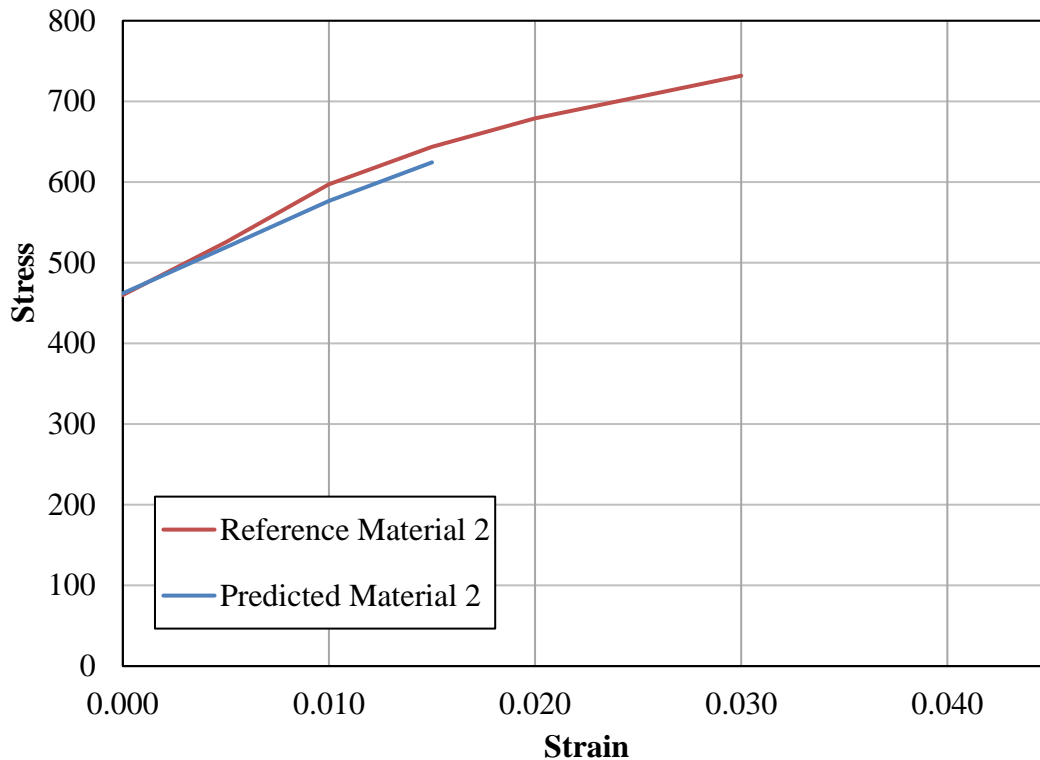


Figure 8.8 Comparison between the stress-strain curves of the reference plastic material model and predicted plastic material model for Material 2.

Looking at Figure 8.7 and Figure 8.8 it is apparent that the two material models have an influence on each other, since the predicted Material 1 model starts to deviate from the reference model, when Material 2 is yielding. During the calibration procedure it was also observed that the material model can be improved upon and refined, if it is recalibrated after every new line which is added to the second plastic material model.

8.2 Test specimen (SAW)

The Matlab code devised for the material calibration of the case study, consisting of a plate with a hole loaded statically was adapted to the statically tested as-welded test specimen, without HFMI treatment (SAW). The main difference consisted in upgrading the code from considering two different materials to three, namely the weld material, the heat affected zone and the base material.

8.2.1 Elastic region

The E-modulus of different material regions was obtained by using one step (13 kN), but comparing simultaneously the experimental strain values obtained by DIC in multiple areas, from every material region with the ones obtained by the Abaqus analysis.

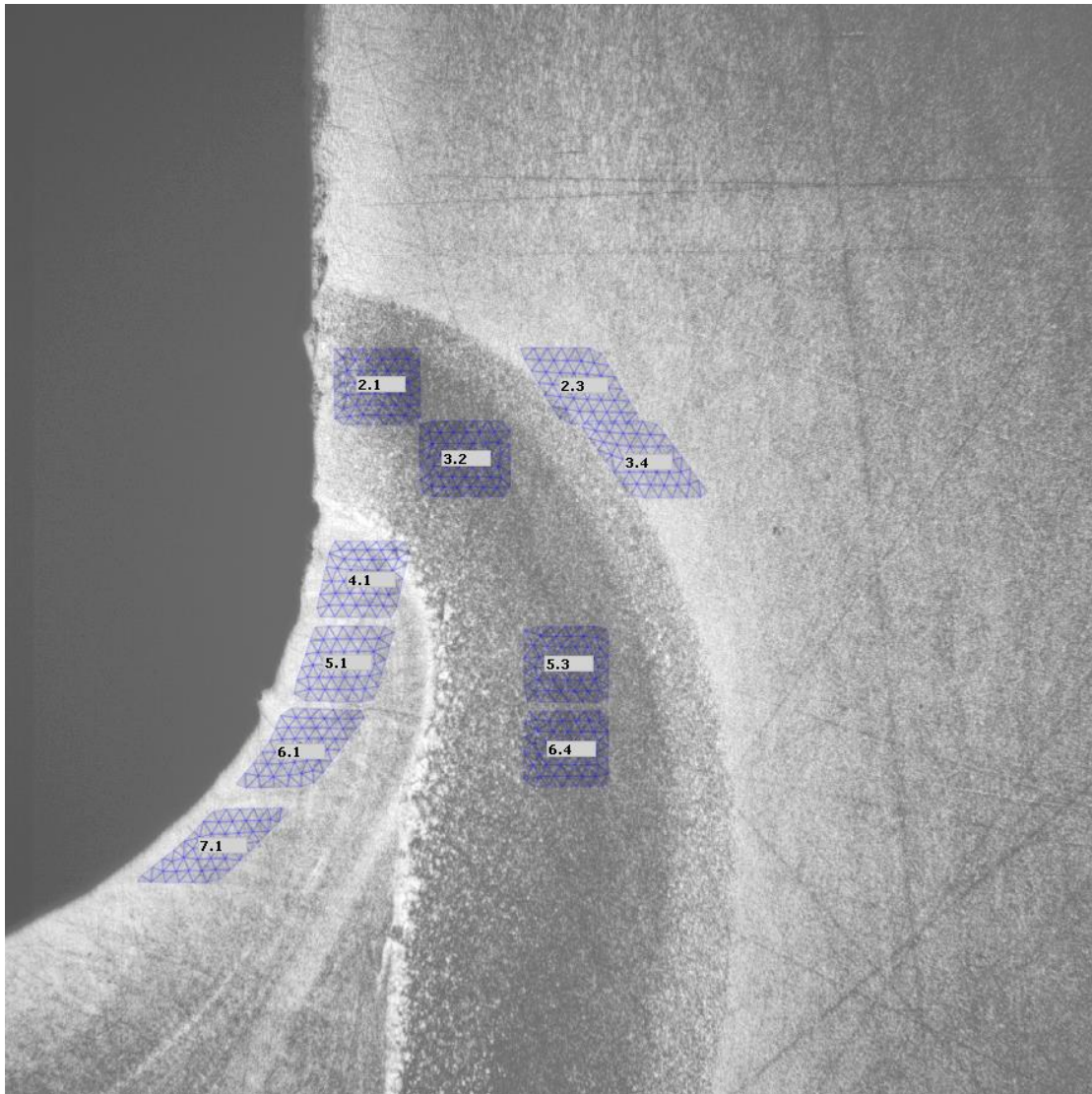


Figure 8.9 Selected areas for the calibration of the E-modulus values.

Four areas were selected from the WM, as well as the HAZ, and two areas from the BM, as presented in Figure 8.9. In order to compare the strain value belonging to an appropriate element from the Abaqus model, to the selected area values from DIC, Figure 8.9 was overlaid with an image showing the elements and the element numbers from the Abaqus model, making it possible to identify the desired elements for the output values, which were later stated in the Abaqus Input file. Thus the desired strain values were calculated by Abaqus only for these specified elements, reducing computation time considerably.

The obtained E-modulus values for the 3 materials are presented in Table 8.6.

Table 8.6 Obtained elastic material parameters for specimen SAW.

	WM	HAZ	BM
E-modulus (GPa)	196.998	219.636	238.449
Poisson's Ratio	0.3	0.3	0.3

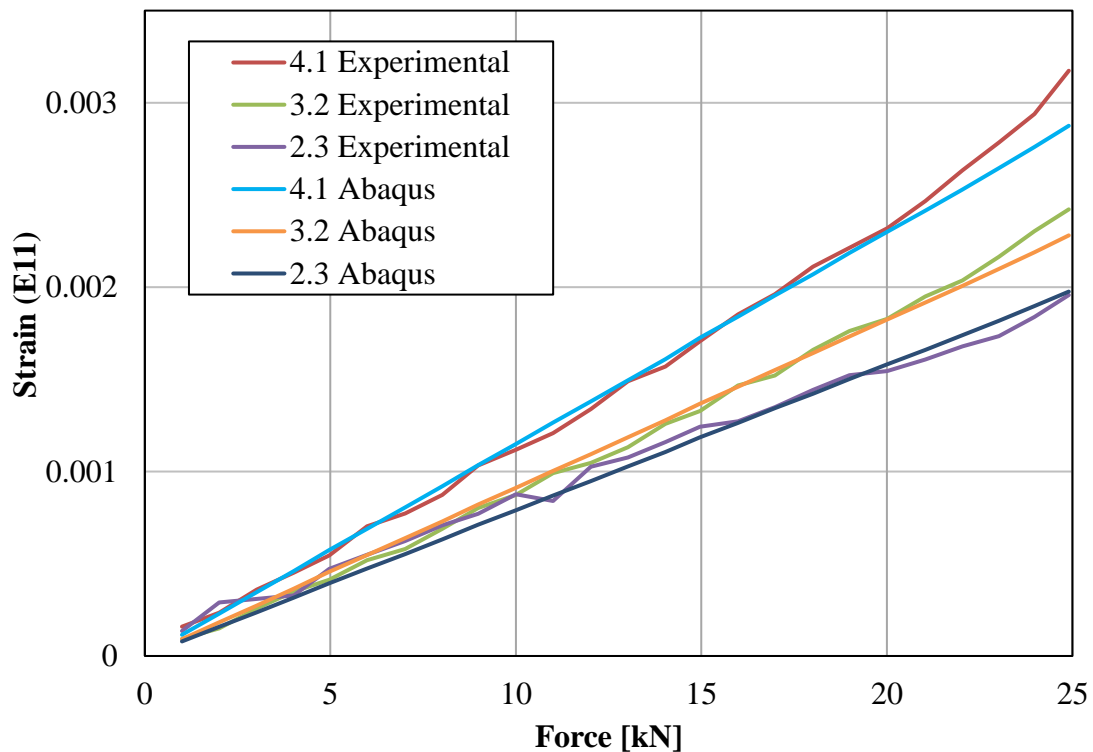


Figure 8.10 Comparison between the experimental strain–force curves and the ones obtained from Abaqus, with only elastic material model input for the three material regions.

The experimental E11 strain and force curves of three selected areas (4.1, 3.2 and 2.3), one from each material region, are compared with the E11 strain and force curves obtained from the FE analysis in Figure 8.10, using the calibrated E-modulus values as elastic material input parameters, in order to check the validity of the obtained E-modulus values.

Good correlation between the experimental E11 strain value and the E11 strain value obtained from the Abaqus analysis was observed in Figure 8.10, showing a deviation from linear behavior in the case of the area in the weld material (4.1) and the area in the heat affected zone (3.2) somewhere beyond an applied load of 20 kN. This deviation can be explained by the occurrence of yielding in these areas.

8.2.2 Plastic region

In order to obtain the plastic material parameters, the number of analyzed areas was reduced to three areas, one from each material, this way reducing the computation time. The areas considered were 4.1, 3.2 and 2.3.

In Figure 8.10 the area located in the weld material (4.1) is deviating at lower load step, than the other areas, thus plastic material model was introduced first for this material. The yield stress and plastic material parameters obtained as a result of material calibration are presented in Table 8.7 and Figure 8.11. The material calibration was performed at one load step, namely when the deviation from linearity was equal to 5 %.

Table 8.7 Obtained plastic material model input for weld material.

Weld material	
Stress (MPa)	Strain
510.391	0
520.635	0.0001
538.405	0.0002
554.402	0.0003

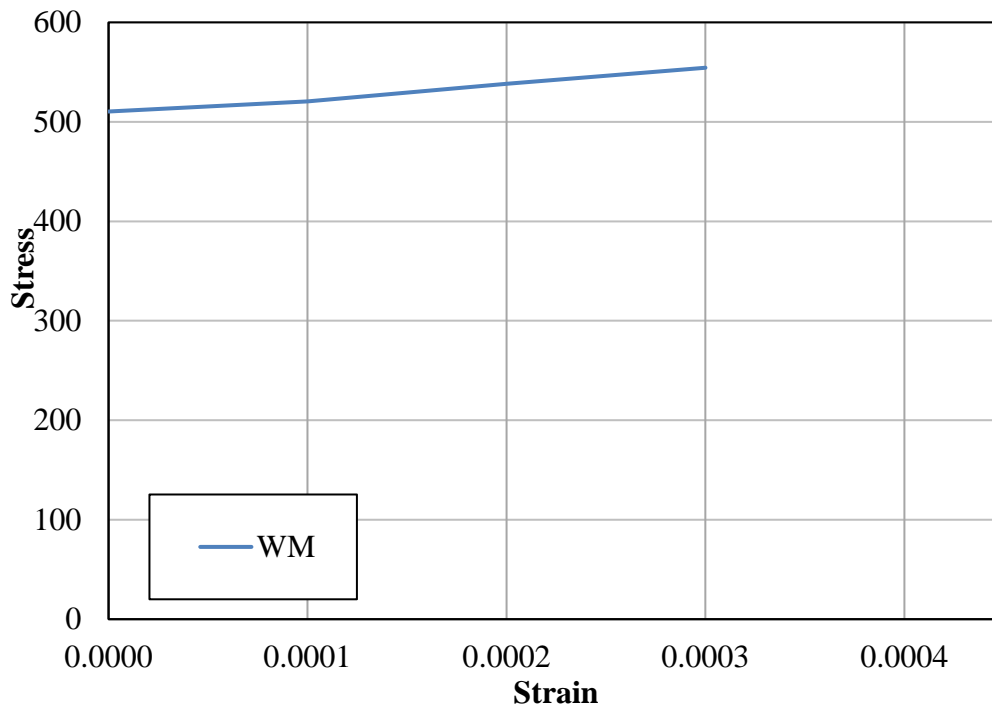


Figure 8.11 The obtained stress-strain curves of the weld material.

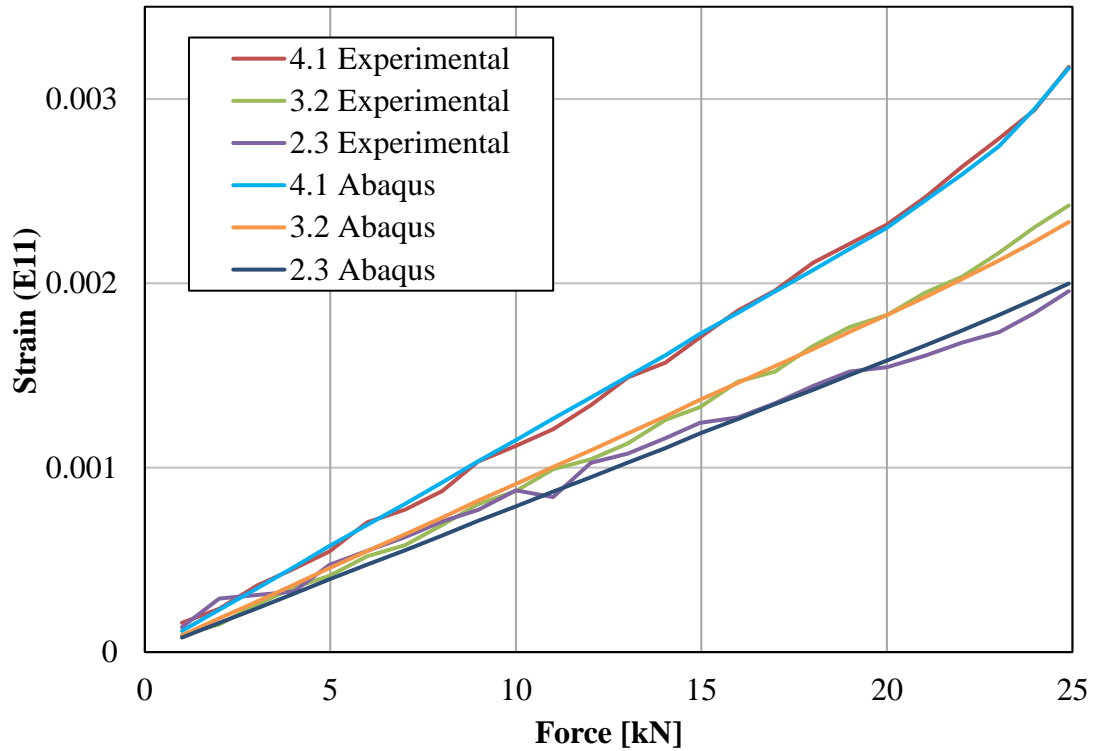


Figure 8.12 Comparison between the experimental strain–force curves and the ones obtained from Abaqus, with elastic material model input for the three material regions, and plastic material input only for the weld material.

After the introduction of plastic material model for the weld material, the E11 strain values follow the experimentally obtained E11 strain values from the same area during loading, as shown in Figure 8.12. A slight deviation from linearity is still observable in the case of the area located in the heat affected zone (3.2), whereas in the case of the area from the base material (2.3) the deviation is decreasing while reaching the maximum applied load. This indicates that the deviation observed considering area 2.3 is rather a consequence of noise in the experimental values, due to the low strain values, rather than the appearance of yielding.

The next step consisted of obtaining the yield stress of the heat affected zone, the value which is presented in Table 8.8. The obtained yield stress of around 510 MPa, for the weld material, as well as the heat affected zone seems reasonable considering the data given by the manufacturer regarding the used materials for the test specimens.

Table 8.8 Obtained plastic material model input for heat affected zone.

Heat affected zone	
Stress (MPa)	Strain
509.668	0

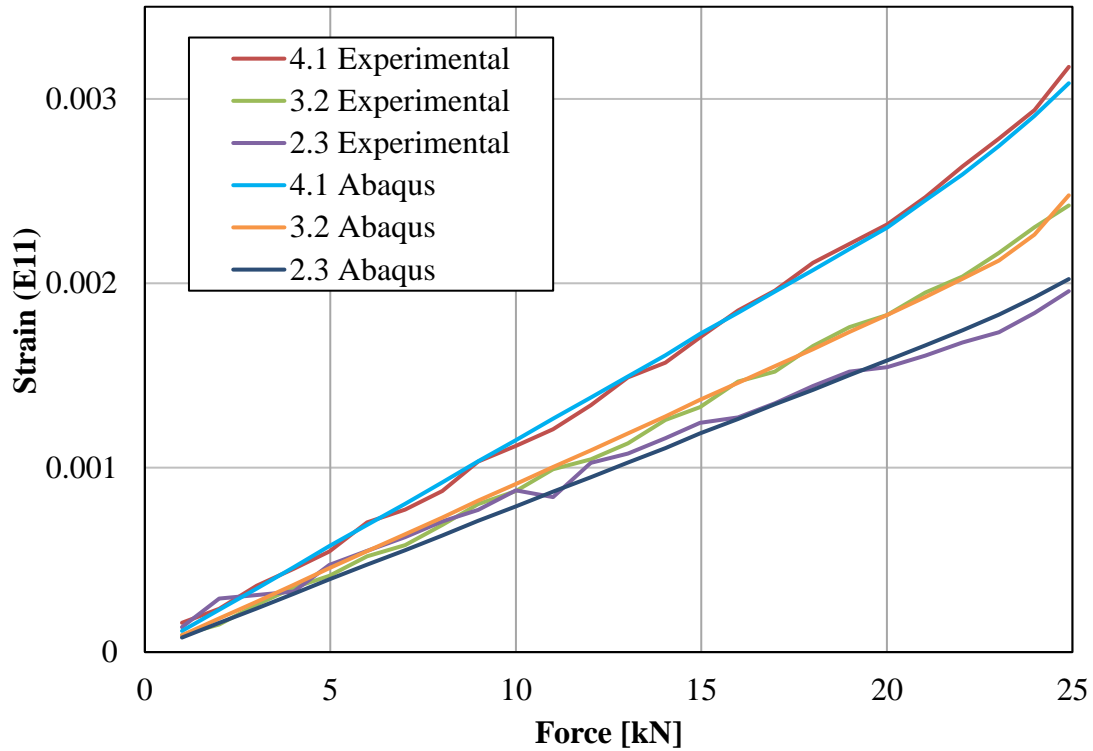


Figure 8.13 Comparison between the experimental strain–force curves and the ones obtained from Abaqus, with elastic material model input for the three material regions, and plastic material input only for the weld material and heat affected zone.

Another comparison between the experimentally obtained E11 strain and the one modelled in Abaqus, during loading for a specific area from each material region is presented in Figure 8.13, when elastic material model is introduced for all three material regions, and plastic material model is defined only for the weld material and the heat affected zone. While the introduction of a plastic material model for the HAZ decreased the difference between the modelled values and the experimental values, it also induced a deviation in the values belonging to area 4.1 (from WM), showing the great influence that one material has on the other, due to their close proximity.

9 Discussion\Conclusion

As a result of the work carried out for the thesis project at hand, it was concluded that it is feasible to use digital image correlation (DIC) in the process of material calibration of a welded detail, in order to obtain the experimental strain field over the area of interest, at the weld toe of a welded detail. However, the obtainment of good results relies on certain aspects of the testing.

It was observed that DIC is not as suitable for the investigation of very small strains, showing signs of significant noise in the experimental values in the elastic region. Thus, in order for the calibration to be possible, large strains are needed in the investigated area, by either making sure that the load level is high enough, or by concentrating the stresses in the area of interest. Due to the presence of noise, even after filtering, it was detected that the E-modulus value even within the same material was different depending on the location of the investigated area. This showed that in the case of small strain it is necessary to investigate multiple areas within the same material, in order to obtain an averaged material model.

Due to the very close proximity of the analyzed material regions, the plastic material input in one material has a large influence on the other materials, making it hard to identify small differences between the analyzed materials. Thus, the calibration procedure works better if there is significant difference between the material inputs, in which case continuous update of the material parameters is recommended after obtaining new plastic material parameters.

The material calibration is an iterative process, which relies on good connection between Abaqus and Matlab. Monitoring the iteration process is recommended in order to observe in time eventual errors that could have appeared.

10 Future research

For further research the test specimen design should be improved, in order to have larger stress concentrations in the investigated area, as well as making sure that the applied load is large enough to capture significant plastic deformation.

After the material calibration is sufficiently optimized, by reducing the number of needed iterations, the procedure could be applied to the statically tested HFMI treated test specimen and later on even capturing the cyclic behavior of the material, using digital image correlation (DIC).

Since DIC is not suitable for monitoring small strains, as those present during elastic deformation, the elastic material model could be obtained by other means, for example by using very small strain gauges.

11 References

- Abaqus Analysis User's Guide, (2013): Version 6.13. Available at <http://129.97.46.200:2080/v6.13/books/usb/default.htm>
- Araújo M. C., (2002): *Non-linear kinematic hardening model for multiaxial cyclic plasticity*. M.Sc. Thesis. Department of Civil and Environmental Engineering, Louisiana State University and Agricultural and Mechanical College, Louisiana, USA, August 2002, 51 pp.
- Barzin B., (2015): *Simulation and Material Calibration of Ultra High Strength Steel (UHSS) S960 Welded Joint under Static Tensile Test utilizing Finite Element Method (FEM)*. M.Sc. Thesis. Department of Mechanical Engineering, Lappeenranta University of Technology, Lappeenranta, Finland, 2015, 39 pp.
- Boumerzoug Z., Derfouf C., Baudin T. (2010): Effect of Welding on Microstructure and Mechanical Properties of an Industrial Low Carbon Steel. *Engineering*, No. 2, July 2010, 502-506 pp.
- Brockenbrough R. L., Merritt F. S. (1999): *Structural Steel Designer's Handbook*. McGraw-Hill Inc., New York.
- Chakrabarty J., (2006): *Theory of Plasticity*. Elsevier Butterworth - Heinemann, Oxford, United Kingdom.
- Dahlberg M., Segle P., (2010): *Evaluation of models for cyclic plastic deformation - A literature study*. Available at www.stralsakerhetsmyndigheten.se .
- Domone P., Illston J. (2010): *Construction Materials: Their nature and behaviour*. Spon Press, Milton Park, Abingdon.
- Dorogoy A., Rittel D., (2009): Determination of the Johnson–Cook Material Parameters Using the SCS Specimen. *Experimental Mechanics*. Vol. 49, December 2009, pp 881-885.
- Easterling K. (1992): *Introduction to the Physical Metallurgy of Welding*. Butterworth - Heinemann, Jordan Hill, Oxford.
- European Standard (2005): *Eurocode 3, Design of steel structures - Part 1-8: Design of joints*, CEN, Brussels.
- Ghahremani K, Safa M, Yeung J, et al, (2014): Quality assurance for high-frequency mechanical impact (HFMI) treatment of welds using handheld 3D laser scanning technology. *Weld World*, Vol. 59, No. 3, May 2015, pp. 391–400.
- GOM mbH, (2015): *GOM Correlate Professional (V8 SR1 Manual Basic): Inspection – 3D Testing*. GOM mbH, Braunschweig, Germany.
- Gorse C., Johnston D., Pritchard M. (2012): *A Dictionary of Construction, Surveying and Civil Engineering*. Oxford University Press, Oxford, United Kingdom.

- Halama R., Sedlák J., Šofer M., (2012): *Phenomenological Modelling of Cyclic Plasticity*, Numerical Modelling, Dr. Peep Miidla (Ed.). InTech, Rijeka, Croatia.
- Herrmann K. (2011): *Hardness Testing: Principles and Applications*. ASM International, Materials Park, Ohio.
- Johnson G. J., Cook W. H., (1983): A constitutive model and data for metals subjected to large strains, high strain rates and high temperatures. *Proceedings of the Seventh International Symposium on Ballistics*, The Hague, The Netherlands, 1983, pp. 541–547.
- Johnson J., ProcessBarron (-): *Fatigue life improvement techniques for welds*. Pelham, Alabama. Retrieved from <http://processbarron.com/wp-content/uploads/Weld-Improvement-Techniques-403.pdf>
- Krenk S., Høgsberg J., (2013): *Statics and Mechanics of Structures*. Springer, Dordrecht, Netherlands.
- Lemaitre J., Chaboche J.-L. (1990): *Mechanics of solid materials*. Cambridge University Press, Cambridge, United Kingdom.
- Marquis G. B., Barsoum Z. (2016): *IIW Recommendations for the HFMI Treatment: For Improving the Fatigue Strength of Welded Joints*. Springer, Singapore.
- Mikkola E. (2016): *A study on effectiveness limitations of high-frequency mechanical impact*. Ph.D. Thesis. Department of Mechanical Engineering, Aalto University, Publication no. 81/2016, Helsinki, Finland, 2016, 117 pp.
- Ottosen N. S., Ristinmaa M., (2005): *The Mechanics of Constitutive Modeling*. Elsevier Ltd., Oxford, United Kingdom.
- Papazafeiropoulos G., Muñoz-Calvente M., Martínez-Pañeda E., (2017): Abaqus2Matlab: a suitable tool for finite element post-processing. *Advances in Engineering Software*. Vol. 105, March 2017, pp 9-16.
- Phillips D. H. (2016): *Welding engineering: An Introduction*. John Wiley & Sons, West Sussex, United Kingdom.
- Samuel K. G., Rodriguez P. (2005): On power-law type relationships and the Ludwingson explanation for the stress-strain behaviour of AISI 316 stainless steel. *Journal of Materials Science*, 40, August 2005, 5727-5731pp.

Appendix I: Matlab code for material calibration of SAW test specimen

Main Matlab code for Elastic material models

Experimental data

```
% Experimental data imported from Excel file, where:  
% first line is the force,  
% upcoming 10 lines are the experimental strain values for the load step of  
% 13 kN, for the areas: 4.1, 5.1, 6.1, 7.1, 2.1, 3.2, 5.3, 6.4, 2.3, 3.4.  
Experiment = xlsread('ExperimentInputE116 13kN.xlsx');  
  
%Given data  
FileName = 'Spline1'; % Input file for running Abaqus
```

Obtain the Elastic material properties - Young's modulus

```
Input0 = [204000, 204000, 204000]; % First guess of Elastic modulus  
E = zeros(1,1); % Pre-allocating  
  
% Experimental strain values for first 25 steps  
ExpStrain = Experiment(2:11,1);  
  
% Function, requesting Abaqus to run the analysis, with the (Input) E-  
modulus  
% Changes the existing E-modulus from the file to the one specified and  
% runs the analysis  
eps = @(Input) simulationE1(FileName, Input);  
  
% Objective function - relative error between experimental strain value  
% and strain value obtained from Abaqus  
Function = @(Input) norm((ExpStrain-eps(Input))./ExpStrain);  
  
%Options for the optimisation function, to display the iteration data,  
%specified maximum number of iterations and tolerances  
options=optimset('display','iter','MaxFunEvals',1000,'TolFun',1.0e-  
07,'TolX',1.0e-07);;  
  
%Optimisation function,  
[Input, objval, exitflag, output] = fminsearch (Function, Input0,options);  
  
E(1,1)= Input; % Storing the obtained E-modulus
```

Testing the obtained E-modulus

```
%Obtain the E11 strain values  
eps = simulation( FileName, 1:25 );  
  
%Experimental E11 values  
ExpStrain1 = Experiment(2:11,1);  
% Values of the objective function, in order to check  
Difference(:,1) = (ExpStrain1 - eps)./ExpStrain1;  
maxdif = max(Difference(:));
```

Main Matlab code for Plastic material models

Initial input:

```
% Experimental data imported from Excel file, where:
% first column is the force,
% second column is Strain E11 at area 4.1 in WM,
% third column is the strain E11 at area 3.2 in the HAZ,
% fourth column is the strain E11 at area 2.3 in the BM
Experiment = xlsread('ExperimentInputE112.xlsx');

% Given data
FileName = 'Spline1'; % Input file for running Abaqus
```

Obtaining Yield stress for the WM:

```
Input0 = [400]; % Initial Yield stress guess

Yieldstress = zeros(3,1); % Pre-allocating

% A value to see after which step it introduces the first yield stress
% The number introduced is to be an initial one, in order to reduce
% computation time, making sure that the chosen step is still in
% the elastic region
j = 16

% Check steps from j to end step, in order to find the yield stress
for i=j:length (Experiment)
    [eps1, eps2, eps3] = simulation(FileName, i); % Strain value for step i
    ExpStrain2 = Experiment(i,2); % Experimental strain value for step i
    Check = abs((ExpStrain2 -eps1)/ExpStrain2)

    % If the difference of strain values is less than 5%, then do not
    % optimise just increase the variable showing the step number
    if (Check < 0.05)
        j=j+1
    else
        % If the difference is larger, then optimise the input E modulus
        IntElas( FileName );
        ExpStrain2 = Experiment(i,2:4); % Experimental strain value for step i
        eps = @(Input2) simulationYield(FileName, i, Input2);
        Function = @(Input2) norm((ExpStrain2-eps (Input2))./ExpStrain2);
        options=optimset('display','iter','MaxFunEvals',100,'TolFun',1.0e-
02,'TolX',1.0e-01);;
        [Input2, objval, exitflag, output] = fminsearch (Function,
Input0,options);

        % Store the obtained Yield stress
        Yieldstress(1,:) = Input2;

        % After obtaining the Yield stress, stop the for loop
        break
    end
end
```

Obtaining Yield stress HAZ

```
Input0 = [500]; % Initial Yield stress guess

% A value to see after which step it introduces the second yield stress
j = 20

% Introduce the guess Yield stress and run the analysis
% simulationYield(FileName, j, Input0);

% Check steps from 27 to 30 to find the yield stress
for i=j:length (Experiment)
    [eps1, eps2, eps3] = simulation(FileName, i); % Strain value for step i
    ExpStrain2 = Experiment(i,3); % Experimental strain value for step i
    Check = abs((ExpStrain2 -eps2)/ExpStrain2)

    % If the difference of strain values is less than 2%, then do not
    % optimise just increase the variable showing the step number
    if (Check < 0.02)
        j=j+1
    else

        % If the difference is larger, then optimise the input E modulus
        IntElas2( FileName );
        ExpStrain2 = Experiment(i,2:4); % Experimental strain value for step i
        eps = @(Input2) simulationYieldHAZ(FileName, i, Input2);
        Function = @(Input2) norm((ExpStrain2-eps (Input2))./ExpStrain2);
        options=optimset('display','iter','MaxFunEvals',100,'TolFun',1.0e-
02,'TolX',1.0e-01);;
        [Input2, objval, exitflag, output] = fminsearch (Function,
Input0,options);

        % Store the obtained Yield stress
        Yieldstress(2,:) = Input2;

        % After obtaining the Yield stress, stop the for loop
        break
    end
end
end
```

Obtaining Plastic material properties for WM

```
Input0 = [480]; % First plastic strain values guess

PlStrain = zeros(8,2); % Pre-allocate
prow = 1; % Number of rows in the plastic material input when starting
YStress1 = Yieldstress (1,1);
Emodulus = 196998.1; %Obtained in the previous elastic material calibration
YStrain1 = YStress1/Emodulus; % Yield strain value
Checkstrain1 = (prow*0.0001) + YStrain1;
ExpStrain1 = Experiment(:,2);
ExpStrain2 = Experiment(:,3);

j = 15; % Starting step for the for loop
```

```

% Analyse each step from starting step until the end step
for i=j:length (Experiment)

    ExpStrain3 = Experiment(i,2:4);
    ExpStrain4 = Experiment(i+1,2);

    [eps1, eps2, eps3] = simulation(FileName, i);
    Check = abs((ExpStrain2(i,1) -eps2)/ExpStrain2(i,1));
    if (Check > 0.1)
        break
    end

    if (ExpStrain4 < Checkstrain1)
        j=j+1
    else
        % If larger than specified value, then optimise the input E modulus
        eps = @(Input3) simulationPl(FileName, i, prow, Input3);
        Function = @(Input3) norm((ExpStrain3 -eps (Input3))./ExpStrain3);
        options=optimset('display','iter','MaxFunEvals',100,'TolFun',1.0e-
02,'TolX',1.0e-02);;
        [Input3, objval, exitflag, output] = fminsearch (Function,
Input0,options);
        PlStrain (prow,1) = Input3;

        Input0 = PlStrain (prow,1); % New guess value for next row
        prow = prow + 1; % Increase the plastic material data row number
        Checkstrain1 = (prow*0.0001) + YStrain1;
        j=j+1
    end
end
end

```

Testing the obtained Plastic material model

```

%Obtain the E11 strain values for all steps
[eps1, eps2, eps3] = simulation( FileName, 1:25 );

%Experimental E11 strain values for first 25 steps
ExpStrain1 = Experiment(:,2);
ExpStrain2 = Experiment(:,3);
ExpStrain3 = Experiment(:,4);
% Values of the objective function, in order to check
Difference(:,1) = (ExpStrain1 - eps1)./ExpStrain1;
Difference(:,2) = (ExpStrain2 - eps2)./ExpStrain2;
Difference(:,3) = (ExpStrain3 - eps3)./ExpStrain3;
maxdif = max(Difference(:));

```

Matlab Function script code: simulationEl

```
function eps = simulationEl( FileName, Input )
%Function script which changes the elastic parameters for the WM material
% in the Abaqus Input file and then runs the Abaqus model, using the
% Abaqus2Matlab toolbox with the new material definition.
% Reference for the Abaqus2Matlab toolbox:
%   G. Papazafeiropoulos, M. Muñiz-Calvente, E. Martínez-Pañeda.
Abaqus2Matlab: a suitable tool for finite element post-processing.
% Advances in Engineering Software. Vol. 105, March 2017, Pages 9-16.
% DOI:10.1016/j.advengsoft.2017.01.006
%
% Input:
% FileName = The name of the Abaqus Input file, which will be modified
% Input = The plastic stress value for the WM material, which is introduced
%         into the Abaqus Input file
%
% Output:
% eps = Matrix containing the E11 strain values, for the 10 specified areas,
%       for the 13 kN load step
```

Change material input data WM

```
file = matlab.lang.makeUniqueStrings(FileName);

fid = fopen([file '.inp']);
% read the entire file, if not too big
s = textscan(fid, '%s', 'delimiter', '\n');
fclose(fid);
% search for your Region:
idx1 = find(strcmp(s{1}, '*Material, name=WM'), 1, 'first');
% now search for the next Region:
idx2 = find(strcmp(s{1}, '** STEP: Step-1'), 1, 'first');
s{1}(idx1+2:idx2-3) = ''; % Deleting previous material properties

Emodulus = Input (1,1)
Poisonsrat = (0.3);

% Emodulus = (2500000);
% Poisonsrat = (Input);

for i=1:1
    s{1,1}{end+1, 1} = ''; % adding empty row at the end
    s{1,1}(idx1+i+2:end+1) = s{1,1}(idx1+i+1:end);
    istress = num2str(Emodulus(i,1), '%.1f');
    istrain = num2str(Poisonsrat(i,1), '%.1f');
    input = {istress, istrain};
    inp = strjoin(input, ', ');
    inp2 = cellstr(inp);
    s{1,1}(idx1+i+1,1) = inp2 (1);
end

% print new file
New = 'NewFile';
fName = [New '.inp'];
% NewFile = genvarname(OldFile)
```

```

fid = fopen(fileName, 'w');           % Open the file
for k=1:numel(s{1,1})
    fprintf(fid, '%s\r\n', s{1,1}{k,1});
end
fclose (fid);

```

Delete old input file and re-name the new file with the previous name

```

delete([file '.inp']);
copyfile ([New '.inp'], [file '.inp']);

rehash
rehash path
rehash pathreset

```

Change material input data HAZ

```

file = matlab.lang.makeUniqueStrings(FileName);

fid = fopen([file '.inp']);
% read the entire file, if not too big
s = textscan(fid, '%s', 'delimiter', '\n');
fclose(fid);
% search for your Region:
idx1 = find(strcmp(s{1}, '*Material, name=HAZ'), 1, 'first');
% now search for the next Region:
idx2 = find(strcmp(s{1}, '*Material, name=WM'), 1, 'first');
s{1}(idx1+2:idx2-1) = ''; % Deleting previous material properties

    Emodulus = Input (1,2)
    Poissonsrat = (0.3);

for i=1:1
    s{1,1}{end+1, 1} = ''; % adding empty row at the end
    s{1,1}(idx1+i+2:end+1) = s{1,1}(idx1+i+1:end);
    istress = num2str(Emodulus(i,1), '%.1f');
    istrain = num2str(Poissonsrat(i,1), '%.1f');
    input = {istress, istrain};
    inp = strjoin (input, ', ');
    inp2 = cellstr (inp);
    s{1,1}(idx1+i+1,1) = inp2 (1);
end

% print new file
New = 'NewFile';
fName = [New '.inp'];

fid = fopen(fName, 'w'); % Open the file
for k=1:numel(s{1,1})
    fprintf(fid, '%s\r\n', s{1,1}{k,1});
end
fclose (fid);

```

Delete old input file and re-name the new file with the previous name

```

delete([file '.inp']);
copyfile ([New '.inp'], [file '.inp']);

rehash
rehash path
rehash pathreset

```

Change material input data BM

```

file = matlab.lang.makeUniqueStrings(FileName);

fid = fopen([file '.inp']);
% read the entire file, if not too big
s = textscan(fid, '%s', 'delimiter', '\n');
fclose(fid);
% search for your Region:
idx1 = find(strcmp(s{1}, '*Material, name=BM'), 1, 'first');
% now search for the next Region:
idx2 = find(strcmp(s{1}, '*Material, name=HAZ'), 1, 'first');
s{1}(idx1+2:idx2-1) = ''; % Deleting previous material properties

    Emodulus = Input (1,3)
    Poisonsrat = (0.3);

for i=1:1
    s{1,1}{end+1, 1} = ''; % adding empty row at the end
    s{1,1}(idx1+i+2:end+1) = s{1,1}(idx1+i+1:end);
    istress = num2str(Emodulus(i,1), '%.1f');
    istrain = num2str(Poisonsrat(i,1), '%.1f');
    input = {istress, istrain};
    inp = strjoin (input, ', ');
    inp2 = cellstr (inp);
    s{1,1}(idx1+i+1,1) = inp2 (1);
end

% print new file
New = 'NewFile';
fName = [New '.inp'];

fid = fopen(fName, 'w'); % Open the file
for k=1:numel(s{1,1})
    fprintf(fid, '%s\r\n', s{1,1}{k,1});
end
fclose (fid);

```

Delete old input file and re-name the new file with the previous name

```

delete([file '.inp']);
copyfile ([New '.inp'], [file '.inp']);

rehash
rehash path
rehash pathreset

```

1st STEP - Run Abaqus FEM model

```
Inp_file = matlab.lang.makeUniqueStrings(FileName);

% Run the input file with Abaqus
system(['abaqus job=' Inp_file]);

% Pause Matlab execution to give Abaqus enough time to create the lck file
pause(10)

% If the lck file exists then halt Matlab execution
while exist([Inp_file '.lck'],'file')==2
    pause(0.1)
end
disp('Simulation Finished')
```

2st STEP - Postprocess Abaqus results file with Abaqus2Matlab

```
% Reading .fil file
Rec = Fil2str([Inp_file '.fil']);

% Obtain the desired output data
% Obtaining desired output data - increment data
IncData = Rec2000(Rec);
incrementno = length (IncData (:,1)); % No of steps

% Obtaining E11 strains
AbaqusStrain = Rec21(Rec);

elemno = length (AbaqusStrain(:,1))/incrementno; % No of elements
j=1;
eps2 = zeros (1,elemno);
for i=1:incrementno
    eps1(i,1:elemno) = AbaqusStrain (j:(j+elemno-1),1);
    j=j+elemno;
    eps2(i, :) = eps1(i,:);
end
eps (1, 1) = (eps2(1, 2)+eps2(1, 4))/2;
eps (2, 1) = (eps2(1, 1)+eps2(1, 8))/2;
eps (3, 1) = (eps2(1, 5)+eps2(1, 7))/2;
eps (4, 1) = (eps2(1, 6)+eps2(1, 3))/2;
eps (5, 1) = (eps2(1, 14)+eps2(1, 15))/2;
eps (7, 1) = (eps2(1, 12)+eps2(1, 17)+eps2(1, 16)+eps2(1, 21))/4;
eps (8, 1) = (eps2(1, 13)+eps2(1, 18))/2;
eps (9, 1) = eps2(1, 25);
eps (10, 1) = (eps2(1, 24)+eps2(1, 26))/2;
eps (:, :)
rehash
rehash path
rehash toolbox
rehash pathreset
rehash toolboxreset
rehash toolboxcache
end
```

Matlab Function script code: simulationYield

```
function eps = simulationYield( FileName, no, Input )
%Function script which changes the yield stress value for the WM material
% in the Abaqus Input file and then runs the Abaqus model, using the
% Abaqus2Matlab toolbox with the new material definition.
% Reference for the Abaqus2Matlab toolbox:
%   G. Papazafeiropoulos, M. Muñoz-Calvente, E. Martínez-Pañeda.
Abaqus2Matlab: a suitable tool for finite element post-processing.
% Advances in Engineering Software. Vol. 105, March 2017, Pages 9-16.
% DOI:10.1016/j.advengsoft.2017.01.006
%
% Input:
% FileName = The name of the Abaqus Input file, which will be modified
% no = The step number, at which the E11 strain value is requested
% Input = The yield stress value for the WM material, which is introduced
%         into the Abaqus Input file
%
% Output:
% eps = Matrix containing the E11 strain values, for the 3 specified areas,
%       for the specified load step
```

Change material input data Material WM

```
file = matlab.lang.makeUniqueStrings(FileName);

fid = fopen([file '.inp'], 'r');
% read the entire file, if not too big
s = textscan(fid, '%s', 'delimiter', '\n');
fclose(fid);
% search for first Region:
idx1 = find(strcmp(s{1}, '*Plastic'), 1, 'last');
% now search for the next Region:
idx2 = find(strcmp(s{1}, '** STEP: Step-1'), 1, 'first');
s{1}(idx1+1:idx2-3) = ''; % Deleting previous material properties

Stressinp = [Input(1,1)]
Straininp = [0];

for i=1:length(Stressinp)
    s{1, 1}{end+1, 1} = ''; % adding empty row at the end
    s{1,1}(idx1+i+1:end+1) = s{1,1}(idx1+i:end);
    istress = num2str(Stressinp(i,1), '%.3f');
    istrain = num2str(Straininp(i,1), '%.6f');
    input = {istress, istrain};
    inp = strjoin (input, ', ');
    inp2 = cellstr (inp);
    s{1,1}(idx1+i,1) = inp2 (1);
end

% print new file
New = 'NewFile';
fName = [New '.inp'];
fid = fopen(fName, 'w'); % Open the file
```

```

for k=1:numel(s{1,1})
    fprintf(fid, '%s\r\n', s{1,1}{k,1});
end
fclose (fid);

```

Delete old input file and re-name the new file with the previous name

```

delete([file '.inp']);
copyfile ([New '.inp'], [file '.inp']);

rehash
rehash path
rehash toolbox
rehash pathreset
rehash toolboxreset
rehash toolboxcache

```

1st STEP - Run Abaqus FEM model

```

% Start simulation
Inp_file = matlab.lang.makeUniqueStrings(FileName);

% Run the input file with Abaqus
system(['abaqus job=' Inp_file]);

% Pause Matlab execution to give Abaqus enough time to create the lck file
pause(10)

% If the lck file exists then halt Matlab execution
while exist([Inp_file '.lck'],'file')==2
    pause(0.1)
end
disp('Simulation Finished')

```

2st STEP - Postprocess Abaqus results file with Abaqus2Matlab

```

% Reading .fil file
Rec = Fil2str([Inp_file '.fil']);

% Obtain the desired output data
% Obtaining desired output data - increment data
IncData = Rec2000(Rec);
incrementno = length (IncData (:,1)); % No of steps

% Obtaining E11 strains
AbaqusStrain = Rec21(Rec);
elemno = length (AbaqusStrain(:,1))/incrementno; % No of elements
j=1;
eps2 = zeros (100,elemno);
for i=1:incrementno
    eps11(i,1:elemno) = AbaqusStrain (j:(j+elemno-1),1);
    j=j+elemno;
end

```

```
    eps2(i, :) = eps11(i,:);
end

eps (1, 1) = (eps2(no, 1)+eps2(no, 2))/2;
eps (1, 2) = (eps2(no, 3)+eps2(no, 4))/2;
eps (1, 3) = eps2(no, 5);
eps (1, :)
fprintf('%.7f \n\n',eps)

rehash
rehash path
rehash toolbox
rehash pathreset
rehash toolboxreset
rehash toolboxcache
end
```

Matlab Function script code: simulationPl

```
function eps = simulationPl( FileName, no, plasticrow, Input )
%Function script which changes the plastic parameters for the WM material
% in the Abaqus Input file and then runs the Abaqus model, using the
% Abaqus2Matlab toolbox with the new material definition.
% Reference for the Abaqus2Matlab toolbox:
%   G. Papazafeiropoulos, M. Muñoz-Calvente, E. Martínez-Pañeda.
Abaqus2Matlab: a suitable tool for finite element post-processing.
% Advances in Engineering Software. Vol. 105, March 2017, Pages 9-16.
% DOI:10.1016/j.advengsoft.2017.01.006
%
% Input:
% FileName = The name of the Abaqus Input file, which will be modified
% no = The step number, at which the E11 strain value is requested
% plasticrow = The row number of the plastic parameter, which is changed
% Input = The plastic stress value for the WM material, which is introduced
%         into the Abaqus Input file
%
% Output:
% eps = Matrix containing the E11 strain values, for the 3 specified areas,
%       for the specified load step
```

Change material input data

```
file = matlab.lang.makeUniqueStrings(FileName);

fid = fopen([file '.inp'], 'r');
% read the entire file, if not too big
s = textscan(fid, '%s', 'delimiter', '\n');
fclose(fid);
% search for your Region:
idx1 = find(strcmp(s{1}, '*Plastic'), 1, 'last');
% now search for the next Region:
idx2 = find(strcmp(s{1}, '** STEP: Step-1'), 1, 'first');
s{1}(idx1+1+plasticrow:idx2-3) = ''; % Deleting previous material properties

Stressinp = [Input(1,1)]
Straininp = [plasticrow * 0.0001];

for i=1:length(Stressinp)
    s{1, 1}{end+1, 1} = ''; % adding empty row at the end
    s{1,1}(idx1+i+1+plasticrow:end+1) = s{1,1}(idx1+i+plasticrow:end);
    istress = num2str(Stressinp(i,1), '%.3f');
    istrain = num2str(Straininp(i,1), '%.6f');
    input = {istress, istrain};
    inp = strjoin (input, ', ');
    inp2 = cellstr (inp);
    s{1,1}(idx1+i+plasticrow,1) = inp2 (1);
end

% print new file
New = 'NewFile';
```

```
fName = [New '.inp'];
fid = fopen(fName,'w'); % Open the file
for k=1:numel(s{1,1})
    fprintf(fid, '%s\r\n', s{1,1}{k,1});
end
fclose (fid);
```

Delete old input file and re-name the new file with the previous name

```
delete([file '.inp']);
copyfile ([New '.inp'], [file '.inp']);

rehash
rehash path
rehash toolbox
rehash pathreset
rehash toolboxreset
rehash toolboxcache
```

1st STEP - Run Abaqus FEM model

```
Inp_file = matlab.lang.makeUniqueStrings(FileName);

% Run the input file with Abaqus
system(['abaqus job=' Inp_file]);

% Pause Matlab execution to give Abaqus enough time to create the lck file
pause(10)

% If the lck file exists then halt Matlab execution
while exist([Inp_file '.lck'],'file')==2
    pause(0.1)
end
disp('Simulation Finished')
```

2st STEP - Postprocess Abaqus results file with Abaqus2Matlab

```
% Reading .fil
Rec = Fil2str([Inp_file '.fil']);

% Obtain the desired output data
% Obtaining desired output data - increment data
IncData = Rec2000(Rec);
incrementno = length (IncData (:,1)); % No of steps

% Obtaining E11 strains
AbaqusStrain = Rec21(Rec);
elemno = length (AbaqusStrain(:,1))/incrementno; % No of elements
j=1;
eps2 = zeros (88,elemno);
```

```

for i=1:incrementno
    eps11(i,1:elemno) = AbaqusStrain (j:(j+elemno-1),1);
    j=j+elemno;
    eps2(i, :) = eps11(i,:);
end

eps (1, 1) = (eps2(no, 1)+eps2(no, 2))/2;
eps (1, 2) = (eps2(no, 3)+eps2(no, 4))/2;
eps (1, 3) = eps2(no, 5);
eps (1, :)
fprintf('%0.7f \n\n',eps)

rehash
rehash path
rehash toolbox
rehash pathreset
rehash toolboxreset
rehash toolboxcache
end

```

Matlab Function script code: simulationYieldHAZ

```
function eps = simulationYieldHAZ( FileName, no, Input )
%Function script which changes the yield stress value for the HAZ material
% in the Abaqus Input file and then runs the Abaqus model, using the
% Abaqus2Matlab toolbox with the new material definition.
% Reference for the Abaqus2Matlab toolbox:
%   G. Papazafeiropoulos, M. Muñoz-Calvente, E. Martínez-Pañeda.
Abaqus2Matlab: a suitable tool for finite element post-processing.
% Advances in Engineering Software. Vol. 105, March 2017, Pages 9-16.
% DOI:10.1016/j.advengsoft.2017.01.006
%
% Input:
% FileName = The name of the Abaqus Input file, which will be modified
% no = The step number, at which the E11 strain value is requested
% Input = The yield stress value for the HAZ material, which is introduced
%         into the Abaqus Input file
%
% Output:
% eps = Matrix containing the E11 strain values, for the 3 specified areas,
%       for the specified load step
```

Change material input data for HAZ Material

```
file = matlab.lang.makeUniqueStrings(FileName);

fid = fopen([file '.inp'], 'r');
% read the entire file, if not too big
s = textscan(fid, '%s', 'delimiter', '\n');
fclose(fid);
% search for first Region:
idx1 = find(strcmp(s{1}, '*Material, name=HAZ'), 1, 'first');
% now search for the next Region:
idx2 = find(strcmp(s{1}, '*Material, name=WM'), 1, 'first');
s{1}(idx1+4:idx2-1) = ''; % Deleting previous material properties

Stressinp = [Input(1,1)]
Straininp = [0];

for i=1:length(Stressinp)
    s{1, 1}{end+1, 1} = ''; % adding empty row at the end
    s{1,1}(idx1+i+4:end+1) = s{1,1}(idx1+i+3:end);
    istress = num2str(Stressinp(i,1), '%.3f');
    istrain = num2str(Straininp(i,1), '%.6f');
    input = {istress, istrain};
    inp = strjoin (input, ', ');
    inp2 = cellstr (inp);
    s{1,1}(idx1+i+3,1) = inp2 (1);
end

% print new file
New = 'NewFile';
fName = [New '.inp'];
fid = fopen(fName, 'w'); % Open the file
```

```

for k=1:numel(s{1,1})
    fprintf(fid, '%s\r\n', s{1,1}{k,1});
end
fclose (fid);

```

Delete old input file and re-name the new file with the previous name

```

delete([file '.inp']);
copyfile ([New '.inp'], [file '.inp']);

rehash
rehash path
rehash toolbox
rehash pathreset
rehash toolboxreset
rehash toolboxcache

```

1st STEP - Run Abaqus FEM model

```

% Start simulation
Inp_file = matlab.lang.makeUniqueStrings(FileName);

% Run the input file with Abaqus
system(['abaqus job=' Inp_file]);

% Pause Matlab execution to give Abaqus enough time to create the lck file
pause(10)

% If the lck file exists then halt Matlab execution
while exist([Inp_file '.lck'],'file')==2
    pause(0.1)
end
disp('Simulation Finished')

```

2st STEP - Postprocess Abaqus results file with Abaqus2Matlab

```

% Reading fil. file
Rec = Fil2str([Inp_file '.fil']);

% Obtain the desired output data
% Obtaining desired output data - increment data
IncData = Rec2000(Rec);
incrementno = length (IncData (:,1)); % No of steps

% Obtaining E11 strains for step no
AbaqusStrain = Rec21(Rec);
elemno = length (AbaqusStrain(:,1))/incrementno; % No of elements
j=1;
eps2 = zeros (100,elemno);
for i=1:incrementno
    eps11(i,1:elemno) = AbaqusStrain (j:(j+elemno-1),1);
    j=j+elemno;
end

```

```
    eps2(i, :) = eps11(i,:);  
end  
  
eps (1, 1) = (eps2(no, 1)+eps2(no, 2))/2;  
eps (1, 2) = (eps2(no, 3)+eps2(no, 4))/2;  
eps (1, 3) = eps2(no, 5);  
eps (1, :)  
fprintf('%.7f \n\n',eps)  
  
rehash  
rehash path  
rehash toolbox  
rehash pathreset  
rehash toolboxreset  
rehash toolboxcache  
end
```

Matlab Function script code: IntElas

```
function IntElas( FileName )
%Function script which Introduces the line '*Plastic' in the Abaqus
% Input file for the WM material, in order to start the plastic material
model definition.
%
% Input:
% FileName = The name of the Abaqus Input file, which will be modified
```

Change material input data

```
file = matlab.lang.makeUniqueStrings(FileName);

fid = fopen([file '.inp'], 'r');
% read the entire file, if not too big
s = textscan(fid, '%s', 'delimiter', '\n');
fclose(fid);

Input = ('*Plastic');

idx3 = find(strcmp(s{1}, '*Material, name=WM'), 1, 'first');
s{1, 1}{end+2, 1} = ''; % adding empty row at the end
s{1,1}(idx3+3:end+1) = s{1,1}(idx3+2:end);
input = {Input};
inp = strjoin (input);
inp2 = cellstr (inp);
s{1,1}(idx3+3,1) = inp2 (1);

Input = ('700.000, 0.000000');

idx3 = find(strcmp(s{1}, '*Material, name=WM'), 1, 'first');
s{1, 1}{end+2, 1} = ''; % adding empty row at the end
s{1,1}(idx3+4:end+1) = s{1,1}(idx3+3:end);
input = {Input};
inp = strjoin (input);
inp2 = cellstr (inp);
s{1,1}(idx3+4,1) = inp2 (1);

% print new file
New = 'NewFile';
fName = [New '.inp'];
fid = fopen(fName,'w'); % Open the file
for k=1:numel(s{1,1})
    fprintf(fid, '%s\r\n', s{1,1}{k,1});
end
fclose (fid);
```

Delete old input file and re-name the new file with the previous name

```
delete([file '.inp']);

copyfile ([New '.inp'], [file '.inp']);
```

```
rehash  
rehash path  
rehash toolbox  
rehash pathreset  
rehash toolboxreset  
rehash toolboxcache  
end
```